Role of translocator protein (18 kDa) (TSPO) in retinal phagocytes in a mouse model of age-related macular degeneration (AMD)

I n a u g u r a l – D i s s e r t a t i o n

Zur

Erlangung des Doktorgrades

der Mathematisch-Naturwissenschaftlichen Fakultät

der Universität zu Köln

vorgelegt von

Anne Wolf

aus Merzig

Köln 2020

For my beloved parents

"A scientist in his laboratory is not a mere technician,
he is also a child confronting natural phenomena that
impress him as though they were fairy tales."

- Marie Curie

Table of contents

Zusammenfassung

Die altersbedingte Makuladegeneration (AMD) ist eine komplex genetische und multifaktorielle degenerative Erkrankung der zentralen Netzhaut, die in der Spätphase zu einem dramatischen Sehverlust führt. Bei allen bis heute untersuchten erblichen Netzhautdegenerationen, einschließlich der AMD, liegt dem Erkrankungsverlauf eine schädliche chronische Aktivierung des angeborenen Immunsystems zugrunde. Vor allem residente Mikrogliazellen, die Gewebsmakrophagen der Netzhaut, spielen eine wichtige Rolle bei der Gewebsintegrität. Durch ihre proinflammatorischen und neurotoxischen Eigenschaften tragen chronisch aktivierte Mikroglia maßgeblich zum Fortschreiten der retinalen Degeneration bei und stellen somit ein Ziel für therapeutische Ansätze dar. Immunmodulatorische, mikrogliagerichtete Therapieansätze zielen dabei darauf ab, die neurotoxischen Eigenschaften zu unterdrücken bei gleichzeitigem Erhalt der homöostatischen Funktionen. Eine Zielstruktur für einen solchen mikrogliagerichteten Therapieansatz stellt das Translokatorprotein (18 kDa) (TSPO) dar. TSPO ist ein mitochondriales Transmembranprotein, das von reaktiven Mikrogliazellen exprimiert wird und als Biomarker für Gliosen dient. In verschiedenen Modellen neurodegenerativer Erkrankungen wie Alzheimer, Parkinson, multiple Sklerose und Netzhautdegenerationen zeigte die Behandlung mit TSPO-Liganden entzündungshemmende und neuroprotektive Effekte. Die zugrunde liegenden molekularen Mechanismen der TSPO-vermittelten Immunmodulation sowie seine biologischen Funktionen sind jedoch noch gänzlich unbekannt.

Die in dieser Arbeit vorgestellten Ergebnisse im laserinduzierten Mausmodell der choroidalen Neovaskularisierung (CNV) als etabliertes Modell für die neovaskuläre Form der AMD, zeigen, dass sowohl die Behandlung mit dem TSPO-Ligand XBD173 als auch die Deletion von TSPO in residenten Mikrogliazellen durch die Erzeugung von Tamoxifen-induzierbaren Cx3cr1^{CreERT2}:TSPO$^{fl/fl}$ Mäusen, eine hemmende Wirkung hinsichtlich der Mikrogliareaktivität als auch der CNV haben. Durch die Analyse von verschiedenen NADPH-Oxidase (NOX)-defizienten Mäusen, konnte TSPO als Schlüsselprotein der NOX1-abhängigen neurotoxischen ROS Produktion in der Netzhaut identifiziert werden. Dabei reguliert TSPO den Einstrom von Ca^{2+}-Ionen aus dem extrazellulären Milieu in das Cytosol, welcher nicht nur für die NOX1 Aktivierung, sondern auch für die NOX1 Expression in Mikrogliazellen notwendig ist. Ebenfalls zeigen wir die Neurotoxizität der NOX1-abhängigen ROS auf Photorezeptorzellen

und damit übereinstimmend eine positive Auswirkung einer NOX1-Defizienz auf den Krankheitsverlauf im laserinduzierten Mausmodell der CNV.

Zusammenfassend zeigt diese Arbeit eine distinkte Rolle für TSPO in retinalen Phagozyten als regulatorisches Schlüsselprotein auf, dass die Funktionen der Mikrogliazellen sowohl durch NOX1-abhängige als auch -unabhängige Mechanismen reguliert und somit TSPO als Zielstruktur zur immunmodulatorischen und antioxidativen Therapie für AMD hervorhebt.

Summary

Aberrant immune responses including reactive phagocytes are implicated in the etiology of age-related macular degeneration (AMD), a major cause of blindness in the elderly. Microglia, the resident phagocytes of the retina, play an active role in driving disease onset and progression and thus represent a broad target for therapy. Pharmacological approaches of microglia-related immunomodulation aim at dampening the harmful microglia response while preserving their homeostatic functions. The translocator protein (18kDa) (TSPO) is described as a biomarker for reactive gliosis and specific TSPO ligands have been shown to potently modulate microglia-related inflammatory responses and improved disease outcome in various preclinical model systems including Alzheimer's, Parkinson's, multiple sclerosis and degenerative diseases of the retina. However, the underlying molecular mechanisms of TSPO-mediated immunomodulation and its biological functions in health and disease remain elusive.

In this study, we report that tamoxifen-induced conditional deletion of TSPO in resident microglia using Cx3cr1^{CreERT2}:TSPO$^{fl/fl}$ mice or targeting the protein with the synthetic ligand XBD173 prevents reactivity of retinal phagocytes in the laser-induced mouse model of neovascular AMD. Concomitantly, the subsequent neoangiogenesis and vascular leakage are also prevented by microglia-specific TSPO knockout or XBD173 treatment.
Using different NADPH oxidase (NOX)-deficient mice, we show for the first time that TSPO is a key regulator of NOX1-dependent neurotoxic ROS production in the retina. Here, TSPO regulates the Ca^{2+} influx from the extracellular milieu into the cytosol that is required for stimulation of NOX1 activity and expression in microglia. We also demonstrate that NOX1-derived ROS induce photoreceptor cell death in a paracrine manner and accordingly, NOX1 knockout mice show the same beneficial effects on CNV and wound healing as XBD173 treatment or microglia-specific TSPO knockout.

Taken together, we showed that TSPO acts as a regulatory node and regulates microglia functions through both NOX1-dependent and independent mechanisms, defining a distinct role for TSPO in retinal phagocyte reactivity and highlights the protein as a drug target for immunomodulatory and antioxidant therapies for AMD.

List of figures

List of tables

List of abbreviations

2-DG	2-Deoxy-D-glucose
AD	Alzheimer's disease
ALS	Amyotrophic lateral sclerosis
AMD	Age-related macular degeneration
ANG-1/2	Angiopoietin 1/2
ANT	Adenine nucleotide translocator
AP-1	Activator protein 1
APS	Ammonium persulfate
ARMS2	Age-related maculopathy susceptibility 2
ATP	Adenosintriphosphate
AUC	Area under the curve
BCA	Bicinchoninic acid
BM	Bruch's membrane
bp	Base pair
BRB	Blood retina barrier
BSA	Bovine serum albumin
C3aR	Complement receptor 3
CCCP	Carbonylcyanide-m-chlorophenylhydrazone
CCL2	C-C Motif Chemokine Ligand 2
CD36	Cluster of differentiation 36
CD68	Cluster of differentiation 68
cDNA	Complementary DNA
CFH	Complement factor H
CNS	Central nervous system
CNV	Choroidal neovascularization
CRAC	Cholesterol-recognition amino acid consensus
Cre	Causes recombination
CSFR1	Colony stimulating factor 1 receptor
Cx3cr1	C-X3-C Motif Chemokine Receptor 1
DAMP	Damage-associated molecular patterns
DBI	Diazepam binding inhibitor protein
DCF	5,6-carboxy-2',7'-dichlorodihydrofluorescein diacetate, di(acetoxymethyl ester)
DHA	Docosahexaenoic acid
DHE	Dihydroethydium
DMEM	Dulbecco's Modified Eagle's Medium
DMSO	Dimethyl sulfoxide
DNA	Desoxyribonucleic acid
Duox	Dual oxidase
E	Embryonic day
E. coli	*Escherischia coli*
EAE	Experimental autoimmune encephalomyelitis
ECL	Enhanced chemiluminescence
EDTA	Ethylenediaminetetraacetic acid
ELISA	Enzyme-linked immunosorbent assay
ETC	Electron transport chain

FCS	Fetal calf serum
FFA	Fundus fluorescein angiography
GA	Geographic atrophy
GABA	Gamma-aminobutyric acid
GCL	Ganglion cell layer
GEWAS	Genome-wide association study
h	Hour
H$_2$DCFDA	2',7'-dichlorohydrofluorescein diacetate
HBSS	Hank's balanced salt solution
HCl	Hydrochloric acid
HMW	Higher molecular weight
HRP	Horseradish peroxidase
HTRA1	High temperature requirement A serine peptidase 1
i.p.	Intraperitoneal
IBA1	Ionizing calcium-binding adaptor molecule 1
IFN-β	Interferon-β
IGF-1	Insulin-like growth factor 1
IgG	Immunoglobulin G
IL	Interleukin
IMM	Inner mitochondrial membrane
IMS	Intermembrane space
INL	Inner nuclear layer
iNOS	Inducible nitric oxide-synthase
IPL	Inner plexiform layer
IR	Infrared fundus picture
IRF8	Interferon regulatory factor 8
IS	Inner segments
IVC	Individual ventilated cages
kDa	Kilodalton
KO	Knockout
LMW	Lower molecular weight
loxP	Locus of X-over P1
LPS	Lipopolysaccharide
MAC	Membrane attack complex
MACS	Magnetic activated cell sorting
MAPK	Mitogen-activated protein kinase
MG	Microglia
min	Minute
MIP	Mean intensity projections
MNP	Mononuclear phagocyte
MPT	Mitochondrial permeability transition
MPTP	Mitochondrial permeability transition pore
mROS	Matrix-derived ROS
MS	Multiple sclerosis
n.d.	Not detected
n.t.	Non-treated
NaCl	Sodium chloride
NADPH	Nicotinamide adenine dinucleotide phosphate

NaOH   Sodium hydroxide
NDS   Normal donkey serum
NF-κB   Nuclear factor 'kappa light chain enhancer' of activated B-cells
NFL   Nerve fiber layer
nm   Nanometer
NMR   Nuclear magnetic resonance
NMS   Normal mouse serum
NOX   NADPH oxidase

o/n   Over night
ODN   Octadecaneuropeptide
OMM   Outer mitochondrial membrane
ONH   Optic nerve head
ONL   Outer nuclear layer
OPL   Outer plexiform layer
OS   Outer segments

PAGE   Polyacrylamide gel electrophoresis
PAMP   Pathogen-associated molecular patterns
PBR   Peripheral benzodiazepine receptor
PBS   Phosphate buffered saline
PCD   Programmed cell death
PCR   Polymerase chain reaction
PD   Parkinson's disease
PET   Positron emission tomography
pH   Potenia Hydrogenii, negative decadic logarithm of the H_3O^+ concentration
PKC   Protein kinase c
PMA   Phorbol 12-myristate 13-acetate
POS   Photoreceptor outer segments
PR   Photoreceptor
PRR   Pattern recognition receptor
PU.1   PU box binding 1

RGC   Retinal ganglion cell
RLU   Relative light unit
RNA   Ribonucleic acid
RNS   Reactive nitrogen species
ROI   Region of interest
ROS   Reactive oxygen species
RPE   Retinal pigment epithelium
RT   Room temperature

s   Seconds
SD-OCT   Spectral domain optical coherence tomography
SDS   Sodium dodecyl sulfate
SEM   Standard error of the mean
SRS   Subretinal space

TBE   Tris-borate-EDTA buffer
TBS   Tris-buffered saline
TEMED   Tetramethylethylendiamine
TLR   Toll-like receptor
TM   Transmembrane
TMRE   Tetramethylrhodamine ethylester
TNF   Tumor necrosis factor

TRIS	Tris(hydroxymethyl)aminomethane
TSPO	Translocator protein
TTN	Triakontatetraneuropeptide
U	Units
V	Volt
VDAC	Voltage-dependent anion channel
VEGF	Vascular endothelial growth factor
w/o	Without
WT	Wild type

1. Introduction

1.1 The structure and function of the mammalian retina

The eye is one of our most important sensory organs responsible for one of the five senses – sight– which enables us to adapt to our environment. Its function is to receive and focus incoming light and transduce it into nerve signals that are sent to the brain for processing. The visual system responds to a narrow spectrum of electromagnetic rays at wavelengths ranging from 400-750 nm also referred to as visible light (Eysel, 1998). Initially, light enters through the transparent cornea and passes through the aqueous humor and the pupil, which will then contract or dilate to control the amount of light passing through the lens and onward towards the retina. Both the cornea and lens are important for focusing the incoming light onto the central area of the retina, the macula. Within the macula lies the *fovea centralis* which represents the center of highest visual acuity (Chader and Taylor, 2013).
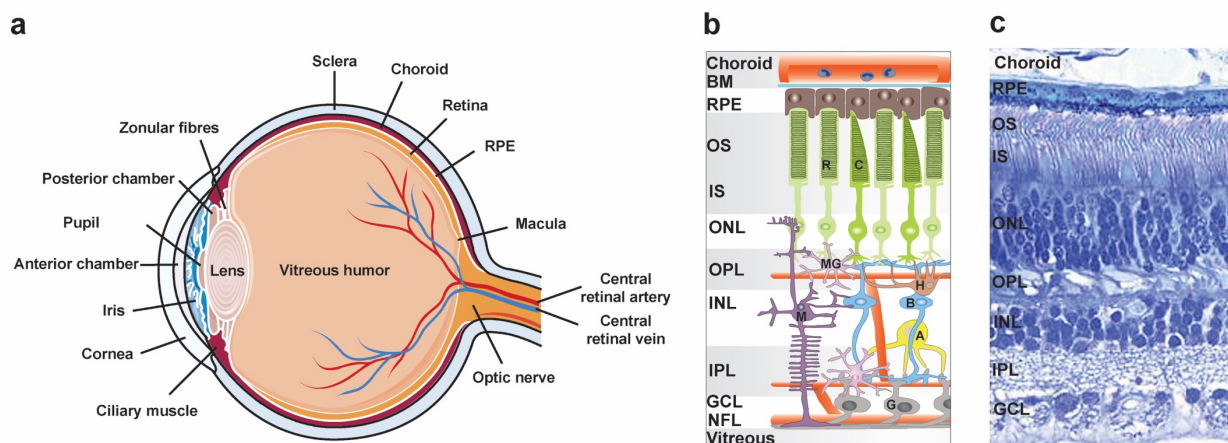
Figure 1: Anatomy of the eye and cross-section of the human retina. a Schematic anatomy of the eye. The retina lines the back of the eye and lies on top of the retinal pigment epithelium (RPE). **b** Schematic overview of the retinal cross-section and the organization of the retinal cells. The retina comprises three distinct cell body layers (nuclear layers) that are separated by synaptic layers (plexiform layers). OS, outer segment; IS, inner segment; ONL, outer nuclear layer; OPL, outer plexiform layer; INL, inner nuclear layer; IPL, inner plexiform layer; GCL, ganglion cell layer; NFL, nerve fiber layer. The outer retina contains the light-sensitive photoreceptor cells: rods (R) and cones (C), whereas the inner retina comprises the bipolar cells (B), Müller glial cells (M), amacrine cells (A), horizontal cells (H) and ganglion cells (G). Microglia (MG) are located in the plexiform layers. **c** A H&E-stained cross-section of the human retina. Adapted from Sung and Chuang, 2010.

The retina is one of the most important parts of the eye as it initiates basic visual processing before the brain receives the information. It converts the light received into chemical and electrical signals which are then transferred to the brain by the optic nerve. Together with the brain and spinal cord, the retina is a part of the central nervous system (CNS) as it derives from the embryonic

diencephalon (Varga et al., 1999). The retina lines the back of the eye adjacent on top of the retinal pigment epithelium (RPE) with a thickness ranging up to 300 µm (Figure 1a). The complexity of the retina is represented by its unique cellular structure bearing more than 55 different highly specialized cell types (Masland, 2001). It is divided into three cellular layers that are separated by synaptic layers. Because of the inverse structure of the retina, incoming light has to pass through all retinal layers in order to stimulate the light-sensitive photoreceptors (Figure 1b, c). In general, we can distinguish between two types of photoreceptors: rods and cones. Both types differ in their sensitivity to specific wavelengths of light, with rods being responsible for dim-light and night vision (scotopic vision) and cones for bright-light and color vision (photopic vision) (Baylor et al., 1979; Brown and Wald, 1964). The human retina contains approximately 130 million photoreceptors of which 95 % represent rods (Sung and Chuang, 2010). The rod population thus exceeds the cone population by 20-fold over the entire retina. Worthy of note is the fact that rods are predominantly found in peripheral areas of the retina but are strikingly absent in the *fovea centralis*, where cones are enriched. In this region the other layers of the retina are displaced concentrically. In contrast to the peripheral retina where one bipolar cell receives stimuli from up to 50-100 rods, the relationship of cones to bipolar cells to ganglion cells within the fovea is 1:1:1, thus representing the locus of highest visual acuity within the macula (Alters, 2000).

The photoreceptor nuclei constitute the tightly packed outer nuclear layer (ONL) and are connected to their outer segments (OS) by the connecting cilium (Horst et al., 1990). The photoreceptor OS are enriched with light-sensitive G-protein-coupled receptors, called opsins. Visual perception begins with the absorption of a photon by an opsin pigment, inducing the isomerization of its 11-*cis*-retinal chromophore to an all-*trans* configuration that triggers the phototransduction cascade including hyperpolarization of photoreceptor cell membranes (Radu et al., 2008). The signal is then forwarded to the inner retinal cells such as bipolar cells via synapses in the outer plexiform layer (OPL). The cell bodies of the inner retinal cells constitute the inner nuclear layer (INL). Signals from these cells are further relayed to the ganglion cells in the ganglion cell layer (GCL) via synapses in the inner plexiform layer (IPL). Two other types of neurons present in the retina are horizontal and amacrine cells. Their cell bodies reside in the INL and are primarily responsible for lateral interactions within the retina. The synaptic transmission of photoreceptors and bipolar cells is modulated by horizontal cells whereas amacrine cells regulate transmission to ganglion cells (Purves et al., 2001). The axons of the ganglion cells converge at the exit of the optic nerve from the eyeball, forming the nerve fiber layer (NFL) that projects into the brain. This exit region is devoid of photoreceptor cells resulting in the so-called blind spot of the retina. Although there is no retinal input in the "blind spot", it is filled with the same visual attributes as its surround

(Komatsu, 2006). In addition to the neuronal cell types, three different types of glia cells are found in the mammalian retina namely astroglia, microglia and Müller glia. Müller cells are the principal glia cells in the retina that serve as support structures. They span radially throughout the entire retina thus connecting the inner with the outer retinal surface. Their terminations form the inner and outer limiting membrane, while their cell bodies are located in the INL. Müller cells contribute to the regulation of the retinal microenvironment and have been described to function as optic fibers conducting light from the retinal surface to the photoreceptors (Franze et al., 2007). Astroglia cells are only found in vascular zones and play a role in constructing the blood-retina barrier (BRB) (Castellano et al., 2012). Microglia cells are the immune cells of the CNS, including the retina which serve as sensors and play important roles in the innate immune system (Karlstetter et al., 2015; Streit, 2002).

Since the retina has a high metabolic turn over, it has to be supplied with nutrients. Neurons within the inner retina are nourished by blood vessels originating from the central retinal artery that span through the INL and GCL, whereas photoreceptor cells depend on the choroidal vasculature for their supply of nutrients (Nau and Blaner, 2012). However, the choroidal vasculature and the photoreceptors are separated by the RPE that forms a component of the BRB. Thus, it controls the flow of nutrients from the choroidal vascular system to the retina. The RPE consists of a single layer of epithelial cells that are highly polarized and play an important role in vitamin A metabolism and maintenance of the retina (Raymond and Jackson, 1995). RPE cells continuously phagocytose the shed discs of photoreceptor outer segments, and recycle the visual pigment (Bok, 1985; Clark, 1986).

Despite the overall consistency of the basic organization of the retina across vertebrates, there are certain distinctions to be considered between humans and mice. In the murine retina, only 3 % of the photoreceptors are cones thus mice predominantly rely on rod-mediated scotopic vision (Dawson and Lavail, 1979). Moreover, while humans are physiologically trichromats, whose cones are separated into three types depending on the expression of different opsins that make the cells either sensitive to short- (S), middle- (M), or long- (L)-wavelength light (Nathans et al., 1986), mice are dichromats expressing only S and M-opsin variants (Jacobs et al., 1991). Lastly, unlike their human counterparts, the murine retina does not have a macula or fovea.

1.2   Age-related macular degeneration (AMD)

1.2.1   Epidemiology and pathophysiology of AMD

Age-related macular degeneration (AMD) is a heterogeneous, complex and progressive chronic disease of the central retina that leads to severe vision loss among the elderly in the industrialized countries (Figure 2). In general, AMD affects 10 % of people older than 65 years with the highest prevalence occurring after the age of 80 (la Cour et al., 2002; Swaroop et al., 2009). Globally, AMD ranks third among the causes of legally blindness, turning into a major medical and socioeconomic challenge since the number of patients is expected to reach 196 million worldwide by 2020 and increase to 288 million by 2040 (Pascolini and Mariotti, 2012; Wong et al., 2014).

Figure 2: Symptoms of AMD. Early signs of vision loss include slight central distorted vision (metamorphopsia) and this area grows larger as the disease progresses, resulting in blind spots and thus in difficulties in seeing colors and fine details until complete central vision loss. Images from https://www.pro-retina.de/simulation/makuladegeneration.

Clinically, early stages of AMD are characterized by pigmentary changes in the macula and the accumulation of insoluble extracellular material, called drusen, at the interface between RPE and Bruch's membrane (BM) (Figure 3) (Fritsche et al., 2014). Drusen deposits contain proteins, lipids, nonfibrillar amyloid oligomers, complement factors and other cellular components and vary in shape, size and distribution (Johnson et al., 2001; Mullins et al., 2000). Hard drusen appear as discrete whitish yellow spots and are commonly found in the population, whereas the presence of larger and less distinct soft drusen is age-related and associated with a higher risk for development of advanced AMD (Cohen et al., 2007; Klein et al., 1992). The appearance of drusen is a hallmark and the earliest visible clinical sign of AMD, which is often found with or proceeded by elastin and collagen degeneration within the BM and its thickening and calcification (Green et al., 1985). Although early AMD is usually asymptomatic, these changes can aggravate and may cause a gradual decline in visual acuity over years (Fritsche et al., 2014).

Late-stage or advanced AMD can manifest either as geographic atrophy (GA) (dry form) or as the wet form characterized by choroidal neovascularization (CNV) (Figure 3). GA is the most common

form, comprising about 90 % of all diagnosed cases and is defined by the presence of well-demarcated atrophic lesions due to loss of RPE cells, followed by degeneration of adjacent photoreceptors and choriocapillaris (Figure 3) (McLeod et al., 2009). Disease progression of GA is slow, and the visual deficits highly depend on the extent of foveal involvement (Danis et al., 2015). Wet AMD is the less common (10 %) but more severe form as vision loss can occur very rapidly. The hallmark of wet AMD is the ingrowth of new blood vessels, known as CNV, from the choriocapillaris through BM into the sub-RPE space. These new vessels, unlike normal ones, are very fragile and leaky, resulting in subretinal fluid, sub-RPE hemorrhage and scarring within the macula (Figure 3) (Colijn et al., 2017; McLeod et al., 2009). Although dry and wet AMD are clinically very different, both forms are not mutually exclusive and are likely to be bilateral (Joachim et al., 2017).
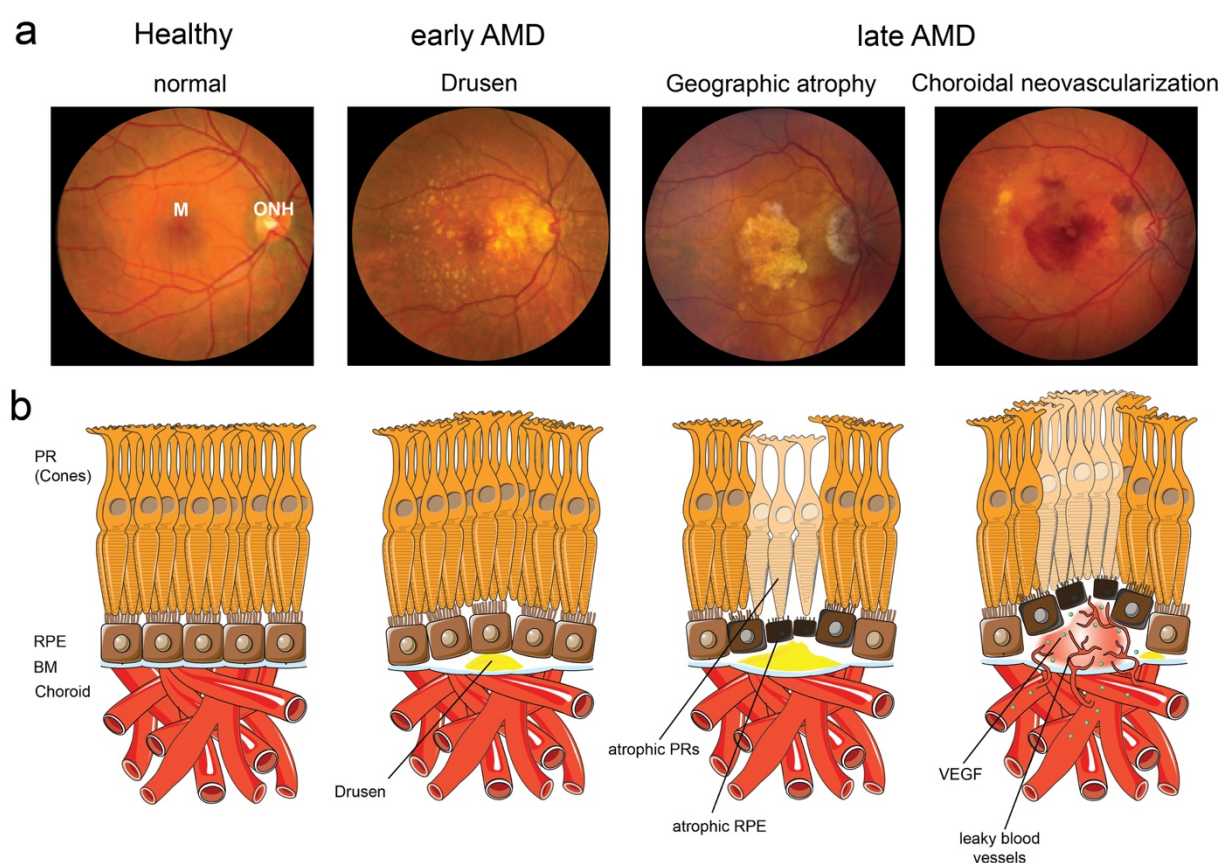
Figure 3: Clinical stages and signs of AMD. a Fundus photographs of the right eye from healthy patients and patients with early or late AMD. **b** Schematic illustrations of photoreceptor-RPE-choroid region depicting features of AMD. Early AMD shows yellow extracellular drusen deposits surrounding macular area (M) that cause a slight RPE detachment. The two forms of late AMD are not mutually exclusive and differ in their clinical appearance. Geographic atrophy is characterized by large drusen and confluent regions of RPE and photoreceptor degeneration centered on the macula. Neovascular (wet) AMD is featured by choroidal neovascularization, resulting in vascular leakage and macular edema. BM, Bruch's membrane; M, macula; ONH, optic nerve head; PR, photoreceptors; RPE, retinal pigment epithelium; VEGF, vascular endothelial growth factor. Fundus pictures adapted from (Swaroop et al., 2009) and schematic illustrations adapted from https://www.webrn-maculardegeneration.com/bruchs-membrane.html.

Angiogenic growth factors like vascular endothelial growth factor A (VEGF-A) promote the formation of abnormal leaky blood vessels (Witmer, 2003) and the treatment of wet AMD currently relies on intravitreal injections of anti-VEGF inhibitors (Ba et al., 2015). However, these anti-VEGF therapies have significant limitations such as the burden of frequent intravitreal injections and resistance to treatment (Yang et al., 2016). In contrast, dry AMD has no approved treatment so far and basically depends on documentation and surveillance of changes in the central visual field. Nevertheless, several promising therapeutic approaches for dry AMD are in progress such as the concept of targeting inflammasomes (Gao et al., 2015), complement factors (Geerlings et al., 2017; Rhoades et al., 2015), modulators of the visual cycle (Kubota et al., 2012) or stem-cell therapy (Schwartz et al., 2015).

1.2.2   Risk factors associated with AMD

The etiology of AMD is still not fully understood due to complex interactions of environmental and genetic factors that influence the susceptibility to risk (Chakravarthy et al., 2010). Age is one of the strongest predictors of AMD as the risk of acquiring the disease is threefold higher in patients older than 75 compared to patients at the age of 65 (Chakravarthy et al., 2010; Klein et al., 1992). The retina is among the most metabolically active tissues of the body, which requires excessive amounts of adenosine triphosphate (ATP) to support its functions (Hurley et al., 2015; Sung and Chuang, 2010; Winkler, 1981). Due to the high metabolism and oxygen consumption rates, the RPE is constantly exposed to insults and damage as it is responsible for the rapid clearance of metabolic by-products of the retinal metabolism and heterophagy of the photoreceptor outer segments (POS) (Winkler et al., 1999). Advanced age is accompanied with increased oxidative stress and a decline in function of photoreceptors and RPE cells resulting in increased vulnerability of the retina and RPE to injury (Beatty et al., 2000; Winkler et al., 1999).

Besides aging, smoking is one major modifiable risk factor of AMD that is known to increase oxidative damage and reduce the antioxidant defense (Espinosa-Heidmann et al., 2006; Khan et al., 2006). Other controllable risk factors, such as high fat diet and obesity, are associated with gut dysbiosis that has been shown to exacerbate CNV (Andriessen et al., 2016; Parekh et al., 2009). In addition to the impact of the individual lifestyle on the prevalence of AMD, gender and ethnicity play also an important role. Women are 1.3 times at greater risk for developing AMD with Caucasians having the greatest disease burden (Rudnicka et al., 2015; Wong et al., 2014).

Heritability has been shown to have a major role in determining AMD risk, as there is an increased susceptibility in individuals with a positive family history of AMD (Maller et al., 2006; Priya et al., 2012). There are a plethora of genome-wide association studies (GEWAS) elucidating the genetic architecture of AMD. To date, 52 common and rare genetic variants across 34 genetic loci have been linked to AMD (DeAngelis et al., 2017; Fritsche et al., 2016). Many of these culprit genes are involved in retinal homeostasis, inflammatory processes and code for various components of the alternative complement pathway (Francis et al., 2009). Two major loci, harboring coding and non-coding variants at chromosome 10q in the two nearby genes, high-temperature requirement A serine peptidase 1 (HTRAl) and age-related maculopathy susceptibility 2 (ARMS2) and at chromosome 1q in the complement factor H (CFH) gene, have demonstrated the strongest replicable associations with AMD (Fritsche et al., 2008; Klein et al., 2005; Rivera et al., 2005).

The complement system, as a part of the innate immune system, consists of a series of soluble proteins that interact in a highly regulated manner to eliminate foreign pathogens. Although the three complement pathways, classical, alternative and mannose-binding lectin pathway, differ in their initiation, all result in complement activation and the formation of the membrane attack complex (MAC). Despite these complement factors circulate through the body, the retina also expresses a variety of these factors and receptors that have also been found in drusen of AMD patients (Anderson et al., 2010; Crabb et al., 2002; Mullins et al., 2000). There is now ample evidence that AMD is connected to a dysregulation of the innate immune system, mainly involving the complement system and reactive mononuclear phagocytes (MNPs), including microglia (Fritsche et al., 2014; Gupta et al., 2003).

1.3   Microglia – immune regulators of the retina

1.3.1   Origin and maintenance of microglia

Microglia represent the primary resident immune cell population of the CNS, including the retina, where they constitute 5-12 % of all CNS cells. Beside their traditional role as representatives of the innate immune system, microglia play pivotal roles during development and proper functioning of the CNS (Kettenmann et al., 2011; Streit, 2002). Initially described by Pío del Río Hortega in 1919 as distinct cells with small cell bodies and long cellular processes within the brain parenchyma, this cell type was termed microglia based on their morphology. He was the first to provide evidence of their mesodermal origin, their surveillance function and phagocytic capacity as mobile cells during pathology (Sierra et al., 2016). The origin of microglia in the CNS has been discussed for

many years but recent studies based on fate mapping confirmed that they derive from primitive hematopoietic progenitors from the yolk sac (Figure 4a) (Kierdorf et al., 2013; Perdiguero et al., 2015). These progenitors colonize the CNS from embryonic day (E) 8.5-9 before the blood-brain barrier (BBB) is established at E13.5 (Tay et al., 2017) and represent a self-maintaining and long-lived cell population that persists for months or even the entire life span of the organism (Figure 4b) (Ajami et al., 2007; Lawson et al., 1992). Microglia development highly depends on colony-stimulating factor 1 receptor (CSF1R) signaling but PU box binding 1 (PU.1)- and interferon regulatory factor 8 (IRF8)-dependent pathways are also essential, as either blockage of CSF1R (Elmore et al., 2014) or deficiency in the factors PU.1 (Mezey et al., 2000) and IRF8 (Kierdorf et al., 2013) resulted in microglia depletion in the CNS (Figure 4b).
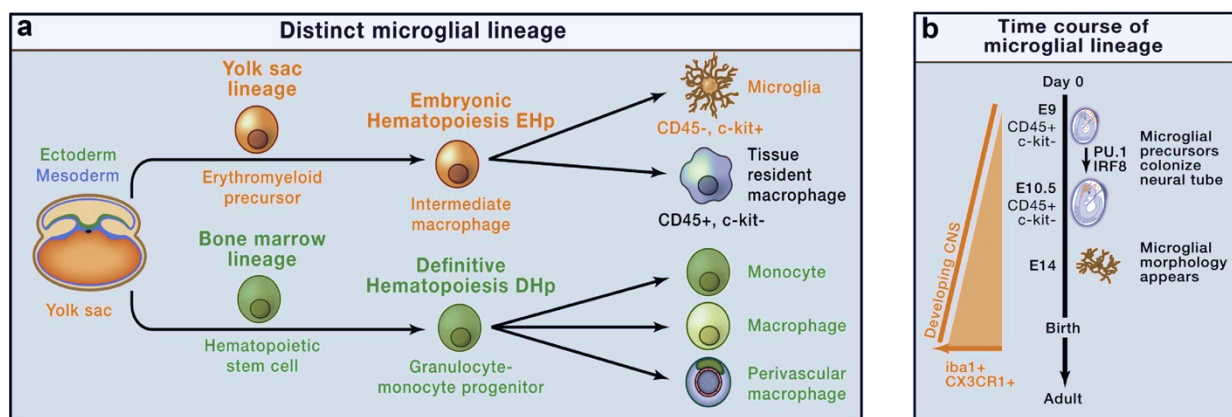
Figure 4: The origin and cell lineage of microglia. a Microglia originate from primitive erythromyeloid progenitors in the yolk sac (embryonic hematopoiesis, indicated in orange) distinct from the definitive hematopoiesis (indicated in green) from which the majority of macrophages are derived. **b** Microglia originate from PU.1-dependent precursors in the yolk sac that proliferate and invade the neuroectoderm-derived developing CNS, as indicated by an increase in the markers CX3CR1 and Iba1. Adapted from Salter and Beggs, 2014.

The idea of microglia having self-renewal ability was challenged by a study showing that latent Nestin[+] non-microglial precursors in the brain can differentiate into microglia and repopulate the brain after pharmacological ablation of microglia (Elmore et al., 2014). However, this concept was recently shattered by a study from Huang et al., demonstrating that all repopulated microglia were solely derived from few surviving microglia after acute depletion (Huang et al., 2018b). Interestingly, the same group could show that retinal microglia are also not derived from Nestin[+] non-microglial precursors but rather have a dual extra-retinal origin (Huang et al., 2018a). The majority (85 %) of new microglia derive from residual microglia in the optic nerve, which repopulate the retina along the center-to-periphery axis, whereas the periphery-emerging less ramified microglia derive from macrophages in the ciliary body/iris (Huang et al., 2018a).

1.3.2 Microglia in the retina: Roles in development and homeostasis

Microglia fulfill significant functions in the retina across different stages of life (Figure 5). During development, microglia are present in the mouse retina around E11.5 and are thought to invade by either crossing the vitreal surface or by migrating from peripheral non-neural ciliary regions (Santos et al., 2008). Microglia entry into the retina coincides spatiotemporally with events of programmed cell death (PCD), which eliminates the superfluous number of neurons that are generated during development, such as retinal ganglion cells (RGC) (Bodeutsch and Thanos, 2000; Marín-Teva et al., 2004). As phagocytic cells, microglia migrate to different regions in the retina and engulf dead neurons, enabling a clean removal without inducing inflammation and tissue necrosis (Ravichandran, 2003). Besides their clearance function, microglia can actively promote PCD of developing neurons (Frade and Barde, 1998; Marín-Teva et al., 2004), as the depletion of microglia with clodronate liposomes decreased developmental apoptosis (Marín-Teva et al., 2004). Not only do microglia play a role in shaping neuronal development and populations in the retina but also in sculpting neuronal circuits by a process called "synaptic pruning" (Katz and Shatz, 1996; Schafer et al., 2012). In the retina, microglia eliminate excessive synaptic connections from the RGCs into the dorsal lateral geniculate nucleus of the thalamus, in an activity- and complement-dependent manner (Schafer et al., 2012). Notably, the complement factors C1q and C3 differentially tag RGC synapses based on their activity, promoting their recognition by microglia via complement receptor C3aR and subsequent elimination by phagocytosis (Schafer et al., 2012). During development of the retinal vasculature, microglia have been found in close proximity with endothelial tip-cells at the vascular front and are thought to play supportive and guidance roles during vasculogenesis (Checchin et al., 2006; Fantin et al., 2010). These roles have been corroborated by studies showing that microglia depletion reduces intraretinal vessel growth and density, while microglia replenishment by intravitreal injection restored the vessel pattern (Checchin et al., 2006; Kubota et al., 2009; Ritter et al., 2006). Interestingly, a two-way communication between microglia and endothelial cells via secreted soluble factors have been identified to shape vascular growth and branching (Rymo et al., 2011) by either promoting (Chen et al., 2017) or limiting vessel sprouting (Stefater et al., 2011).

Taken together, microglia colonization and the absolute number are spatiotemporally coordinated with key events of retinal development. Consistent with this idea, localization and morphology of developmental microglia is dissimilar to those found in the mature retina. At birth, amoeboid microglia are predominantly found at the basal side of the retina but become progressively ramified as the retina matures (Li et al., 2019).
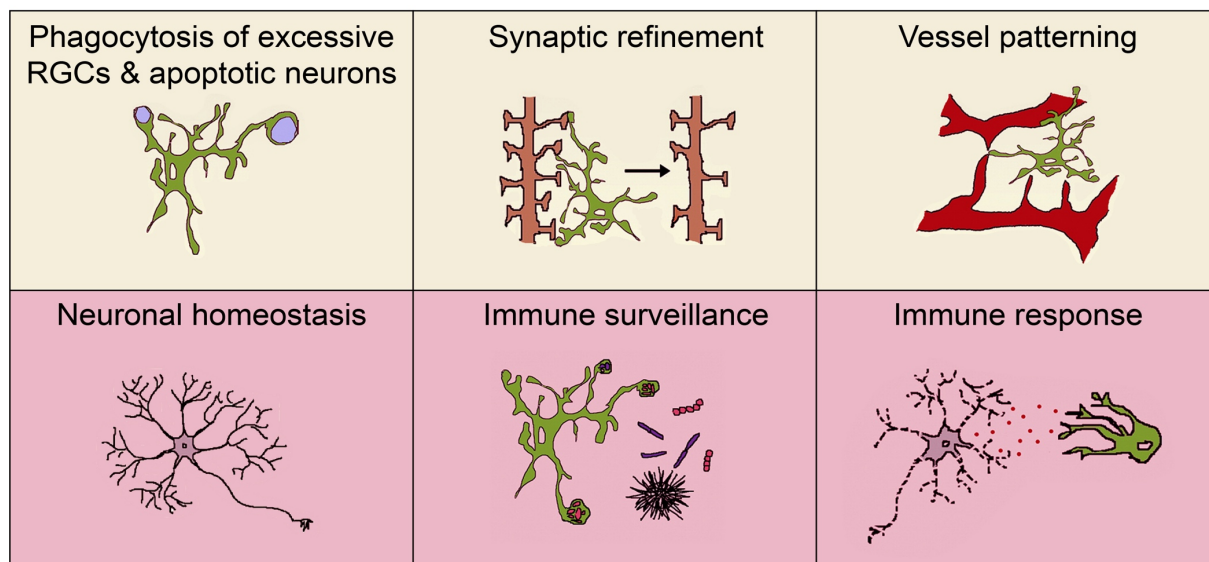
Figure 5: Diverse roles of microglia in the retina. Yellow and red boxes show schematic representation of microglia roles in the retina during developmental stages and general homeostatic and immune-related functions, respectively. RGC, retinal ganglion cells. Modified from Casano and Peri, 2015.

In the adult retina, microglia form a network of non-overlapping cells that are distributed throughout the plexiform layers (Figure 6a). Under homeostatic conditions, microglia have a ramified morphology with small somata and highly dynamic and long motile cellular protrusions that are continuously surveying the integrity of the surrounding environment (Figure 6b) (Hume et al., 1983; Karlstetter et al., 2015; Langmann, 2007; Nimmerjahn et al., 2005). Beyond acting as immune sentinels, microglia are necessary for maintaining neuronal activity, synaptic function and plasticity in the mature retina, as prolonged microglia depletion results in synaptic degeneration that leads to deficits in visual perception (Figure 5) (Wang et al., 2016).

In the healthy retina, a continuous bi-directional crosstalk between microglia and neurons is required to limit microglia activation and to maintain retinal homeostasis (Marinelli et al., 2019; Szepesi et al., 2018). Therefore, microglia express a large variety of different receptors, whose activation modulates microglia sensing and housekeeping functions. The CD200/CD200R axis, together with CX3CL1/CX3CR1, are among the most studied signaling pathways in the context of microglia regulation (Broderick et al., 2002; Cardona et al., 2006; Liang et al., 2009; Manich et al., 2019). Retinal neurons express the transmembrane glycoprotein CD200 and the chemokine CX3CL1 (fractalkine) and binding to their corresponding receptors CD200R and CX3CR1, expressed on microglia, regulates immune vigilance by controlling key microglial functions such as cytokine production, motility and phagocytosis (Cardona et al., 2006; Carter and Dick, 2009; Hernangómez et al., 2012; Hoek et al., 2000; Liang et al., 2009). During pathological conditions, these complex cell interactions fail and cause an activated microglia immune response that drives retinal degeneration.
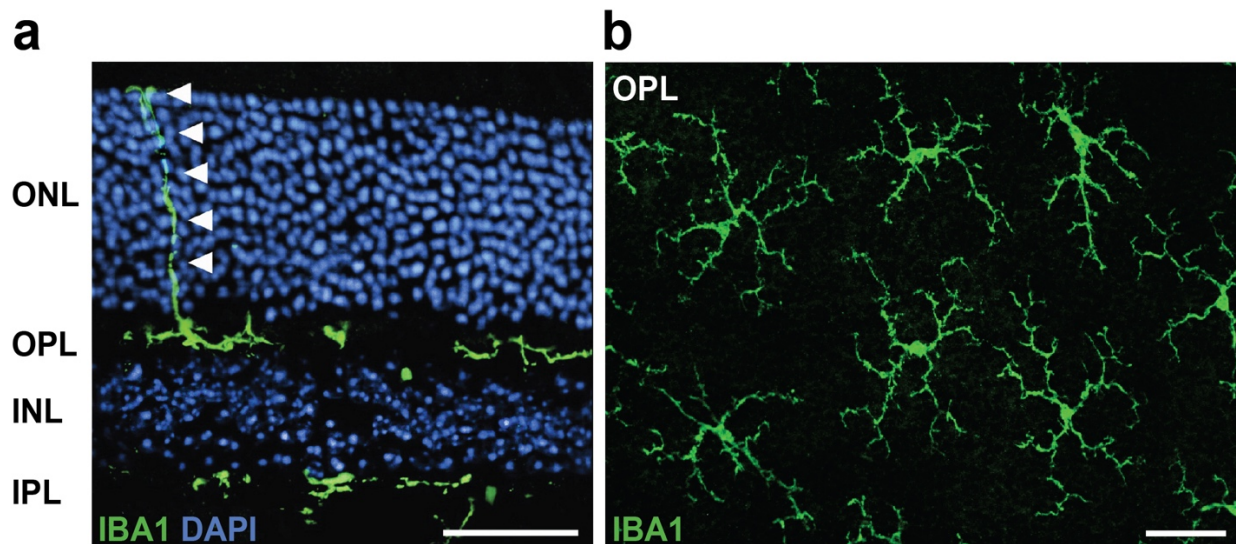
Figure 6: Localization and morphology of microglia in the mature retina. a Immunohistochemical analysis of Iba1^{+} microglia in retinal cross sections shows the distribution of ramified cells throughout the plexiform layers (OPL, IPL) of the healthy retina. Using their long cellular protrusions (white arrowheads), microglia constantly screen their microenvironment and crosstalk with other retinal neurons. Nuclei were counterstained with DAPI. Scale bar: 50 µm. **b** Iba1-stained retinal flat mount shows a highly ordered network of microglia in the OPL of the retina. This view allows the detailed characterization of the microglia phenotype including analysis of cell density, ramification and relative position. Scale bar: 50 µm. ONL, outer nuclear layer; OPL, outer plexiform layer; INL, inner nuclear layer; IPL, inner plexiform layer. Modified from Karlstetter et al., 2015.

1.3.3 Microglia in the diseased retina: Key players in neuroinflammation

A tightly controlled immune system has evolved in the retina to protect it from external and internal noxious insults. Apart from the immune privileged status, mediated by an intact BRB and an immunosuppressive microenvironment, the retina is protected by its own specialized innate immune defense composed of the complement system and microglia (Chen et al., 2019). In order to mediate the host defense, microglia express dedicated pattern recognition receptors (PRRs), such as Toll-like receptors (TLRs), that sense and recognize pathogen-associated molecular patterns (PAMPs) and damage-associated molecular patterns (DAMPs) (Hickman et al., 2013). In addition to PRRs, microglia express various purinergic receptors that are activated by nucleotides secreted by damaged neurons (Burnstock et al., 2011; Calovi et al., 2019; Davalos et al., 2005). Once microglia detect danger signals, they convert from a ramified homeostatic cell into an activated amoeboid-shaped phagocyte and migrate towards the site of damage, e.g. to the degenerating ONL and subretinal space (Figure 7) (Karlstetter et al., 2015; Karperien et al., 2013). Simultaneously, microglia not only enhance their phagocytic capacity to eliminate cellular debris and dead neurons, but also release a variety of pro-inflammatory cytokines and chemokines (Jurgens and Johnson, 2012; Karlstetter et al., 2015; Wynn and Vannella, 2016). Among them, the chemokine (C-C motif)

ligand 2 (CCL2), plays a crucial role during microglia activation and inflammation, as it attracts other mononuclear phagocytes to the lesion site, that are activated in a paracrine manner by released cytokines like interleukin-6 (IL-6) and IL-1β (Ferreira et al., 2012; Hinojosa et al., 2011; Krady et al., 2008). In addition, microglial reactive oxygen species (ROS) production is considered a major contributor to neuronal damage and death (Block and Hong, 2007; Gao et al., 2012; Haslund-Vinding et al., 2017). Under physiological conditions, ROS are generated in a regulated manner by nicotinamide adenine dinucleotide phosphate (NADPH) oxidases (NOX) or by mitochondria as by-products during oxidative phosphorylation. This regulated ROS generation contributes to tissue homeostasis as it plays important roles in host defense, oxygen sensing and signal transduction (Geiszt and Leto, 2004; Holmstroem and Finkel, 2014; Lambeth, 2004; Nayernia et al., 2014). However, when exaggerated ROS production overwhelms the cellular antioxidant defense capacity, oxidative stress occurs that results in cellular toxicity (Halliwell, 2006; Haslund-Vinding et al., 2017).

Microglia, in collaboration with Müller cells mediate and shape the magnitude of retinal immune response through reciprocal interactions. Here, microglia-derived neurotrophic factors directly trigger or inhibit the release of secondary trophic factors from Müller cells either to support photoreceptor survival or mediate apoptosis (Harada et al., 2003; 2000; Shen et al., 2013; Wang and Wong, 2014; Wenzel et al., 2005). Conversely, activated Müller cells secrete the diazepam binding inhibitor (DBI) protein, a ligand for the translocator protein (18 kDa) (TSPO), expressed in activated microglia, to limit microglia reactivity (Wang et al., 2014b).

While a short period of controlled microglia activation is considered to be neuroprotective (Shastri et al., 2013) excessive or chronic activation lead to degeneration of healthy neuronal tissue and irreversible cell damage (Karlstetter et al., 2010).
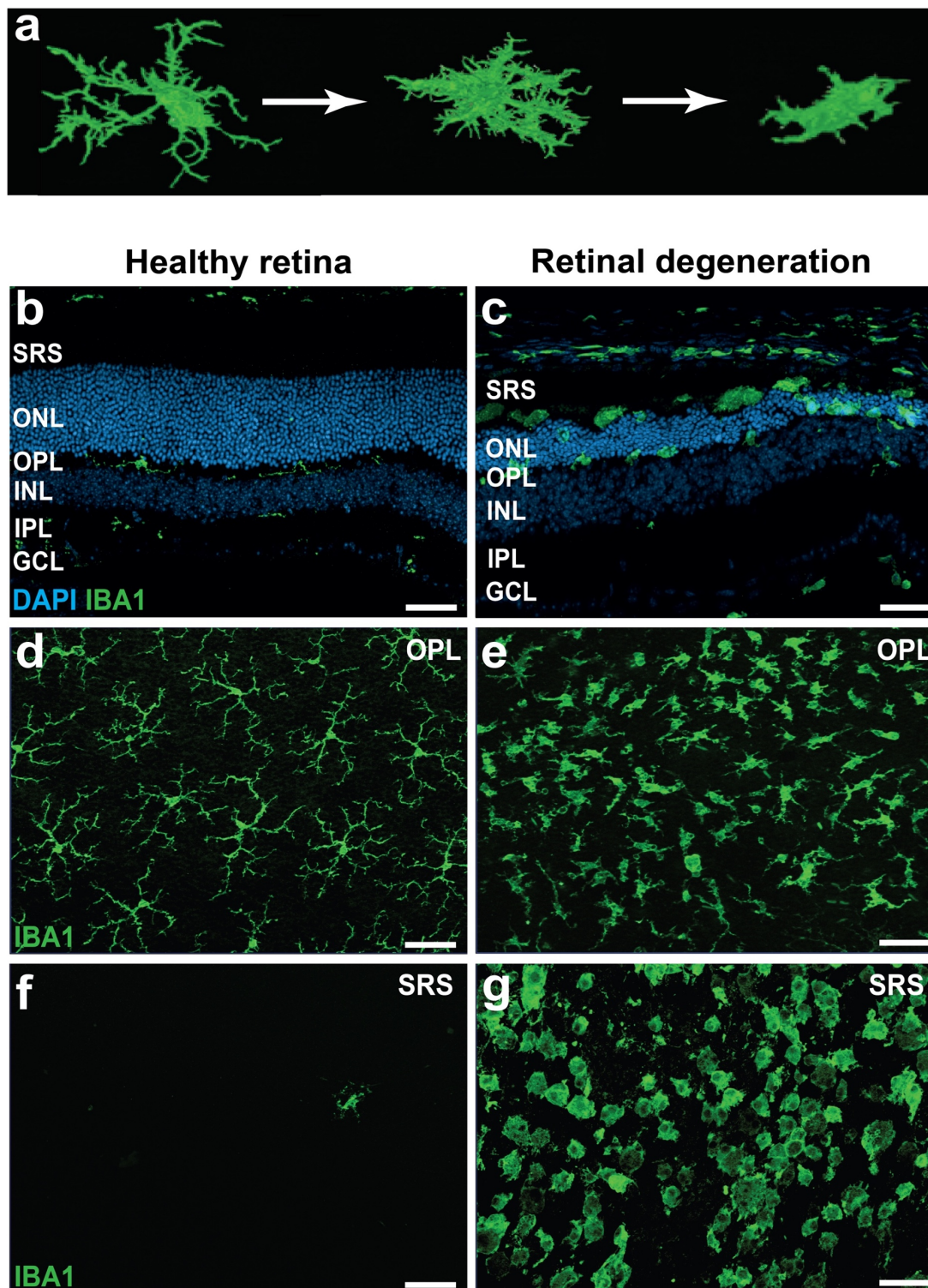
Figure 7: Microglia reactivity in a moue model of retinal degeneration. **a** Schematic 3D skeleton analysis of microglia in Iba1-stained brain sections show the progressive morphological changes in microglia after activation. **b-g** Immunohistochemical analysis of Iba1^{+} microglia in retinal cross-sections **(b, c)** and flat-mounts **(d-g)** in retinas from healthy and degenerated retina. In the healthy retina, microglia are located in the IPL, OPL and GCL, where they form a network of evenly distributed non-overlapping cells and exhibit a surveillant ramified phenotype. In retinal degeneration microglia transform into an amoeboid-shaped full blown phagocyte, that is either completely devoid of processes or has very few unbranched processes, and start to migrate towards the degenerating ONL and the subretinal space where they are not only involved in the phagocytic clearance of cellular corpses and debris, but also actively contribute to the degenerative processes. Scale bar: 50 μm. ONL, outer nuclear layer; OPL, outer plexiform layer; INL, inner nuclear layer; IPL, inner plexiform layer; GCL, ganglion cell layer; SRS, subretinal space. Panel a modified from Martyanova et al., 2015.

1.3.3.1 Microglia reactivity in AMD

Retinal microglia and recruited macrophages play an important role in the maintenance of tissue homeostasis and the clearance of debris from the subretinal space. However, age is one of the main factors that induce changes in the immune system leading to increased tissue stress and damage (Nikolich-Žugich, 2018). Indeed, aged microglia are primed and show an exaggerated response to homeostatic disturbances compared to naïve microglia, favoring age-related para-inflammation (Buchanan et al., 2008; Perry and Holmes, 2014; Sierra et al., 2007; Xu et al., 2009). While the etiology of AMD is still not well understood, GEWAS and experimental animal models have unequivocally shown dysregulated innate immune responses in AMD. Retinal transcriptome analysis from AMD and healthy human donor eyes revealed the involvement of inflammatory genes along with increased levels of chemokines and complement factors in all AMD phenotypes (Newman et al., 2012). In line with this, bloated phagocytic microglia have been shown to accumulate in the subretinal space and are closely associated with drusen and CNV in AMD patients (Figure 8) (Combadière et al., 2007; Gupta et al., 2003). It is suggested that the widespread accumulation of drusen represents a potent pro-inflammatory stimulus and attracts macrophages and microglia (Buschini et al., 2011; Doyle et al., 2012; Killingsworth et al., 1990). Apart from microglia accumulation within the subretinal space, retinas from AMD patients with GA also show microglia reactivity in the ONL, where they phagocytose apoptotic photoreceptors (Gupta et al., 2003). However, activated microglia and other mononuclear phagocytes can also execute photoreceptor death by phagocytosing stressed but living photoreceptors in their vicinity (Zhao et al., 2015). This indicates that microglia reactivity is a driving force in photoreceptor demise and disease progression and cannot be simply regarded as bystander.
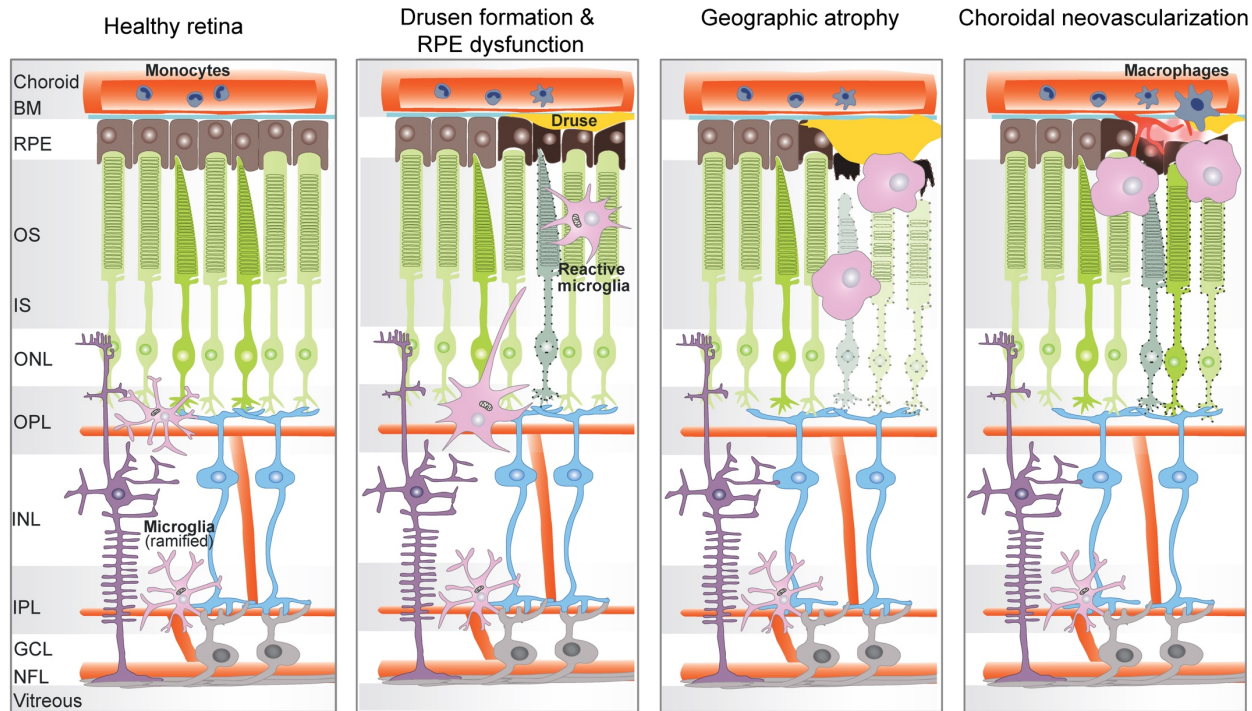
Figure 8: Schematic representation of microglial activity in AMD. In the healthy retina, microglia reside in the plexiform layers where they continuously scan their environment and phagocytose cell debris. Early signs of AMD including drusen formation or RPE dysfunction rapidly alert microglia, which transform into amoeboid phagocytes and migrate to the subretinal space in an attempt to restore homeostasis. In both types of late AMD, geographic atrophy and choroidal neovascularization, chronically activated microglia contribute to tissue damage and exacerbate disease progression. BM, Bruch's membrane; RPE, retinal pigment epithelium; OS, outer segments; IS, inner segments; ONL, outer nuclear layer; OPL, outer plexiform layer; INL, inner nuclear layer; IPL, inner plexiform layer; GCL, ganglion cell layer; NFL, nerve fiber layer. Figure modified from Karlstetter et al., 2015.

1.3.4 Microglia as targets for therapy

Microglia reactivity is not a phenomenon unique to AMD, it is a common hallmark in many neurodegenerative diseases and broadly independent of the underlying genetic defect or cause (Amor et al., 2014; Karlstetter et al., 2015; Langmann, 2007). Thus, microglia-directed immunotherapy could represent an early and feasible strategy to attenuate progression of a variety of retinal degenerative diseases.

Microglia depletion via pharmacological CSF1R inhibition has been found to reduce neuroinflammation in distinct diseases (Kokona et al., 2018; Li et al., 2017a; Rice et al., 2015). However, ablation of microglia does not always result in tissue homeostasis, as shown in the context of Parkinson's disease (PD), brain ischemia and encephalitis (Jin et al., 2017; Rubino et al., 2018; Szalay et al., 2016; Wheeler et al., 2018; Yang et al., 2018). Due to the variation of beneficial or detrimental effects of microglia depletion, a microglia-replacement strategy would be more suitable (Rice et al., 2017). The self-renewal ability of microglia after depletion enables them to repopulate the CNS niche within a short time with the new cells still able to surveille the

15

environment and to respond to injuries (Varvel et al., 2012; Zhang et al., 2018). Nevertheless, the potential side-effects of microglia depletion have to be considered, as the ablation may induce a transient immunodeficiency and elicit secondary effects that could be harmful to the CNS (Parkhurst et al., 2013). In the mature retina, prolonged microglia cessation results in synaptic and photoreceptor degeneration that leads to deficits in visual perception (Wang et al., 2016). Therefore, therapy concepts of microglia-related immunomodulation should dampen the harmful microglia response while preserving their homeostatic functions. Such treatment strategies involve the targeting of microglia surface receptors or the modulation of intracellular molecules, as their activation induces signaling pathways that play essential roles in controlling microglia functions (Akhtar-Schäfer et al., 2018; Karlstetter et al., 2015).

For instance, ATP-mediated purinergic signaling evokes an excess inflammatory response by releasing cytokines via the protein kinase c (PKC)/mitogen-activated protein kinase (MAPK) pathway, while its inhibition with the selective P2X7 receptor antagonist A438079 delayed the death of retinal neurons and ganglion cells after optic nerve injury (He et al., 2017; Nadal-Nicolás et al., 2016). In addition, blocking TLR2 and TLR4 signaling with the semi-synthetic tetracycline derivative minocycline via inhibition of IkBα degradation, prevents microgliosis and preserves photoreceptor function in the light-damaged retina (Nikodemova et al., 2006; Scholz et al., 2015b; Zhang et al., 2004). Apart from that, interferon-β (IFN-β), polysialic acid and natural compounds like curcumin and docosahexaenoic acid (DHA) show also immunomodulatory effects on microglia (Ebert et al., 2009; Karlstetter et al., 2017; 2011; Lückoff et al., 2016).

Thus, markers for microglia activation may serve as a tool for evaluating and monitoring the efficacy of these therapeutic interventions during the course of disease. Among them, TSPO is a key biomarker for measuring neuroinflammation via positron emission tomography (PET), as it is highly and specifically expressed in activated microglia (Karlstetter et al., 2014; Vivash and O'Brien, 2016). The fact that Müller cell-microglia interactions via TSPO-mediated signaling negatively regulates features of microglial activation, makes TSPO also an attractive target for therapy (Karlstetter et al., 2014; Wang et al., 2014b). Indeed, several TSPO ligands are under investigation as treatment options for neurological disorders (Rupprecht et al., 2010).

16

1.4 Translocator protein (18 kDa) (TSPO)

1.4.1 Structure and expression of TSPO

The translocator protein (18 kDa) (TSPO), formerly known as the peripheral benzodiazepine receptor (PBR), was first identified in 1977 as a high affinity benzodiazepine binding site in peripheral tissues that was distinct from the central benzodiazepine receptor as it was not coupled to gamma-aminobutyric acid (GABA) receptors (Braestrup et al., 1977; Gavish et al., 1999). The *Tspo* gene is composed of four exons, while exon 1 and half of exon 4 remain untranslated (Casalotti et al., 1992; Lin et al., 1993). It encodes a five α-helical transmembrane protein composed of 169 amino acids that is primarily located in the outer mitochondrial membrane (OMM) (Figure 9a-b) (Anholt et al., 1986). From the cytosolic view, these five transmembrane helices (TM1-5) are tightly packed together in a clockwise order TM1-TM2-TM5-TM4-TM3, with the longest loop located in between TM1 and TM2 (Jaremko et al., 2015). The C-terminal part in TM5 resides in the cytoplasm and harbors a cholesterol-recognition amino acid consensus (CRAC) motif (residues 147–159) that binds cholesterol in nanomolar concentration (Figure 9b) (Jamin et al.; Li et al.). TSPO is a highly conserved protein found in many Archae, Bacteria and Eukarya (Balsemão-Pires et al., 2011; Fan et al., 2012). Both human and mouse TSPO share an 81.1 % sequence homology (Figure 9a) (Selvaraj and Stocco, 2015). Together with the fact that mammalian TSPO can compensate for the loss of function of the TSPO homolog in the proteobacterium *Rhodobacter sphaeroides*, suggests that its functions are, at least in part, evolutionarily conserved (Yeliseev et al., 1997).

Although TSPO is expressed in every mammalian tissue including heart; lung; spleen; kidney; liver; skin; bone marrow; adipose tissue; brain and retina, highest expression levels are found in steroidogenic tissues such as adrenal glands, gonads, placenta and testis (Anholt et al., 1985; De Souza et al., 1985; Gehlert et al., 1985; Wang et al., 2012). In the healthy CNS, TSPO expression is extremely weak but increases predominantly in activated microglia and astrocytes during neuropathological conditions (Daugherty et al., 2013; Maeda et al., 2007; Rupprecht et al., 2010). In the retina, apart from the damage-induced TSPO expression specifically in microglia, the RPE shows a constitutive expression of TSPO (Figure 9c) (Karlstetter et al., 2014; Scholz et al., 2015a).
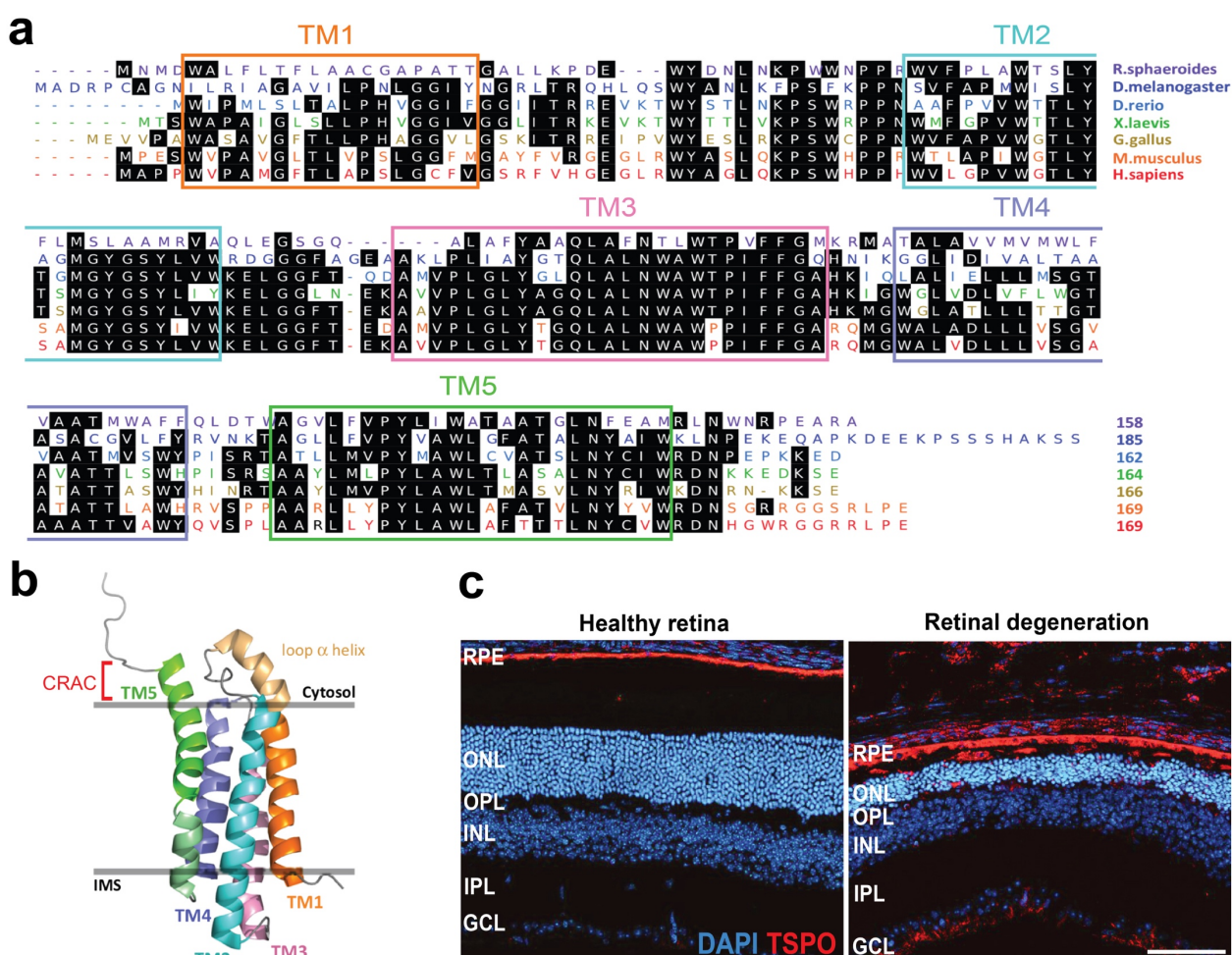
Figure 9: TSPO structure and retinal expression. a TSPO protein sequence homology. TSPO sequence comparisons showing relatively conserved consensus sequences (black shaded) in various model organisms. Percentage identity with *Homo sapiens*: *Rhodobacter sphaeroides*, 33.5 %; *Drosophila melanogaster*, 42.6 %; *Danio rerio*, 54.3 %; *Xenopus laevis*, 57.3 %; *Gallus gallus*, 60.4 % and *Mus musculus*, 81.1 %. **b** Structure of TSPO in the OMM membrane (side view) showing the five α-helix transmembrane structure (TM1–5). The location of the cholesterol-recognition amino acid consensus (CRAC) motif at the C-terminus in TM5 (residues 147–159) point outside the TSPO structure. IMS, intermembrane space. **c** Immunohistochemical analysis of retinal cross sections stained with TSPO. In the healthy retina, TSPO is constitutively expressed in the RPE but not in microglia. Upon retinal degeneration, TSPO is upregulated in activated microglia present in the subretinal space. Nuclei were counterstained with DAPI. Scale bar: 100 μm. ONL, outer nuclear layer; OPL, outer plexiform layer; INL, inner nuclear layer; IPL, inner plexiform layer; RPE, retinal pigment epithelium. Subpanel a and b adopted from Selvaraj and Stocco, 2015.

1.4.2 TSPO and its elusive functions

The robust TSPO expression in steroidogenic tissues and the discovery as a high-affinity cholesterol binding protein suggested a link between TSPO and steroidogenesis (Midzak et al., 2015; Mukhin et al., 1989; Papadopoulos et al., 1997a). Thereby, TSPO has been described as indispensable for cholesterol transport across the mitochondrial membrane, which is the rate-limiting step of steroid formation. First evidence came from studies which showed that TSPO ligands stimulate steroid synthesis in steroidogenic cells *in vitro*, while this process was impaired

in TSPO-deficient cells (Mukhin et al., 1989; Papadopoulos et al., 1997a). The fact that TSPO full-body knockout (KO) mice were embryonic lethal, reinforced the role of TSPO in steroidogenesis and pointed towards a broader role in basic functions that are critical for embryonic development (Papadopoulos et al., 1997b). However, recent findings from independent research groups using steroidogenic-tissue-specific or global TSPO-KO mice have challenged the previous literature and refuted the involvement of TSPO in steroidogenesis (Banati et al., 2014; Morohaku et al., 2014; Tu et al., 2014). These studies revealed that global TSPO-KO mice are viable and showed no phenotypic abnormalities nor changes in steroid production (Banati et al., 2014; Tu et al., 2014). In addition, conditional TSPO-KO in testicular Leydig cells also showed that TSPO is not required for steroidogenesis (Morohaku et al., 2014). Indeed, it was shown that the pharmacological effect of the TSPO ligand PK11195 on steroid production in TSPO-deficient Leydig cells is not mediated through TSPO but rather represent off-target effects (Tu et al., 2015). Of note, the human adrenocortical cell line H295R, which has no endogenous TSPO expression, is still capable of producing steroids (Tu et al., 2014). Moreover, a recent high-resolution nuclear magnetic resonance (NMR) structure of TSPO refuted the previously assumed channel-like core formation of TSPO for cholesterol binding (Rupprecht et al., 2010), as the side chains of the CRAC motif are located on the outside pointing towards the membrane (Jaremko et al., 2014). Altogether, this led to a reappraisal of the essential role of TSPO in steroidogenesis and its importance throughout the body (Selvaraj and Stocco, 2015).

TSPO has also been considered as a component of the mitochondrial permeability transition pore (MPTP), as it was co-purified with voltage-dependent anion channel (VDAC) and adenine nucleotide translocator (ANT), two core components of the MPTP (McEnery et al., 1992). This conclusion was strengthened by the findings that the TSPO ligands PK11195 and Ro5-4864 were able to induce mitochondrial permeability transition (MPT) *in vitro* (Chelli et al., 2001; Kinnally et al., 1993). However, a recent study using TSPO-deficient mitochondria revealed that TSPO is neither involved in the regulation of MPT nor do TSPO ligands regulate MPTP activity through TSPO (Sileikyte et al., 2014). Additional genetic analysis of the putative MPTP components also excluded a role for VDAC (Baines et al., 2007) and ANT (Kokoszka et al., 2004) while recent findings indicate that the MPTP is formed by dimers of F_0F_1 ATP synthase (Giorgio et al., 2013). Interestingly, TSPO ligands have been shown to interact with the F_0F_1 ATP synthase suggesting that the observed effects on MPT are indeed TSPO independent (Cleary et al., 2007; Johnson et al., 2006). Other functions where TSPO has been implicated include regulation of mitochondrial metabolism (Gatliff et al., 2017; Liu et al., 2017); tetrapyrrole biosynthesis (Batoko et al., 2015), ROS production (Gatliff et al., 2014) and more general cellular processes such as proliferation,

survival, and apoptosis (Caballero et al., 2013; Rechichi et al., 2008; Veenman and Gavish, 2012). However, some of these effects were evidenced by means of TSPO ligands, which were proven to have off-targets effects, thus further experiments are needed to conclude that these effects reflect a direct involvement of TSPO.

Despite the lack of a precise molecular function, TSPO has emerged as an important biomarker, as it is specifically upregulated in activated microglia in a variety of neurodegenerative diseases including multiple sclerosis (MS) (Daugherty et al., 2013), Alzheimer's disease (AD) (Edison et al., 2008), PD (Ouchi et al., 2005) and Huntington's disease (Meßmer and Reynolds, 1998). Thus, numerous TSPO PET ligands have been developed and used to monitor the dynamics of neuroinflammation (Banati et al., 2014). Similar to the brain, TSPO is also highly induced in microglia during retinal pathologies, which marks the duration and extent of retinal inflammation (Scholz et al., 2015a; Wang et al., 2014b). Although the significance of TSPO induction and especially its role during these pathologies is still not fully clear, it has been shown to play a role during inflammation. In the retina, the synchronously regulated expression of TSPO in microglia and its ligand DBI in Müller cells provides a mechanism of reciprocal modulatory microglia-macroglia interactions that drive the resolution of inflammatory responses and facilitate a return to quiescence (Wang et al., 2014b).

1.4.2.1 TSPO as a target for immunomodulation

Increased TSPO density has been observed in various neurodegenerative diseases and colocalizes to reactive microglia and astrocytes. Although TSPO ligands have mostly been used for non-invasive diagnostic imaging *in vivo*, several studies have also demonstrated their ability to mitigate microglia reactivity and to promote neuronal survival (Ferzaz et al., 2002; Ryu et al., 2005; Veiga et al., 2005). Hence, TSPO may be relevant as a disease-modifying gene and represents an attractive target for therapeutic interventions.

Several endogenous TSPO ligands exist such as cholesterol (Li et al., 2001) and porphyrins (Verma et al., 1987), which bind TSPO in nanomolar and micromolar affinity, respectively. Other TSPO ligands including endozepines such as DBI and its proteolytic products octadecaneuropeptide (ODN) and triakontatetraneuropeptide (TTN) have been shown to bind both TSPO and the $GABA_A$ receptor and to stimulate mitochondrial steroid synthesis (Costa and Guidotti, 1991; Mocchetti and Santi, 1991; Papadopoulos et al., 1991). In the retina, Müller cell-derived DBI was shown to

negatively regulate microglial reactivity by suppression of ROS production, pro-inflammatory cytokine expression and microglia proliferation (Figure 10) (Wang et al., 2014b).

Classical synthetic TSPO ligands such as the isoquinoline carboxamide PK11195 and the benzodiazepine derivative Ro5-4864, that bind TSPO with nanomolar affinity, have been shown to exert anti-inflammatory effects in two mouse models with autoimmune arthritic conditions (Torres et al., 2000). Additionally, in a mouse model for late-stage AD, PK11195 treatment was effective in reducing both soluble and deposited β-amyloid, thus improving behavioral and pathological disease outcomes (Christensen and Pike, 2018). Another established TSPO ligand is the benzoxazine etifoxine, which is not only selective for TSPO, but also binds to $GABA_A$ receptors (Hamon et al., 2003). In a mouse model for MS, administration of etifoxine before disease onset was protective and improved symptomatic recovery. Notably, in this model etifoxine reduced pro-inflammatory cytokine expression and peripheral immune cell infiltration in the spinal cord (Daugherty et al., 2013). Moreover, other studies have shown beneficial effects of etifoxine on reducing microglial reactivity and promoting neural survival after intracerebral hemorrhage or traumatic brain injury (Li et al., 2017b; Simon-O'Brien et al., 2016).

The phenylpurine XBD173, also termed AC-5216 or Emapunil, is a selective and high-affinity second generation TSPO ligand that has a more beneficial side-effect profile than benzodiazepine derivatives (Kita et al., 2004; Rupprecht et al., 2009). Treatment with XBD173 reduced degeneration of dopaminergic neurons and recovered motor dysfunction in a mouse model of PD (Gong et al., 2019). In addition, we recently exploited the endogenous TSPO ligand-mediated immunomodulation in the retina and showed that XBD173 has immunomodulatory and neuroprotective effects in a mouse model of light-induced retinal degeneration. Here, XBD173 administration reduced the expression of pro-inflammatory cytokines and the accumulation of reactive microglia in the outer retina with concomitant preservation of photoreceptors (Figure 10) (Scholz et al., 2015a).

Taken together, these findings highlight TSPO as an immunomodulatory target and emphasize the anti-inflammatory and neuroprotective properties of TSPO ligands and their potential as pharmacological therapies in the treatment of neurodegenerative diseases. However, how TSPO and its different ligands exert these beneficial effects is still not fully clear and further experimental approaches are needed to elucidate the underlying mechanisms.
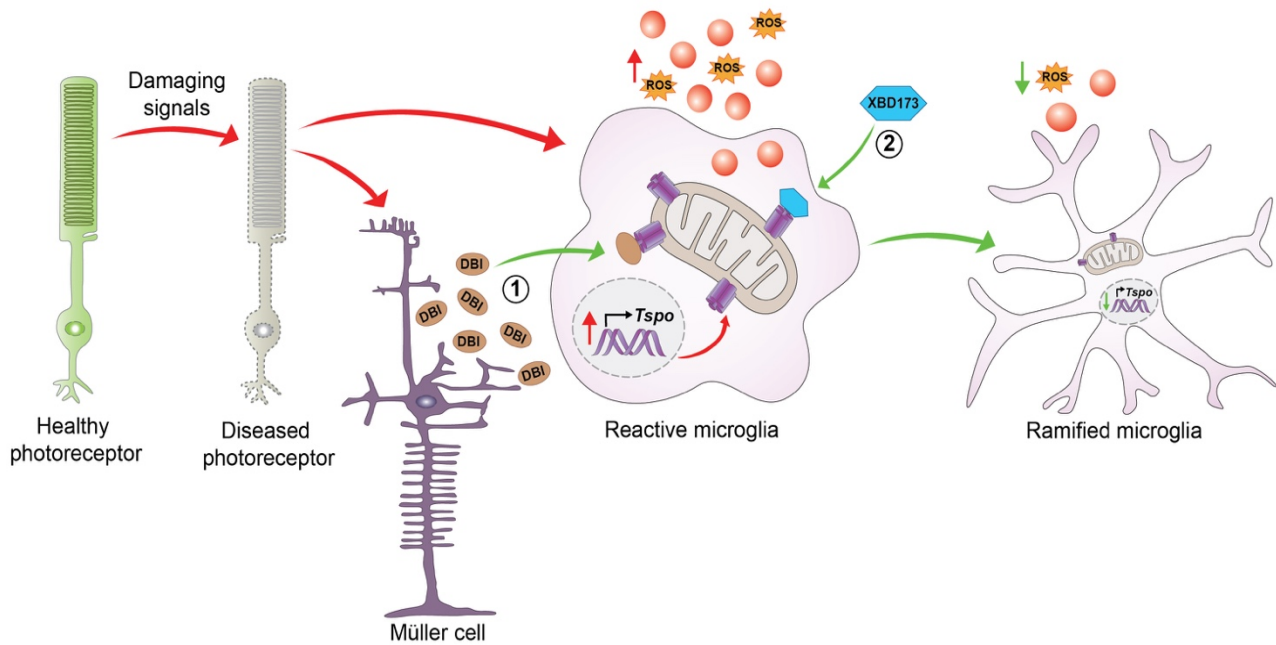
Figure 10: Immunomodulatory effects of endogenous and synthetic TSPO ligands. Specific signals from dying photoreceptors strongly induce TSPO expression in microglia and signal to Müller cells, resulting in upregulation of the expression and secretion of endogenous TSPO ligand diazepam binding inhibitor (DBI) protein. ① Secreted DBI is subsequently taken up by microglia and binding of DBI limits the magnitude and duration of microglia inflammatory responses and promotes their return to baseline quiescence. ② Exploiting this endogenous TSPO ligand-mediated immunomodulatory mechanism using the specific synthetic TSPO ligand XBD173 also negatively regulates features of microglial activation. Figure modified from Rashid et al., 2018.

1.5   Aim of the study

Microglia cells are the resident phagocytes of the CNS, including the retina, and play pivotal roles in innate immune responses and regulation of homeostasis in the healthy and degenerating CNS. Microgliosis is a common hallmark of neurodegenerative diseases and chronic pro-inflammatory microglia reactivity negatively contributes to disease progression. Thus, pharmacological approaches of microglia-related immunomodulation that inhibit dysregulated microglia inflammatory responses while preserving their beneficial neuroprotective functions, represent promising therapeutic strategies to attenuate progression of a variety of neurodegenerative diseases. We and others have previously shown, that TSPO is a biomarker for reactive microglia and an attractive target for microglia-directed immunotherapy in degenerative diseases of the retina. However, the underlying molecular mechanisms of TSPO-mediated immunomodulation and neuroprotection remain largely elusive.

Thus, in this study we aimed on elucidating the molecular function of TSPO in retinal immune homeostasis and angiogenesis using the laser-induced CNV model, an established system to study key aspects of neovascular AMD. Based on the concept of endogenous TSPO ligand-mediated immunomodulation of retinal microglia, we investigated whether the synthetic TSPO ligand XBD173 possesses immunomodulatory and neuroprotective effects in the mouse model of neovascular AMD. Additionally, we aimed to assess the direct function of TSPO in retinal immune cells using conditional microglia-specific knockout mice.

2. Material and methods

2.1 Mouse experiments

2.1.1 Mouse husbandry

All animal procedures were conducted in compliance with protocols approved by the local government authorities (Tierschutzkommission acc. §15 TSchG of the Landesamt für Natur, Umwelt und Verbraucherschutz Nordrhein-Westfalen) and were in accordance with the National Institutes of Health (NIH) guidelines. Mice were housed in individually ventilated caging (IVC) systems (GM 500, Tecniplast® Greenline) with a maximum cage density of five adult mice per cage. Light was adjusted to a 12h/12h light/dark cycle with light on at 6 am, temperature and relative humidity were regulated to $22 \pm 2°C$ and 45-65 % relative humidity. Mice were fed irradiated phytoestrogen-free standard diet for rodents (Altromin 1314; 59 % carbohydrates, 27 % protein, 14 % fat) and had access to food and acidified water *ad libitum.*

2.1.2 Experimental mouse lines

$Cx3cr1^{CreERT2}$:$Tspo^{fl/fl}$ mice ($TSPO^{\Delta MG}$) were generated by crossing $Cx3cr1^{CreERT2}$ mice (Yona et al., 2013) to $TSPO^{fl/fl}$ mice (Sileikyte et al., 2014). Nox1- (Gavazzi et al., 2006), Nox2- (Pollock et al., 1995), Nox4- (Carnesecchi et al., 2011) and $p22^{phox}$-KO (Nakano et al., 2008) mice were kindly provided by M. Schramm (Institute for Medical Microbiology, University of Cologne). C57BL/6J mice and homozygous transgenic knockout mice and corresponding wild type littermates, eight to ten-week-old with an averaged body weight of 19 g $\pm$ 1.5 g for females and 25 g $\pm$ 2 g for males, were used for experiments.

2.1.3 XBD173 administration

The phenylpurine XBD173 (AC-5216, Emapunil) was obtained by custom synthesis from APAC Pharmaceuticals. The mice received intraperitoneal (i.p.) injections of XBD173 at a dose of 10 mg/kg dissolved in DMSO or DMSO as a vehicle control daily starting one day before laser photocoagulation, while the first two days the mice received twice a day XBD173 or DMSO.

2.1.4 Tamoxifen administration

The tamoxifen dependent Cre recombinase (Cre[ERT2]) is used for the generation of conditional somatic mouse mutants, that allows one to control gene activity over the location and time. After tamoxifen administration, the synthetic estrogen receptor ligand is metabolized in the liver to 4-OH tamoxifen, resulting in the translocation of Cre[ERT2] into the nucleus. For this, tamoxifen powder was partially dissolved in 100 % ethanol and vortexed for 5 minutes (min). Filter-sterilized corn oil was added to a 9:1 oil:ethanol mixture ratio to a final concentration of 20 mg/ml tamoxifen and incubated at 37°C until complete dissolution. The prepared tamoxifen working solution was stored at -20°C protected from light. For induction of Cre recombinase activity, 4−6-week-old TSPO[ΔMG] mice and littermates carrying the respective *loxP*-flanked alleles but lacking expression of Cre recombinase (TSPO^{fl/fl}), were treated with 4 mg tamoxifen injected i.p. twice two days apart.

2.1.5 Laser photocoagulation

Laser photocoagulation was carried out as described previously (Balser et al., 2019). In brief, mice were anesthetized with a mixture of ketamine (100 mg/kg body weight, Ketavet) and xylazine (5 mg/kg body weight, 2 % Rompun) diluted in 0.9 % sodium chloride by i.p. injection and their pupils dilated with a topical drop of phenylephrine 2.5 %–tropicamide 0.5 %. A slit-lamp-mounted diode laser system (Quantel Medical Vitra, 532 nm green laser, power 100 mW, duration 100 ms and spot size 100 μm) was used to generate three equal laser burns around the optic nerve in each eye with a cover glass as a contact lens. For gene expression and protein analysis, 20 laser burns were applied to both eyes. To validate rupture of Bruch's membrane, infrared (IR) images were recorded using Spectralis[TM] HRA/OCT device to analyze post-laser retinal structure and laser lesion size *in vivo*. In case of cataract and corneal epithelial edema before laser photocoagulation, unsuccessful laser burns without Bruch's membrane rupture or severe choroidal hemorrhages, eyes were excluded from further analysis.

2.1.6 Fundus photography and fundus fluorescein angiography (FFA)

Vascular leakage was analyzed 3, 7 and 14 days after laser photocoagulation. After anesthesia and pupil dilatation, mice received i.p. injection of 0.1 ml of 2.5 % fluorescein diluted in 0.9 % sodium chloride. Late phase angiograms were recorded 10 min after fluorescein injection using

Spectralis™ HRA/OCT. Simultaneously, IR fundus images were acquired to analyze the laser lesion size.

2.1.7 Isolation and immunomagnetic enrichment of primary microglia

Brains from 8-10-week-old mice were harvested in cold HBSS without Ca^{2+} and Mg^{2+} and after removal of the meninges enzymatically dissociated into single cell suspensions with a papain-based Neural Tissue Dissociation Kit on the GentleMACS® Dissociator according to the manufacturer's instructions. The single cell suspension was passed through a 70 μm cell strainer and depleted of myelin by suspension in 30 % isotonic Percoll® followed by a 10 min centrifugation at 700 x g at 4°C. The cell pellet was resuspended in MACS buffer (97.5 μl per brain) and CD11b-specific monoclonal antibodies conjugated to paramagnetic beads (2.5 μl per brain) were added and cells labeled on ice for 15 min with 300 rpm. After labeling, cells were washed three times and sorted in combination with LS columns (Miltenyi Biotec) and QuadroMACS™ magnetic separator according to the manufacturer's instructions. After elution from the LS columns, cells were resuspended in DMEM high glucose supplemented with 10 % heat-inactivated FCS and counted using Trypan Blue exclusion in a Neubauer chamber.

2.1.8 Trans-well co-culture of photoreceptor cells and primary microglia

2.1.8.1 Culturing of 661W photoreceptor cells

661W photoreceptor cells were a gift from Prof. Muayyad Al-Ubaidi (Department of Cell Biology, University of Oklahoma Health Sciences Center, USA). Cells were grown in a monolayer in DMEM high glucose supplemented with 10 % heat-inactivated FCS and 1 % Penicillin-Streptomycin (P/S) and maintained at 37°C in a humidified atmosphere of 5 % CO_2. At about 90 % confluency, 661W cells were washed twice with 1x PBS and incubated with 1x trypsin-EDTA for 3 min at 37°C to detach the adherent cells from the culture surface. The reaction was stopped by addition of an equal volume of serum containing DMEM high glucose medium. Cells were collected, centrifuged at 300 x g for 5 min and the cell pellet resuspended in DMEM high glucose supplemented with 10 % heat-inactivated FCS and 1 % P/S and counted using Trypan Blue exclusion in a Neubauer chamber.

2.1.8.2 Trans-well co-culture of 661W cells and primary microglia

Primary microglia at the bottom and 661W photoreceptor cells on top were separated in a trans-well culture with 0.4 µm inserts (Corning). As a basal culture medium, DMEM supplemented with 10 % FCS, 1 % P/S, was used. Primary microglia were seeded at a density of 2.5 x 10^5 cells/well in a 24 well-plate and 661W photoreceptor cells at a density of 2.5 x 10^4 cells/well in 0.4 µm trans-well inserts. After 4 h, trans-wells with 661W cells were removed, placed in a new sterile 24 multi well-plate (Corning) and primary microglia were stimulated with 661W photoreceptor cell debris by synchronization at 450 x g for 5 min at 4°C. Where indicated, primary microglia were treated with 50 mM XBD173. After incubation for 15 min at 37°C, trans-wells with 661W cells were transferred back to the primary microglia and the trans-well co-culture incubated for another 24 h.

2.2   Molecular biology

2.2.1   Isolation of genomic DNA

Genomic DNA was isolated from ear punches obtained between P18 - P21 using the HotSHOT method as described previously (Truett et al., 2000) with some modifications. Briefly, the samples were incubated 15 min in alkaline lysis buffer (Table 7) at 95°C followed by 5 min on ice. An equal volume of neutralization buffer (Table 7) was added, mixed and the DNA diluted to a working concentration of 25 ng/µl.

2.2.2   Quantification of nucleic acids

Nucleic acid concentration was assessed by measuring the sample absorption at 260 nm with a NanoDrop® ND-2000 UV-Vis Spectrophotometer. The 260/280 nm absorbance ratio was used as a measure of purity of nucleic acid samples. Ratios of approximately 1.8 and 2.0 were accepted as pure DNA and pure RNA, respectively.

2.2.3   Genotyping and ΔTSPO PCR

Genotyping was performed by PCR with customized primers (purchased from IDT) listed in table 1. Reactions were performed in a thermocycler PCR machine. All amplifications were performed in a total reaction volume of 25 µl containing a minimum of 50 ng DNA template, 25 pmol of each

primer, 25 μM dNTP Mix, 1 x reaction buffer S and 1 unit of Taq Polymerase. Standard PCR programs started with 5 min of denaturation at 94°C, followed by 35 cycles consisting of denaturation at 94°C for 40 seconds (s), annealing at oligonucleotide-specific temperatures for 44 s and elongation at 72°C for 45 s, and a final elongation step at 72°C for 5 min. Amplified DNA fragments were analyzed on 1-2 % (w/v) agarose gels which were electrophoresed at 120 mV.

Genotyping for the NMF333 mutation (p22^{phox} mouse strain) was done with PCR amplification and subsequent *BslI* digestion (New England BioLabs) of a fragment of the *Cyba* gene according to the manufacturer's instructions. The WT allele produces digestion products of 202 and 89 bp and the *NMF333* allele products of 162, 89, and 40 bp.

Table 1: Genotyping primer.

Mouse line	Primer	Sequence 5' – 3'	Orientation	Annealing site
Cx3cr1^{CreERT2}	Cx3cr1-A	cctctaagactcacgtggacctg	forward	Intron 1
	Cx3cr1-B	gacttccgagttgcggagcac	reverse	Exon 1
	Cx3cr1-C	gccgcccacgaccggcaaac	reverse	Cre^{ERT2}
Nox1	N1WT-F	tagcctggctgttccctcacccaaa	forward	Intron 2
	N1WT-R	gggacagcttcctgcatccctctgt	reverse	Intron 2
	N1neo-R	tcggatcgagcgctctgaagttcct	reverse	NEO cassette
Nox2 (gp91^{phox})	N2WT-F	aagagaaactcctctgctgtgaa	forward	Intron 2
	N2WT-R	cgcactggaacccctgagaaagg	reverse	Exon 3
	N2neo-R	gttctaattccatcagaagcttatcg	reverse	NEO cassette
Nox4	N4WT-F	gttgctggcttctgcttctt	forward	Intron 2
	N4WT-R	ctttgtgtggttgcttaggaga	reverse	Intron 2
	N4neo-R	aagcttccgattcccattct	reverse	NEO cassette
NMF333 (p22^{phox}) (Point mutation Y121H)	P22-F	cagatgcccactgactgcta	forward	Intron 4
	P22-R	cgagccacagtacagcttca	reverse	Intron 5
TSPO$^{fl/fl}$	Tspo_loxp-F	ggattaccacacccaaccag	forward	Intron 1
	Tspo_loxp-R	taggagtgcaaagccagtca	reverse	Intron 1

The ΔTSPO PCR were performed with primers spanning the *loxP*-flanked exons 2 and 3 of the *Tspo* gene (Table 2) using the above-mentioned conditions. PCR amplification of complementary DNA (cDNA) isolated from retina and RPE/choroidal tissues from tamoxifen-treated TSPO$^{fl/fl}$ mice resulted in a 526 bp fragment and from TSPO^{ΔMG} mice in 526 bp and 176 bp fragments, respectively.

Table 2: ΔTSPO PCR primer.

Target	Primer	Sequence 5' – 3'	Orientation	Annealing site
Tspo	Tspo-P1	taccaacctctgtgcgcag	forward	Exon 1
	Tspo-P2	atgctctaagggcatgcctg	reverse	Exon 4

2.2.4 RNA isolation, cDNA synthesis and qPCR

RNA was isolated from retinal and RPE/choroidal tissue or primary microglia using the RNeasy Micro Kit according to the manufacturer's instructions. First-strand cDNA was synthesized from the total mRNA using the RevertAid™ H Minus First strand cDNA Synthesis Kit. Transcript levels were analyzed by quantitative real-time PCR performed in LightCycler® 480 II with either SYBR® Green (Takyon No Rox SYBR Master Mix dTTP blue) or probe-based (Takyon No ROX Probe MasterMix blue dTTP) detection according to the manufacturer's instructions with the primers listed in table 3 and table 4, respectively. *Actin* and *Atp5b* were used as housekeeping genes. Measurements were performed in technical duplicates and delta delta CT threshold calculation was used for relative quantification of results. UPL probes used for probe-based detection were purchased from Roche.

Table 3: Primer for probe-based quantitative real-time PCR.

Gene	NM accession number	Forward primer (5' – 3')	Reverse primer (5' – 3')	UPL Probe
Atp5b	NM_016774.3	ggcacaatgcaggaaagg	tcagcaggcacatagatagcc	77
Cd68	NM_001291058.1	ctctctaaggctacaggctgct	tcacggttgcaagagaaaca	27
Nox1	NM_172203.2	ggatggatctctcgcttctg	aatgctgcatacatcactgtca	19
Tspo	NM_009775.4	actgtattcagccatggggta	accatagcgtcctctgtgaaa	33

Table 4: Primer for SYBR® Green.

Gene	NM accession number	Forward primer (5' – 3')	Reverse primer (5' – 3')
Actin	NM_007393.5	aggaggagcaatgatcttg	agacctgtacgccaacacag
Duox1	NM_001099297.1	agcccctgaaagaaccctac	tccccatgcgggatgtaaatg
Duox2	NM_177610.2	tccattagtgagtctgattgtc	gtttgtcaaggacctgcagact
Nox2	NM_007807	ggttccagtgcgtgttgct	gcggtgtgcagtgctatcat
Nox3	NM_198958.2	gtgataacaggcttaaagcagaaggc	ccactttcccctacttgactt
Nox4	NM_015760.5	ggagactggacagaacgattc	tgtataacttagggtaatttctagagtgaatga

2.3   Biochemistry

2.3.1   Immunohistochemistry of retinal and RPE/choroidal flat mounts

Mice were euthanized by cervical dislocation and the eyes enucleated and fixed in 4 % of Roti Histofix for 2 h at room temperature (RT). The dissected retinal and RPE/choroidal flat mounts were permeabilized and blocked overnight in Perm/Block buffer (Table 7) at 4°C. The flat mounts were subsequently incubated with anti-IBA1 antibody for 48 h at 4°C (Table 5). After washing three times with PBST-X, the flat mounts were incubated 1 h with donkey anti-rabbit AlexaFluor^{TM} 488 (Table 5). RPE/choroidal flat mounts were stained in addition with TRITC-conjugated isolectin B4 from *Bandeiraea simplicifolia* (Table 5). After several washing steps, retinal and RPE/choroidal flat mounts were mounted on a microscope slide and embedded with Vectashield HardSet H-1400 fluorescence mounting medium. Images were taken with a Zeiss Imager.M2 equipped with an ApoTome.2.

Table 5: List of antibodies and stains used for immunohistochemistry.

Antibodies / Stains	Species	Dilution	Manufacturer, Cat. No.
anti-IBA1	Rabbit, polyclonal	1:500	Wako, 019-19741
Alexa Fluor® 488	Donkey anti-rabbit IgG	1:1000	Invitrogen, A21206
Isolectin B4-TRITC conjugate	*Bandeiraea simplicifolia*	1:100	Sigma, L5264

2.3.2   Mitochondrial staining of primary microglia

For fluorescence microscopic analysis of the mitochondrial network of primary microglia, mitochondria were stained with 100 nM of the mitochondrial membrane potential-sensitive dye MitoTracker Red CMXRos for 15 min at 37°C. Primary microglia were also stained with recombinant monoclonal anti-TSPO/PBR antibody (Abcam, ab109497; rabbit), diluted 1:1000 in PBST-X and nuclei were counterstained with DAPI. Where indicated, primary microglia were treated with 200 μM carbonyl cyanide m-chlorophenyl hydrazone (CCCP) as a positive control for mitochondrial network fragmentation.

2.3.3   Protein extraction

Shock-frozen tissue samples and primary microglia were lysed by sonication in ice cold PBS supplemented with protease and phosphatase inhibitors (Complete protease inhibitor cocktail) followed by centrifugation at 12,000 x *g* at 4°C for 30 min. Supernatants were transferred to new tubes and protein concentration was determined by BCA Protein Assay according to the manufacturer's instructions and lysates stored at -80°C.

2.3.4   Western blot

Isolated proteins extracts were diluted to 0.6-0.8 µg/µl with PBS and 6x non-reducing Laemmli buffer, incubated at 95°C for 5 min and separated by size via SDS-PAGE. Resolving gels contained 12 % and stacking gel 5 % acrylamide (Table 6). Equal amounts of samples were loaded onto the 0.75 mm gels and gel electrophoresis was carried out in 1x Running buffer at 120 V for 2 h.

Table 6: SDS-PAGE gel recipes.

SDS-PAGE Gel	Ingredients
Resolving gel	12 % v/v Acrylamide 400 mM w/v TRIS pH 8.8 0.1 % w/v SDS 0.1 % w/v APS 0.01 % v/v TEMED
Stacking gel	5 % v/v Acrylamide 125 mM w/v TRIS pH 6.8 0.1 % w/v SDS 0.1 % w/v APS 0.005 % v/v TEMED

For immunoblotting, proteins were electrophoretically transferred onto a 0.45 µm nitrocellulose membrane in 1x Transfer buffer at 100 V for 1 h. Membranes were blocked in M-TBST for 1 h at RT before incubation with primary antibodies (Table 7) for 1 h at RT or overnight at 4°C. After several washing steps in TBS-T, membranes were incubated with horseradish peroxidase (HRP)-conjugated secondary antibodies (Table 7). Membranes were washed thrice and the immune complex was visualized using SignalFire™ Elite ECL Reagent and a MultiImage II system. PageRuler pre-stained protein ladder was used for identification of protein size. Band intensities were quantified using ImageJ.

Table 7: List of antibodies used for Western blot.

Antibodies, 1st and 2nd	Species	Dilution	Manufacturer, Cat. No.
anti-Actin	Mouse, monoclonal	1:1000	Sigma, A5441
anti-PBR (TSPO)	Rabbit, monoclonal	1:1000	Abcam, ab109497
IgG-HRP conjugate	Goat anti-mouse, polyclonal	1:4000	Dako, P0447
IgG-HRP conjugate	Goat anti-rabbit, polyclonal	1:4000	Dako, P0448

2.3.5 Enzyme-linked immunosorbent assays (ELISA)

The concentration of cytokines in total retinal and RPE/choroidal lysates (see 2.3.3) were measured by ELISA as per manufacturer's instructions (Table 10). Absorbance was measured with a TECAN infinite M 1000.

2.3.6 Quantification of ROS

Primary microglia (see 2.1.7) were plated out at a density of 1×10^5 cells/well as triplicates in DMEM supplemented with 10 % FCS in sterile 96F plates. White or black closed bottom 96F plates were used for luminescence or fluorescence measurements, respectively. Primary microglia were pre-treated with either 50 µM XBD173 or DMSO as vehicle control for 1 h at 37°C as indicated. Cells were centrifuged at 650 x g at 4°C and washed once with HBSS with Ca^{2+} and Mg^{2+} to remove non-adherent cells and added substances for pre-treatment. Primary microglia were stimulated with 661W photoreceptor cell debris by synchronization at 850 x g for 5 min at 4°C or with 100 ng/ml ultrapure LPS from *E. coli* O111:B4. After three washing steps, cells were covered in HBSS with or without Ca^{2+} and Mg^{2+} supplemented with 5 % heat-inactivated normal mouse serum (NMS) as indicated. As a positive control for extra- and cytosolic ROS measurements phorbol 12-myristate 13-acetate (PMA), a chemical stimulator of ROS, was added with a final concentration of 1 ng/ml. For ROS measurement in the mitochondrial matrix rotenone, an inhibitor of complex I of the electron transport chain, was used as a positive control with a final concentration of 100 µM. Where indicated, 100 µM of the Ca^{2+} ionophore ionomycin was added to the medium after stimulation with 661W photoreceptor cell debris to raise intracellular Ca^{2+} levels.

2.3.6.1 Extracellular ROS production

For detection of extracellular ROS, ice-cold solution of 50 µM cell-impermeable isoluminol and 3.2 U/ml HRP in HBSS with Ca^{2+} and Mg^{2+} was used (Herb et al., 2019). The enzyme HRP uses the produced ROS to catalyze the conversion of isoluminol to the excited 3-aminophtalate. This product decays to lower energy state and emits light during the process. After stimulation with 661W photoreceptor cell debris and treatment with different substances (see 2.3.6) isoluminol/HRP solution was added to the wells and chemiluminescence was recorded for 120 min with 60 s intervals at 37°C in TriStar^2 LB 942 Multimode Plate Reader. To calculate cell-specific luminescence, the luminescence of cell-free wells containing HBSS with or without used substances was subtracted.

2.3.6.2 Cytosolic ROS production

For detection of cytosolic ROS, the substance 5,6-carboxy-2',7'-dichlorodihydroflurescein diacetate, di(acetoxymethyl ester) (DCF) was used (Herb et al., 2019). Primary microglia were incubated in 20 µM DCF in HBSS with Ca^{2+} and Mg^{2+} at 37°C for 15 min. DCF is a hydrophilic molecule, which readily enters cells by diffusion during incubation. After reaching the cytosol, ester groups of the DCF molecule are cleaved by cytosolic esterases, leading to the loss of hydrophilicity. Lipohilic DCF is trapped in cytosol as dihydrofluorescein. Cleaving of the ester groups also leads to the exposure of functional groups that are able to react with ROS. After reaction with ROS, dihydrofluorescein is converted to its oxidized and fluorescent derivate fluorescein. After incubation, cells were centrifuged and washed for two times with ice cold HBSS with Ca^{2+} and Mg^{2+} and primary microglia were stimulated as described in 2.3.6. After stimulation with 661W photoreceptor cell debris and treatment with different substances, cells were covered with ice cold HBSS with Ca^{2+} and Mg^{2+} supplemented with 5 % heat-inactivated NMS. Fluorescein was excited at 495 nm and emitted fluorescence at 520 nm was recorded for 120 min with 60 s intervals at 37°C in TriStar^2 LB 942 Multimode Plate Reader. To calculate cell-specific fluorescence, the fluorescence of cell-free wells containing HBSS with or without used substances was subtracted.

2.3.6.3 Mitochondrial matrix-derived ROS production

ROS production in the mitochondrial matrix was detected by using the fluorescence probe MitoSOX Red (Herb et al., 2019). Primary microglia were incubated with 5 µM MitoSOX Red in

HBSS with Ca^{2+} and Mg^{2+} at 37°C for 15 min. MitoSOX Red accumulates in the mitochondrial matrix and is oxidized exclusively by superoxide. After incubation, cells were centrifuged and washed for two times with ice cold HBSS with Ca^{2+} and Mg^{2+} and primary microglia were stimulated as described in 2.3.6. After stimulation with 661W photoreceptor cell debris and treatment with different substances, cells were covered with ice cold HBSS with Ca^{2+} and Mg^{2+} supplemented with 5 % heat-inactivated NMS. MitoSOX Red was excited at 510 nm and emitted fluorescence at 580 nm was recorded for 120 min with 60 s intervals at 37°C in a TECAN infinite M 1000 microplate reader. To calculate cell-specific fluorescence, the fluorescence of cell-free wells containing HBSS with or without used substances was subtracted.

2.3.7 Quantification of calcium levels

2.3.7.1 Mitochondrial calcium levels

Primary microglia were seeded at a density of 1 x 10^5 cells/well in triplicates in DMEM + FCS in black 96-well plates. To analyze mitochondrial calcium levels, primary microglia were incubated in 2 μM Rhod-2-AM in HBSS with Ca^{2+} and Mg^{2+} supplemented with 5 % heat-inactivated normal mouse serum for 15 min at 37°C before stimulation with 661W photoreceptor cell debris and treatment with different substances (see 2.3.6). Rhod-2-AM fluorescence was measured at 1-min intervals using a Tecan Infinite M 1000 microplate reader.

2.3.7.2 Cytosolic calcium levels

Primary microglia were seeded at a density of 1 x 10^5 cells/well in triplicates in DMEM + FCS in black 96-well plates. To analyze mitochondrial calcium levels, primary microglia were incubated in 2 μM Fura-2-AM in HBSS with Ca^{2+} and Mg^{2+} supplemented with 5 % heat-inactivated NMS for 15 min at 37°C before stimulation with 661W photoreceptor cell debris and treatment with different substances (see 2.3.6). Fura-2-AM fluorescence was measured at 1-min intervals using a Tecan Infinite M 1000 microplate reader.

2.3.8 Analysis of mitochondrial membrane potential

Primary microglia were seeded at a density of 1 x 10^5 cells/well in triplicates in DMEM + FCS in black 96-well plates, incubated in 1 μM tetramethylrhodamine, ethyl ester (TMRE) in HBSS with Ca^{2+} and Mg^{2+} for 20 min at 37°C and then stimulated with 661W photoreceptor cell debris (see

2.3.6). TMRE accumulates in the mitochondrial matrix due to its cationic properties and the negative charge of the matrix. The negative charge is stable as long as protons are pumped across the inner mitochondrial membrane and the charge separation across the membrane causes the mitochondrial membrane potential (MMP). Accumulated TMRE shows a red shift in its fluorescence properties and represents stable membrane potential, while loss of the MMP results in release of TMRE from mitochondria and thus in a decreased fluorescence signal. The proton shuttling substance CCCP at a final concentration of 200 µM was used as a positive control. TMRE fluorescence was measured for 300 min at 60-min intervals using a Tecan Infinite M 1000 microplate reader.

2.3.9 Analysis of cellular ATP levels

Primary microglia were seeded at a density of 1×10^5 cells/well in triplicates in DMEM + FCS in white 96-well plates and stimulated with 661W photoreceptor cell debris or treated with 200 µM CCCP as a positive control. Where indicated, 500 µM 2-Deoxy-D-glucose or 10 µM oligomycin A was added to the medium after stimulation with 661W photoreceptor cell debris. Cellular ATP levels were determined by using the CellTiter-Glo® Luminescent Cell Viability Assay in accordance with the manufacturer's instructions. Chemiluminescence was measured for 120 min at 60-min intervals using a TriStar² LB 942 Multimode Plate Reader.

2.3.10 Flow cytometry

Medium of 661W cells from the inlays (see 2.1.8.2) was collected, cells were washed with 1x PBS and harvested using 1x trypsin-EDTA for 20 s at RT. Collected medium and cells were centrifuged at 650 x *g* at 4°C for 5 min and resuspended in MACS buffer. To assess cell death of 661W cells after trans-well co-culturing with stimulated or unstimulated primary microglia, Annexin V/Propidium iodide staining was performed according to the manufacturer's instructions.
Cells were analyzed via flow cytometry with a BD FACSCanto™ Flow Cytometer (BD Biosciences) and data were obtained and analyzed with BD FACSDiva™ software (BD Biosciences).

2.4 Computational analysis

2.4.1 Image analysis

Morphological analysis of Iba1$^+$ mononuclear phagocytes in lasered retinas and RPE/choroidal flat mounts was done using a grid system as previously described (Lückoff et al., 2017) and the evaluation of Iba1$^+$ area per laser lesion was performed using ImageJ. The average grid crossing points and Iba1$^+$ area per laser lesion was calculated.

The size of laser lesions and vascular leakage was determined using the measuring tool of the HEYEX software. The analysis of vascular leakage by measuring pixel intensities was performed as described previously (Lückoff et al., 2017). In brief, pixel intensity was quantified in two regions of interest (ROI) within and one ROI outside each laser lesion using FIJI. The background pixel intensity was then subtracted from the laser lesion values and the data of three laser lesions averaged to obtain the mean laser-induced leakage per eye.

CNV area in RPE/choroidal flat mounts were measured with the spline function of the graphic tool included in the ZEN blue software. The average CNV area per eye was calculated.

Morphometric parameters in retinal flat mounts were analyzed using MotiQ, a fully automated analysis software. MotiQ was developed as an ImageJ plugin in Java and is publicly available (https://github.com/hansenjn/MotiQ, V3.1.1). All segmentation and quantification were performed on 2D mean intensity projections (MIPs) of 3D image data.

2.4.2 Statistical analysis

Statistical analysis was conducted on data from at least three independent experiments. Western blots from XBD173-treated, microglia-specific TSPO and Nox1-KO retinas or RPE/choroids were performed two times with three biological different samples each time. All micrographs shown are representative images of at least three independent experiments. Statistical analysis was performed using GraphPad Prism 8 software. Differences between two groups were analyzed by a two-tailed unpaired Student's t test. In order to analyze the data from the laser-induced CNV mouse model and to take into account simultaneously the correlation between measurements from the same mouse, assuming that eyes were exchangeable and the correlation for repeated measurements in the same eye (in case of repeated laser burns), a linear mixed model was used,

including treatment (or genotype) and time as fixed effects and mouse as random effect (Ando et al., 2002; Zhao et al., 2019). Data are presented as means ± SEM, * P< 0.05, ** P<0.01, *** P≤ 0.001.

2.5   Buffers, chemicals and kits

All buffers and solutions used in this study are listed in table 8, chemicals and kits used in this study are listed in table 9 and table 10, respectively.

Table 8: List of all buffers and solutions.

Buffer / Solution	Chemical composition / Manufacturer, Cat. No.
Alkaline lysis buffer	25 mM NaOH 200 mM EDTA pH 12 in ddH$_2$O
DMEM – high glucose	Sigma, D1145
DNA Loading dye (6x)	30 % w/v Glycerol 0.25 % w/v bromophenol blue in ddH$_2$O
DPBS (1x)	Gibco, 14190
HBSS (1x, w/o Ca^{2+}, Mg^{2+})	Gibco, 14175
HBSS (1x, with Ca^{2+}, Mg^{2+})	Gibco, 14025
Laemmli buffer (6x), non-reducing	375 mM TRIS pH 6.8 60 % Glycerol 0.2 % SDS, 0.01 % bromophenol blue in ddH$_2$O
M-TBST (Blocking buffer)	5 % milk powder in 1x TBS-T
MACS buffer	0.5 % BSA 200 mM EDTA pH 8.0 in PBS
Neutralization buffer	40 mM TRIS-HCl pH 5 in ddH$_2$O
PBST-X	0.3 % Triton X-100 in PBS
Percoll 100% (isotonic)	9 parts v/v Percoll 1 part v/v 1.5 M NaCl
Perm/Block buffer	5 % NDS 0.2 % BSA 0.3 % Triton X-100 in 1x PBS
Running buffer (10x)	192 mM Glycine 250 mM TRIS 1 % w/v SDS in ddH$_2$0
TBE buffer (10x)	1 M Boric acid 1 M Tris pH 7.5 20 mM EDTA pH 8.0 in ddH$_2$O
TBS (10x)	150 mM NaCl 200 mM TRIS in ddH$_2$O
TBS-T (1x)	0.1 % Tween 20 in 1x TBS

Transfer buffer (10x)	192 mM Glycine
	250 mM TRIS pH 7.4
	0.1 % w/v SDS in ddH$_2$O
Transfer buffer (1x)	10 % Transfer buffer 10x
	70 % ddH$_2$O
	20 % v/v Methanol
Trypsin-EDTA (0.05 %, phenol red)	Thermo Scientific, 25300054

Table 9: List of chemicals and reagents.

Name	Manufacturer, Cat. No.
β-Mercaptoethanol	Sigma-Aldrich, M-7154
2-Deoxy-D-glucose (2-DG)	Sigma-Aldrich, D8375
5,6-carboxy-2',7'-dichlorodihydroflurescein diacetate, di(acetoxymethyl ester) (DCF)	Thermo Scientific, C2938
Acrylamide/Bis- solution 30 % (29:1)	Roth, A124.1
Agarose	Biozym, 84004
Ammonium persulfate (APS)	Sigma-Aldrich, A3678
Artelac® Splash EDO®	Bausch + Lomb, PZN 07706996
Boric acid	Sigma-Aldrich, B6768
Bovine Serum Albumin (BSA)	Sigma-Aldrich, A9418
Bromophenol blue	Sigma-Aldrich, B-6131
Bsl1, Restriction enzyme	New England BioLabs, R0555S
Carbonyl cyanide 3-chlorophenylhydrazone (CCCP)	Sigma-Aldrich, C2759
Cd11b MicroBeads human/mouse	Miltenyi biotec, 130-093-634
cOmplete Mini, Protease Inhibitor Cocktail	Roche, 11836153001
Corn oil	Sigma-Aldrich, C8267
Dimethyl sulfoxide (DMSO)	Sigma-Aldrich, D5879
Ethanol, absolute	AppliChem, A3678
Ethidium bromide	Sigma-Aldrich, 46067
Ethylenediaminetetraacetic acid (EDTA)	Sigma-Aldrich, E9884
Fetal Calf Serum (FCS)	Gibco, 10270
Fluorescein ALCON® 10 %	Alcon®, PZN 01467007
Fura-2-AM	Sigma-Aldrich, F0888
GeneRuler 100 bp plus	Thermo Scientific, SM0332
Glycerol	Sigma-Aldrich, 49781
Glycine	Roth, 3790.2
Horseradish peroxidase (HRP)	Merck, 516531-5KU
Hydrochloric acid (HCl), 37 %	Roth, X942.1
Ionomycin	Sigma-Aldrich, I3909

Isoluminol	Sigma-Aldrich, A8264
Isopropanol (2-propanol)	ChemSolute, 1136
Ketaset 100 mg/ml	Zoetis, PZN 12467832
LPS, ultrapure from *E. coli* O111:B4	InvivoGen, tlrl-eblps
Methanol	ChemSolute, 1437.2511
Methocel® 2 %	OmniVision, PZN 04682367
MitoSox™	Thermo Scientific, M36008
MitoTracker Red CMXRos	Thermo Scientific, M7512
N, N, N', N'-Tetramethylethylendiamin (TEMED)	Roth, 2367.1
Normal donkey serum (NDS)	Linaris, ADI-NDKS-10
Normal mouse serum (NMS)	Dunn Lab, N14010M
Oligomycin A	Sigma-Aldrich, 75351
PageRuler, prestained	Thermo Scientific, 31985
Percoll™	GE Healthcare, 17-0891-02
Phenylephrine 2.5 % / Tropicamide 0.5 %	University Hospital Cologne, Pharmacy
Phorbol-12-myristate-13-acetate (PMA)	Sigma-Aldrich, P1585
Powdered milk	Roth, T145.3
Rhod-2-AM	Enzo, ENZ-52010
Rompun 2 % (Xylazine)	Bayer, PZN 1320422
Rotenone	Sigma, R8875
Roti Histofix 4 %	Roth, P087.4
Sodium chloride (NaCl)	Sigma-Aldrich, S9888
Sodium Chloride 0.9 %, injection	Fresenius Kabi, PZN 06605514
Sodium dodecyl sulfate (SDS)	Serva, 20765.03
Sodium hydroxide (NaOH)	Merck, 1.06462
Sucrose	Roth, 4621.1
Tamoxifen	Sigma-Aldrich, T5648
TRIS	Roth, 4855.3
Triton X-100	Sigma-Aldrich, X100
Trypan Blue 0.4 %	Thermo Scientific, 15250061
Tween 20	Sigma-Aldrich, P1379
Vectashield® HardSet™ Mounting Medium	Vectashield®, H1400
XBD173 (AC-5216, Emapunil)	APAC Pharmaceuticals, 828072

Table 10: List of all kits used in this study.

Kit	Manufacturer, Cat. No.
BD OptEIA™ TMB Substrate Kit for ELISA	BD Biosciences, 555214
CellTiter-Glo® Luminescent Cell Viability Assay	Promega, G7570
FITC AnnexinV/ Propidium iodide Detection Kit	BD Pharmigen, 556547

Mouse Angiopoietin-1 ELISA	MyBioSource, MBS727480
Mouse CCL2/JE/MCP-1 DuoSet® ELISA	R&D Systems, DY479
Mouse IL-1 beta /IL-1F2 DuoSet® ELISA	R&D Systems, DY401
Mouse IL-6 DuoSet® ELISA	R&D Systems, DY406
Mouse TNF DuoSet® ELISA	R&D Systems, DY410
Mouse VEGF DuoSet® ELISA	R&D Systems, DY493
Mouse/Rat Angiopoietin-2 Quantikine® ELISA	R&D Systems, MANG20
Mouse/Rat IGF-I/IGF-1 DuoSet® ELISA	R&D Systems, DY791
Neural Tissue Dissociation Kit (P)	Miltenyi Biotec, 130-092-628
Pierce™ BCA Protein Assay Kit	Thermo Scientific, 23225
RevertAid RT Kit	Thermo Scientific, K1691
RNeasy® Micro Kit	Qiagen, 74004
SignalFire™ Elite ECL Reagent	Cell Signaling Technology, 12757
Takyon™ No ROX Probe MasterMix blue dTTP	Eurogentec, UF-NPMT-B0701
Takyon™ No ROX SYBR® MasterMix blue dTTP	Eurogentec, UF-NSMT-B0701
Taq-S PCR Kit	Genaxxon bioscience, M3313
TMRE Mitochondrial Membrane Potential Assay Kit	Abcam, ab113852

2.6 Devices and software

All devices used in this study are listed in table 11 and software are listed in table 12.

Table 11: List of all devices used in this study.

Device	Manufacturer
Adventurer Pro balance	Ohaus®
BD FACSCanto™ Flow Cytometer	BD Biosciences
BlueMarine™ 200 Electrophoresis unit	SERVA Electrophoresis GmbH
Centrifuge 5415 R	Eppendorf
Centrifuge Mini Star	VWR International
Cryostat CM3050	Leica
Explorer R Ex 124 balance	Ohaus®
Galaxy 170S CO2 incubator	Eppendorf
GentleMACS® Dissociator	Miltenyi Biotec
Heraeus Megafuge 40R Centrifuge	Thermo Scientific
Infinite® F200 Pro plate reader	Tecan Trading AG
Intas Gel iX20 Imager	Intas
LightCycler® 480 Instrument II	Roche Applied Science
Matrix™ Multichannel Pipette	Thermo Scientific
Mini-Protean® Tetra System	Bio-Rad

MiniTrans-Blot® Cell Module	Bio-Rad
MSC-Advantage hood	Thermo Scientific
MultiImageII	Alpha Innotech
NanoDrop 2000 Spectrophotometer	Thermo Scientific
Neubauer counting chamber	OptikLabor
PeqSTAR 2x cycler	Peqlab
PowerPac™ basic	Bio-Rad
QuadroMACS™ Separator	Miltenyi Biotec
See-saw rocker SSL4	Stuart®
Slit lamp BQ900®	Haag-Streit International
Spectralis™ HRA+OCT	Heidelberg Engineering
Thermomixer compact	Eppendorf
Vibracell 75115 Sonicator	Fisher Bioblock Scientific
Vitra Monospot Laser	Quantel Medical
Vortex-Genie™	Scientific Industries
Zeiss Stemi 508 Stereo microscope	Zeiss

Table 12: List of software used in this study.

Software	Manufacturer
Adobe creative suite	Adobe Systems
AlphaView FluorChem FC2	Cell Biosciences
BD FACSDiva™ software (V5.0.3)	BD Bioscience
FIJI/ Image J (V1.9.13.0)	Wayne Rasband, NIH
GraphPad Prism 8 (V8.4.1)	GraphPad Software, Inc.
Heidelberg Eye Explorer (HEYEX)	Heidelberg Engineering
i-control 1.9	Tecan Trading AG
Intas Gel Documentation Software (V3.39)	Intas Science Imaging
LightCycler® 480 Software (V1.5.1)	Roche Applied Science
Microsoft Office 365 pro plus	Microsoft Corporation
Nanodrop 2000/2000c Software	Thermo Scientific
Papers 3	Read Cube
Zen blue 2012 (V3.1.0.00002)	Zeiss

3.   Results

3.1   Immunomodulatory and neuroprotective effects of the TSPO ligand XBD173 in laser-induced CNV

3.1.1   XBD173 alleviates MNP reactivity in laser-damaged retinas and RPE/choroids

We have previously shown that microglia activation and light-induced retinal degeneration can be prevented by TSPO ligands. However, the underlying molecular mechanisms of TSPO-mediated immunomodulation and neuroprotection remain largely elusive. To investigate if targeting TSPO with the synthetic ligand XBD173 has also immunomodulatory potential in an *in vivo* model of neovascular AMD, laser photocoagulation in C57BL/6J mice that were treated daily with intraperitoneal injections of XBD173 or vehicle DMSO, were performed. The laser-induced CNV mouse model is extensively used in retinal research since it recapitulates several main features of wet AMD (Lambert et al., 2013). The laser damage results in the rupture of BM and an acute local inflammatory response concomitant with a rapid recruitment of MNPs and ingrowth of choroidal capillaries into the avascular retina within a few days (Combadière et al., 2007; Karlstetter et al., 2017; Lückoff et al., 2016).

First, the immune-related effects of XBD173 on laser-induced CNV were assessed. Here, confocal images of retinal flat mounts from DMSO-treated mice revealed massive accumulation of reactive ameboid-shaped Iba1$^+$ cells within the lesions at 3d post-laser injury whereas retinas from XBD173-treated mice had less Iba1$^+$ phagocytes and these cells showed mainly a ramified morphology (Figure 11a, b). The infiltration of immune cells in the retina 7d after laser injury was overall less than at 3d, indicating an inflammation-related wound healing process. Nevertheless, XBD173 treatment significantly attenuated phagocyte reactivity at both time points (Figure 11b, c). The mRNA expression of *Cd68* and *Tspo* itself were then quantified to determine the magnitude of immune cell activation. Indeed, retinal *Tspo* and *Cd68* transcript levels strongly increased after laser injury compared to naïve mice and the XBD173-treated groups showed diminished activation marker expression especially at the earlier time points (Figure 11d). Since TSPO protein oligomerization has been reported in human and mouse cells (Delavoie et al., 2003), retinal TSPO levels under non-reducing conditions were analyzed. After laser injury, Western blot analysis revealed a higher TSPO-specific molecular weight band at 25 kDa (referred to as higher molecular weight "HMW1"), that was absent in non-lasered naïve or XBD173-treated mice (Fig. 11e). In contrast, monomeric TSPO levels (referred to as lower molecular weight "LMW"), were significantly

lower compared to naïve mice. The ratio of HMW1 to LMW was higher after laser injury than in naïve mice and XBD173 prevented lesion associated formation of HMW1 TSPO (Figure 11e, f). Next, secretion of pro-inflammatory cytokines was analyzed. Six hours after laser injury, increased levels of CCL2 and IL-6 were found in the retina, whereas levels of IL-1β and TNF did not change (Figure 11g). Notably, XBD173-injected mice had strongly reduced CCL2 and IL-6 secretion comparable to the level of naïve mice (Figure 11g).
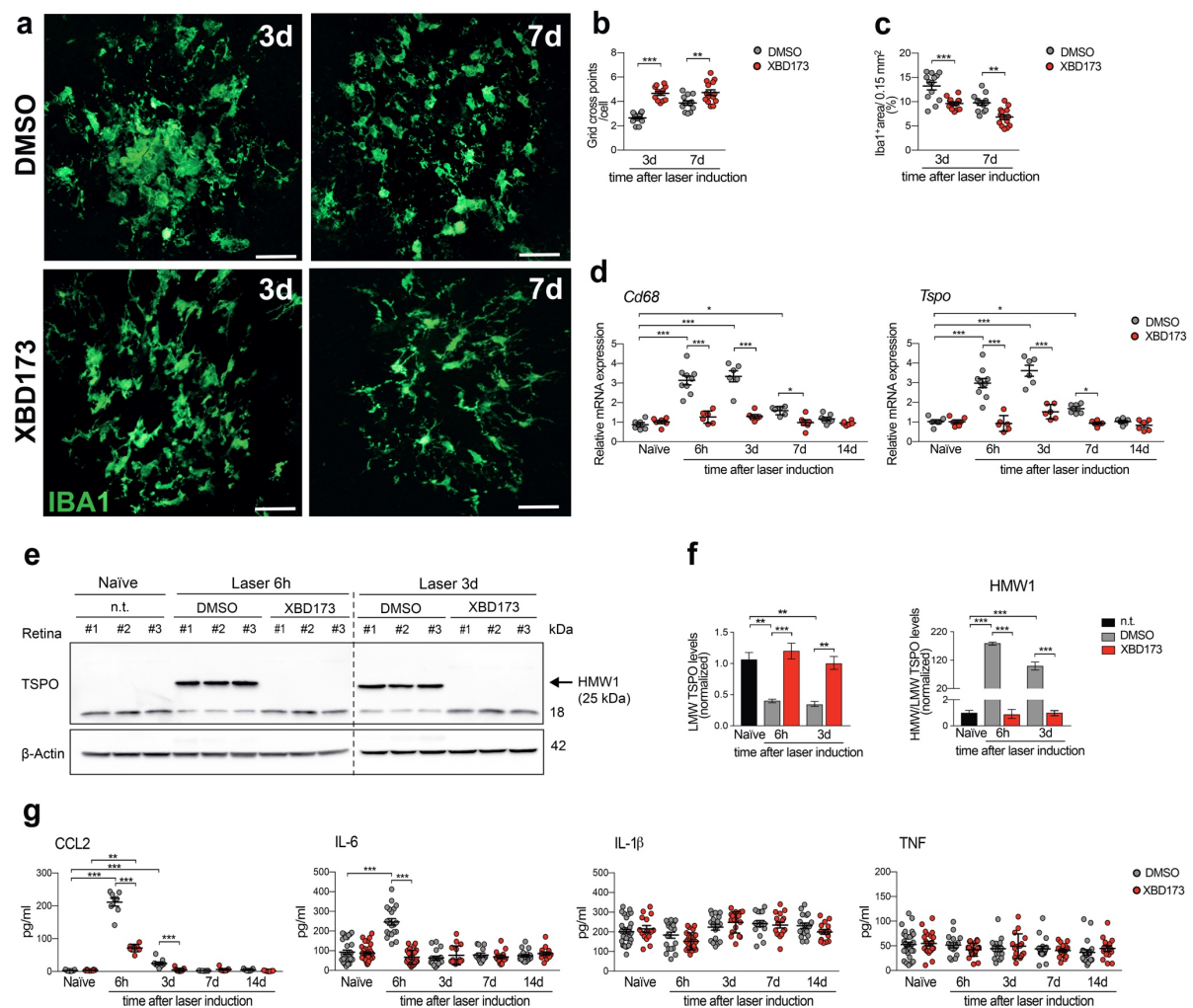
Figure 11: XBD173 dampens mononuclear phagocyte reactivity in the retina after laser-induced CNV in mice. a Representative images show accumulation of Iba1+ mononuclear phagocytes within the laser lesion in retinal flat mounts. Scale bar: 50 μm. **b** Analysis of Iba1+ cell morphology within laser lesions. n= 13-17 spots. **c** Quantification of Iba1+ area of the laser lesions. n= 13 spots. **d** *Cd68* and *Tspo* mRNA levels in retina from DMSO- or XBD173 treated mice at indicated time points after laser-induced CNV. n= 6 retinas. **e** TSPO protein levels in whole retinal lysates of naïve and lasered mice at indicated time points. Each lane represents an individual retina. Dotted line indicates individual blots, which were processed in parallel. **f** Densitometric analysis of Western blots. LMW TSPO (18 kDa) signals were normalized to β-Actin and HMW:LMW TSPO ratio determined. n= 6 retinas from two independent experiments. LMW, lower molecular weight; HMW, higher molecular weight; n.t., non-treated. **g** Pro-inflammatory cytokine levels in retinas of naïve and lasered mice at indicated time points. CCL2 (n= 8 retinas); IL-6 (n= 17-32 retinas), IL-1β (n= 17-33 retinas) and TNF (n= 17-33 retinas). Data are presented as mean ± SEM. Linear mixed model was used for statistical analyses; * P< 0.05, ** P<0.01, *** P≤ 0.001.

To explore the effects of targeting TSPO with XBD173 on subretinal and RPE-associated phagocytes, Iba1$^+$ cells were imaged in RPE/choroidal flat mounts. Similarly, as in the retina, XBD173 treatment reduced phagocyte infiltration and reactivity in the RPE/choroid compared to DMSO treatment (Figure 12a-c). Laser-induced *Cd68* and *Tspo* expression were also reduced after XBD173 treatment (Figure 12d). Of note, Western blot analysis of RPE/choroids revealed an additional TSPO-specific HMW band (36 kDa) (referred to as "HMW2") (Figure 12e). Again, LMW TSPO levels were significantly lower and the ratio of HMW1 to LMW and HMW2 to LMW was higher after laser-injury than in naïve mice and significantly reduced in XBD173-treated mice (Figure 12f). Moreover, increased levels of CCL2, IL-6 and IL-1β were found in the RPE/choroids after laser-injury, while XBD173 treatment prevented their laser-induced secretion. Levels of TNF did not change after laser injury or XBD173 treatment (Figure 12g).
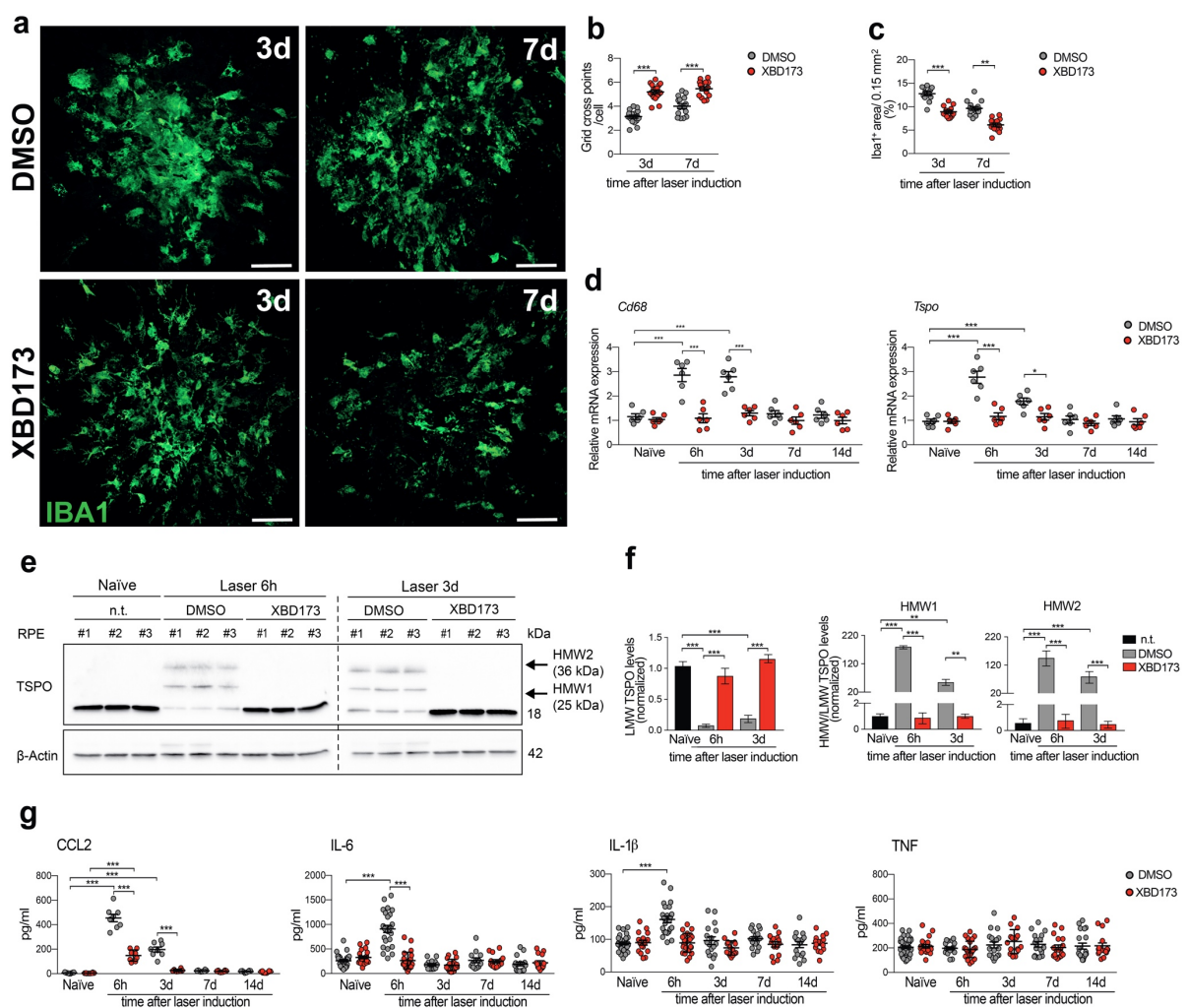
Figure 12: XBD173 dampens mononuclear phagocyte reactivity in the RPE/choroid after laser-induced CNV in mice. a Representative images of Iba1$^+$ cells within the laser lesion in RPE/choroidal flat mounts. Scale bar: 50 μm. **b** Analysis of Iba1$^+$ cell morphology within laser lesions. n= 13 spots. **c** Quantification of Iba1$^+$ area

of the laser lesions. n= 13 spots. **d** *Cd68* and *Tspo* mRNA levels in RPE/choroid from DMSO- or XBD173 treated mice at indicated time points after laser-induced CNV. n= 6 RPE/choroids. **e** Western blots showing TSPO expression in whole RPE/choroidal lysates of naïve and lasered mice at indicated time points. Each lane represents an individual RPE/choroid. Dotted line indicates individual blots, which were processed in parallel. **f** Densitometric analysis of Western blots. LMW TSPO (18 kDa) signals were normalized to β-Actin and HMW:LMW TSPO ratio determined. n= 6 RPE/choroids from two independent experiments. LMW, lower molecular weight; HMW, higher molecular weight; n.t., non-treated. **g** Pro-inflammatory cytokine levels in RPE/choroids of naïve and lasered mice. CCL2 (n= 8 RPE/choroids); IL-6, IL-1β and TNF (n= 17-30 RPE/choroids). Data are presented as mean ± SEM. Linear mixed model was used for statistical analyses; * P< 0.05, ** P<0.01, *** P≤ 0.001.

3.1.2 XBD173 blocks stimulation-induced extracellular ROS production in microglia

Since reactive MNPs are a rich source for ROS, which have been suggested as drivers of neurodegeneration, we next analyzed if targeting TSPO with XBD173 also affects ROS production of mouse primary microglia (pMG). ROS can be produced in different subcellular locations such as the lumen of phagosomes and the extracellular milieu (extracellular ROS), the cytoplasm (intracellular ROS) or in the mitochondrial matrix. Extracellular and phagosomal ROS can be assessed with the cell-impermeable dye isoluminol (Lundqvist and Dahlgren, 1996), while intracellular ROS levels are measured with the cell-permeable dye DCF derivative 5,6-carboxy-2',7'-dichlorodihydrofluorescein diacetate, di(acetoxymethyl ester) that exclusively detects ROS in the cytosol (Hempel et al., 1999) (Figure 13a). ROS that is produced in the mitochondrial matrix as a by-product of the respiratory electron transport chain (ETC) can be analyzed with MitoSOX Red (Robinson et al., 2006) (Figure 13a).

First, we analyzed extracellular and phagosomal ROS production in pMG after different stimuli (Figure 13b). Here, ROS levels strongly increased after stimulation of pMG with phorbol 12-myristate 13-acetate (PMA), a chemical stimulator of ROS, or after phagocytosis of photoreceptor cell debris but not after LPS treatment (Figure 13b). As phagocytic clearance of dead cells by microglia is a physiological process that is overreactive during disease, stimulation with photoreceptor cell debris was used for further experiments.

Culture of pMG in the presence of XBD173 strongly diminished stimulation-induced ROS production (Figure 13c). In contrast, cytosolic ROS (Figure 13d) or ROS produced in the mitochondrial matrix (Figure 13e) was not detected in stimulated microglia. These data indicate that the TSPO ligand XBD173 blocks extracellular and phagosomal ROS production of microglia after stimulation.
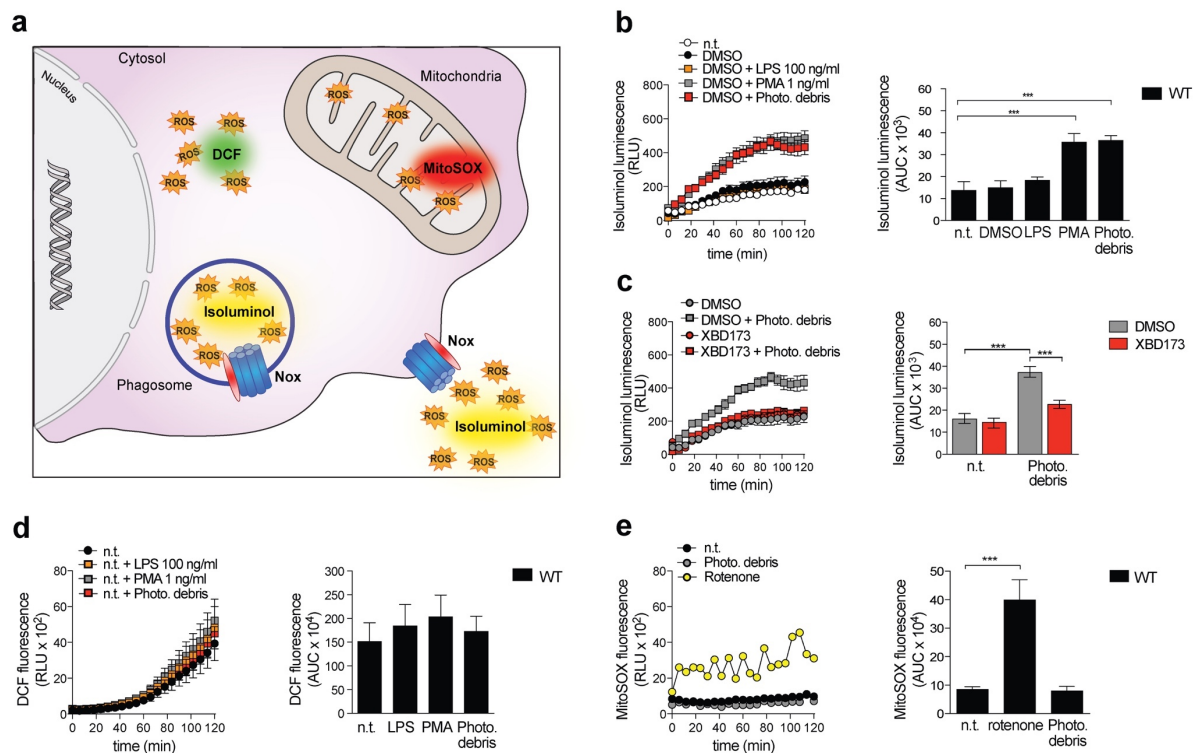
Figure 13: XBD173 blocks stimulation-induced extracellular ROS production in primary microglia. a Schematic representation of three different ROS detection methods. Isoluminol detects ROS in the lumen of phagosomes and the extracellular milieu (extracellular ROS). DCF detects cytosolic (intracellular) ROS and MitoSOX Red measures ROS inside the mitochondrial matrix. **b** Quantification of extracellular ROS production by primary microglia from WT mice. Primary microglia were stimulated with LPS, PMA or photoreceptor cell debris. Kinetics of ROS production and the area under the curve (AUC) are shown. n= 4 independent experiments. **c** Quantification of stimulation-induced extracellular ROS production by primary microglia from WT mice treated with XBD173. Kinetics of ROS production and the area under the curve (AUC) are shown. n= 11 independent experiments. **d** Cytosolic ROS production in WT mice. Primary microglia were stimulated with LPS, PMA or photoreceptor cell debris. Kinetics of ROS production and the area under the curve (AUC) are shown. n= 4 independent experiments. **e** Matrix-derived ROS (mROS) production in WT mice. Primary microglia were stimulated with photoreceptor cell debris or rotenone as a positive control to induce ROS production into the mitochondrial matrix. Kinetics of ROS production and the area under the curve (AUC) are shown. n= 4 independent experiments. Data are presented as mean ± SEM; unpaired two-tailed Student's *t* test; ***P≤ 0.001.

3.1.3 XBD173 limits laser-induced vascular leakage and neoangiogenesis

To investigate the anti-angiogenic potential of XBD173, we assessed its effects on inflammation-induced vascular leakage with late-phase fundus fluorescein angiography (FFA). While DMSO-injected mice showed prominent vascular leakage after laser injury, strongly reduced vascular leakage was seen in XBD173-treated mice at all analyzed time points (Figure 14a). Both, leakage intensity and area were significantly lower in the XBD173 group than in controls (Figure 14b, c). These findings were confirmed by monitoring CNV formation using lectin staining of RPE/choroidal flat mounts. The CNV size was significantly

smaller in the XBD173 treatment groups compared to DMSO-treated control mice (Figure 14d, e). To elucidate whether targeting of TSPO with XBD173 also affects angiogenic growth factors, the protein levels of VEGF-A, angiopoietin-1 (ANG-1), ANG-2, and insulin-like growth factor-1 (IGF-1) levels were measured in the retina and RPE/choroid. The secretion of all growth factors was significantly increased in both tissues after laser injury, but strongly reduced in XBD173-treated mice especially at early time points of the analysis (Figure 14f, g). As laser-induced CNV is also accompanied by a wound healing process, we monitored the lesion size and the formation of a fibrotic scar over time after laser injury *in vivo* using SD-OCT. Notably, XBD173 treatment attenuated the lesion-associated fibrosis significantly at all time points compared to controls, indicating a faster wound healing process (Figure 15a, b). These findings demonstrate that XBD173 attenuates both vascular leakage and neoangiogenesis.
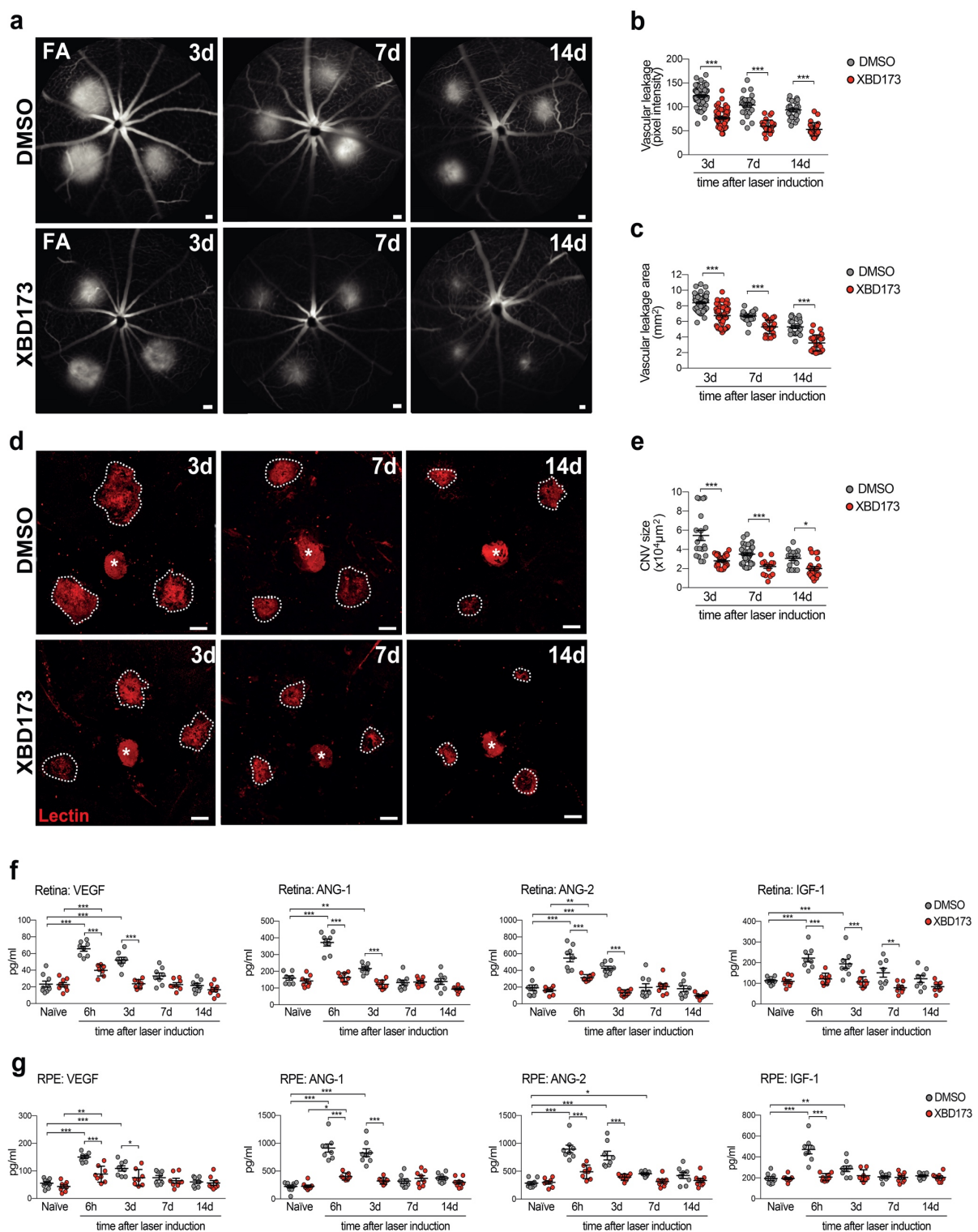
Figure 14: XBD173 inhibits laser-induced vascular leakage and pathological CNV in mice.
a Representative late phase fundus fluorescein angiography (FFA) images at indicated time points post laser injury. Scale bar: 200 µm; FA, fluorescein angiography. **b** Quantification of vascular leakage intensity after laser-induced CNV. n= 25-56 eyes. **c** Quantification of vascular leakage area after laser-induced CNV. n= 25-56 eyes. **d** Representative images of laser-induced CNV stained with isolectin B4 in RPE/choroidal flat mounts. Scale bar: 100 µm. **e** Quantification of laser-induced CNV area in RPE/choroidal flat mounts. n= 17-38 RPE/choroids. **f** Pro-angiogenic growth factor levels in retinas of naïve and lasered mice at indicated time points. n= 8 eyes. **g** Pro-angiogenic growth factor levels in RPE/choroids of naïve and lasered mice at indicated time points. n= 8 eyes. Data are presented as mean ± SEM. Linear mixed model was used for statistical analyses; * P< 0.05, ** P<0.01, *** P≤ 0.001.
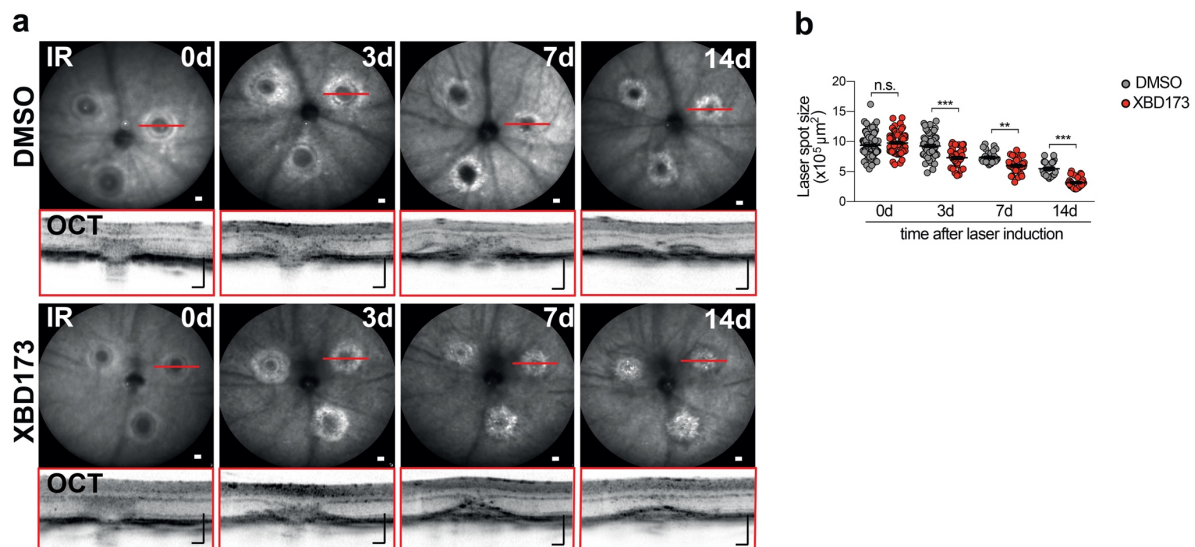
Figure 15: XBD173 attenuates laser lesion size and promotes wound healing. a Representative infrared (IR) fundus images at indicated time points post laser injury. Lower panel shows OCT scan from one laser spot marked by a red line. Scale bar: 200 µm. **b** Quantification of laser spot size. n= 26-106 eyes. n.s., not significant. Data are presented as mean ± SEM. Linear mixed model was used for statistical analyses; ** P<0.01 and *** P≤ 0.001.

3.2 Effects of microglia-specific TSPO-KO on laser-induced CNV

3.2.1 Validation of microglia-specific TSPO-KO

Since we demonstrated a protective and immunomodulatory effect of XBD173 treatment in the mouse model of laser-induced CNV, we next assessed the direct function of TSPO in retinal immune cells. For this, we generated microglia-specific conditional TSPO-KO mice (referred to as TSPO$^{\Delta MG}$) using the tamoxifen inducible Cre-*LoxP* system. TSPO$^{fl/fl}$ mice (Sileikyte et al., 2014) carrying *loxP* sites flanking exons 2 and 3 of the *Tspo* locus were crossed with mice heterozygous for *Cre* recombinase driven by microglia/macrophage-specific Cx3cr1 promoter (Cx3cr1^{CreERT2}) (Yona et al., 2013). As CX3CR1 is expressed by both microglia and macrophages, tamoxifen was applied four weeks before laser photocoagulation. This allows specific targeting of microglia based on their greater longevity and limited self-renewal when compared to the infiltrating myeloid cells (Bruttger et al., 2015).

Next, we assessed TSPO expression in the retina and RPE/choroid prepared from tamoxifen-treated TSPO$^{fl/fl}$ and TSPO$^{\Delta MG}$ mice by two different methods. First, successful recombination at the *Tspo* locus was confirmed by PCR (Figure 16a). Second, the absence of TSPO protein in the retina were confirmed by SDS-PAGE and Western blotting (Figure 16b). However, microglia comprise only 0.2 % of total retinal cells and other glia cells such as Müller cells

and astrocytes also express TSPO, that mask the microglial TSPO-KO efficiency in total retinal lysates. Thus, we also validated the microglia-specific TSPO-KO in primary microglia isolated from TSPO$^{fl/fl}$ and TSPO$^{\Delta MG}$ mice using PCR (Figure 16c) and Western blot (Figure 16d).
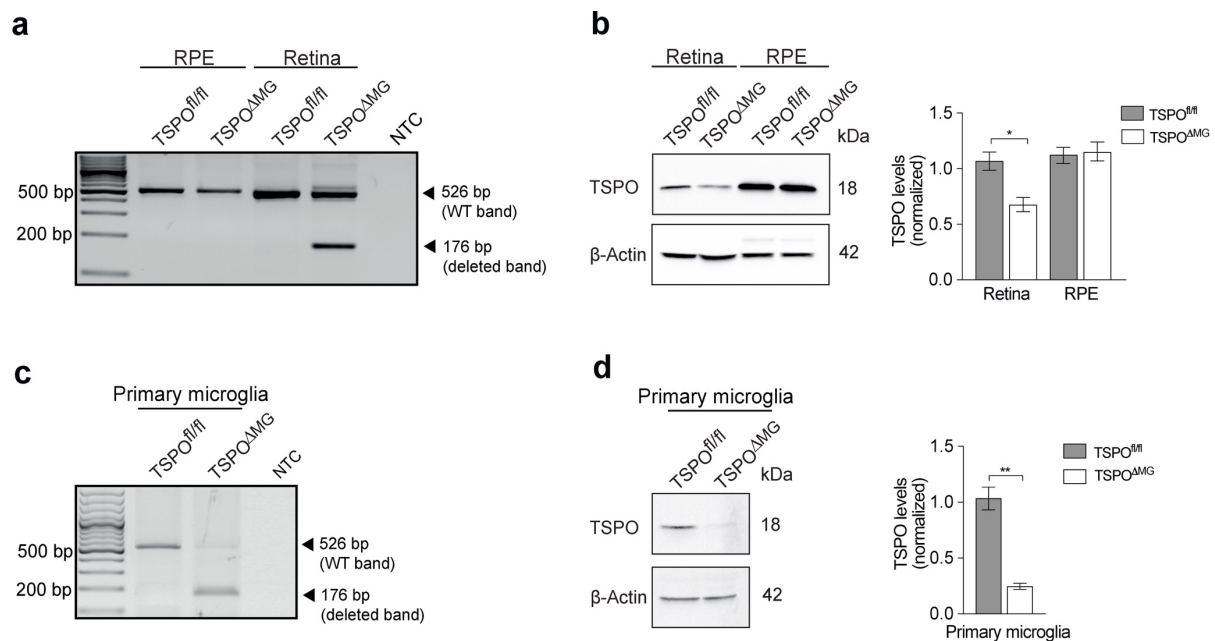
Figure 16: Validation of microglia-specific TSPO knockout. a, c Genomic PCR products spanning exon 1 and 4 of *Tspo* from retina or RPE/choroid **(a)** or from isolated primary microglia **(c)**. WT band, 526 bp; *Tspo* deleted band, 176 bp; NTC, no template control. **b, d** TSPO protein levels from total retina or RPE/choroid lysates **(b)** or from isolated primary microglia **(d)** and densitometric analysis of Western blots. TSPO signals were normalized to β-Actin. n= 3 independent experiments or retinas and RPE/choroids from three independent experiments. Data are presented as mean ± SEM; unpaired two-tailed Student's *t* test *$P < 0.05$ and **$P < 0.01$.

3.2.2 Characterization of TSPO-deficient microglia

Microglia-specific TSPO-KO mice were phenotypically unremarkable when compared with control mice. Notably, microglia from TSPO$^{\Delta MG}$ mice did also not show obvious morphological differences in their ramification or branching network compared with TSPO$^{fl/fl}$ mice (Figure 17).
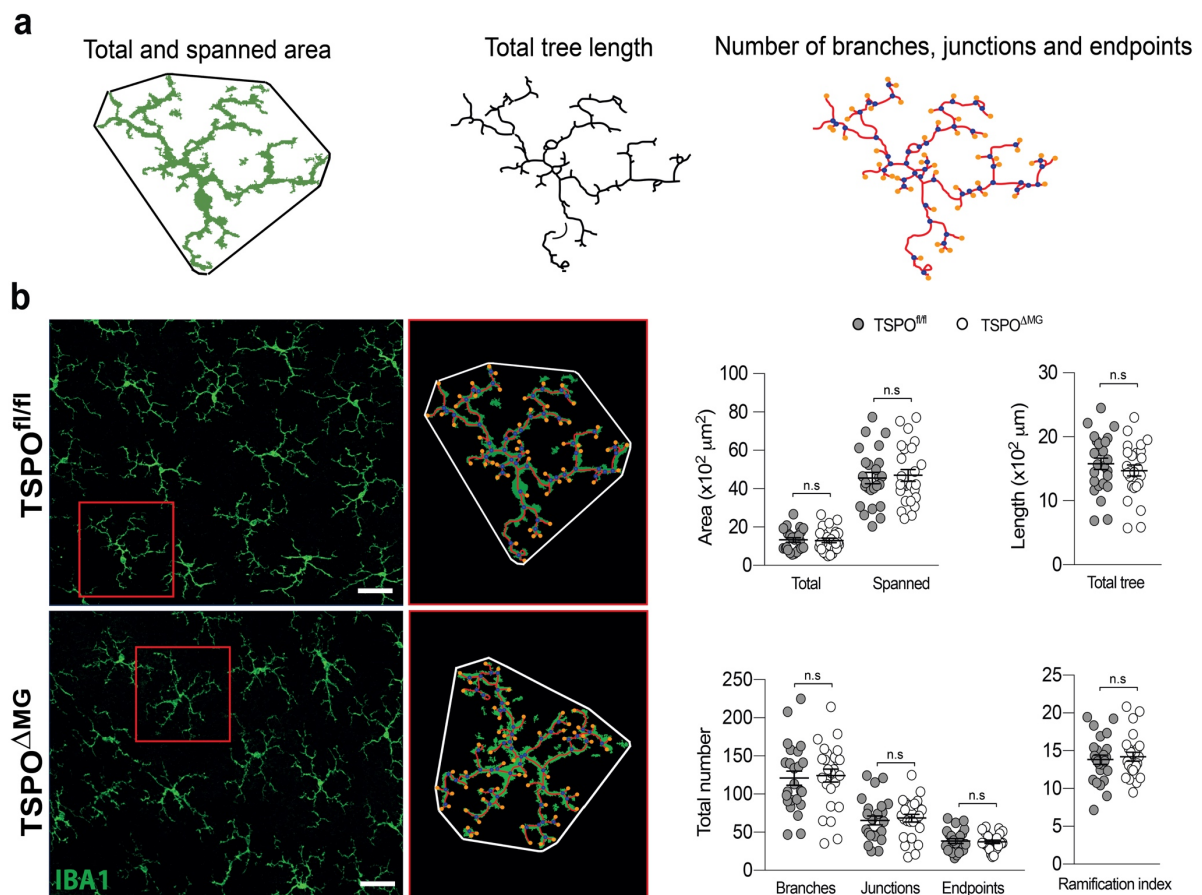
Figure 17: Microglia of TSPO-KO mice exhibit a normal phenotype. a Analysis of microglia phenotype in retinal flat mounts. Three morphological parameters were analyzed: 1) total (area of green arbor) and spanned area (area circumscribed by the polygonal object defined by connecting the outer points of the dendritic arbor (green)); 2) total tree length (sum of all dendritic segments identified in the skeletonized arbor); 3) number of branches (blue dots), junctions (points where more than two branches meet, blue dots) and endpoints (orange dots) (identified in a skeletonized rendition of the arbor). **b** Skeleton analysis of microglia morphologies in Iba1-stained retinal flat mounts. Scale bar: 50 µm. Original photomicrographs (left panel) and skeletons (green) with associated convex hulls (white polygonal) (right panel). Data are presented as mean ± SEM. n= 25 microglia cells from individual retinas, unpaired two-tailed Student's *t* test. n.s., not significant.

Since TSPO may be involved in basic mitochondrial functions (Gatliff et al., 2014; Liu et al., 2017), we next analyzed the mitochondrial network, the mitochondrial membrane potential (MMP) and cellular ATP levels (Figure 18). Confocal image analysis of the mitochondrial network in TSPO$^{\Delta MG}$ microglia showed no mitochondrial fragmentation or other alterations in morphology compared to TSPO$^{fl/fl}$ microglia, where TSPO co-localized with mitochondria (Figure 18a). Interestingly, unstimulated TSPO$^{\Delta MG}$ microglia showed a slight hyperpolarization of the MMP compared to TSPO$^{fl/fl}$ cells, suggesting an increased activity of the ETC (Figure 18b). However, after stimulated phagocytosis of photoreceptor cell debris, the MMP was slightly reduced in both TSPO$^{\Delta MG}$ and TSPO$^{fl/fl}$ cells (Figure 18b). Microglia from TSPO$^{\Delta MG}$ mice showed no differences in cellular ATP levels compared to TSPO$^{fl/fl}$

microglia neither in untreated conditions nor after stimulation with debris (Figure 18c). Inhibition of glycolysis through the glucose derivative 2-Deoxy-D-glucose (2-DG) showed that both resting and stimulated microglia depend to some degree on glycolysis for ATP generation (Figure 18d). However, inhibition of the mitochondrial ATP synthase by oligomycin A treatment showed that ATP is mainly generated through mitochondrial respiration (Figure 18e). Importantly, there was no difference between WT and TSPO-KO microglia. Thus, TSPO-deficient microglia are perfectly capable of generating ATP through mitochondrial respiration further indicating unimpaired mitochondrial function. Taken together, these data implicate that TSPO is not required for mitochondrial integrity, health or energy metabolism in unstimulated or stimulated microglia.
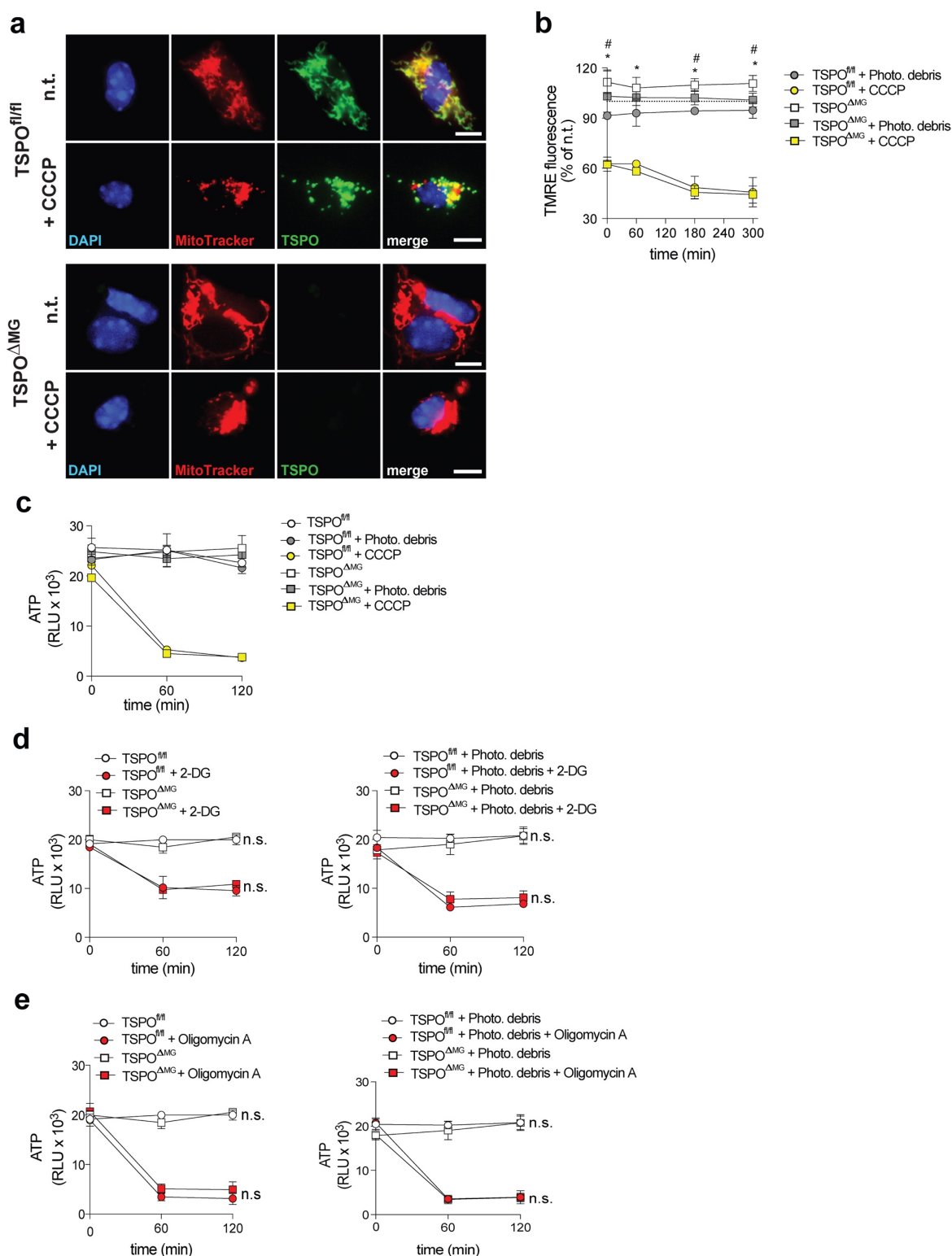
Figure 18: TSPO-KO microglia exhibit a normal energy homeostasis. a Representative images of TSPO- and Mitotracker Red-stained mitochondria in TSPO$^{fl/fl}$ and TSPO$^{\Delta MG}$ primary microglia. Nuclei were counterstained with DAPI. Scale bar: 6 μm. **b** Analysis of mitochondrial membrane potential in TSPO$^{fl/fl}$ and TSPO$^{\Delta MG}$ primary microglia. Where indicated, TSPO$^{fl/fl}$ and TSPO$^{\Delta MG}$ primary microglia were stimulated with photoreceptor cell debris and mitochondrial membrane potential was impaired with CCCP as a positive control. n= 4 independent experiments. **c-e** Analysis of total ATP levels. Where indicated, primary microglia from TSPO$^{fl/fl}$ and TSPO$^{\Delta MG}$ mice were stimulated with photoreceptor cell debris and treated either with 200 μM CCCP to impair the mitochondrial membrane potential **(c)**, 500 μM 2-Deoxy-D-glucose (2-DG) to inhibit glycolysis **(d)** or 10 μM oligomycin A to inhibit complex V of the ETC **(e)**. n= 3 independent experiments. Data are presented as mean ± SEM; unpaired two-tailed Student's *t* test; *$P < 0.01$ when TSPO$^{fl/fl}$ compared to TSPO$^{fl/fl}$ + Photo. debris; #$P < 0.01$ when TSPO$^{fl/fl}$ compared to TSPO$^{\Delta MG}$. n.s., not significant; n.t., non-treated.

3.2.3 TSPO-KO in microglia attenuates their reactivity in laser-damaged retinas and RPE/choroids

We next determined if the absence of TSPO in microglia affects their behavior in the laser-CNV model. TSPO[ΔMG] retinas showed less infiltration of Iba1^{+} cells and reduced reactivity in the laser lesions at all time points analyzed compared to TSPO^{fl/fl} mice (Figure 19a-c). The increased expression of *Cd68* and *Tspo* was also prevented in TSPO[ΔMG] mice (Figure 19d). Notably, naïve TSPO[ΔMG] mice had lower LMW TSPO levels in the retina than TSPO^{fl/fl} mice and the lesion-induced formation of HMW1 TSPO was only detected in TSPO^{fl/fl} but not in TSPO[ΔMG] mice (Figure 19e, f). Furthermore, the laser-induced secretion of CCL2 and IL-6 was prevented in TSPO[ΔMG] retinas, phenocopying the effects of XBD173 treatment (Figure 19g). Again, levels of IL-1β and TNF did not change in the retina after laser damage (Figure 19g).
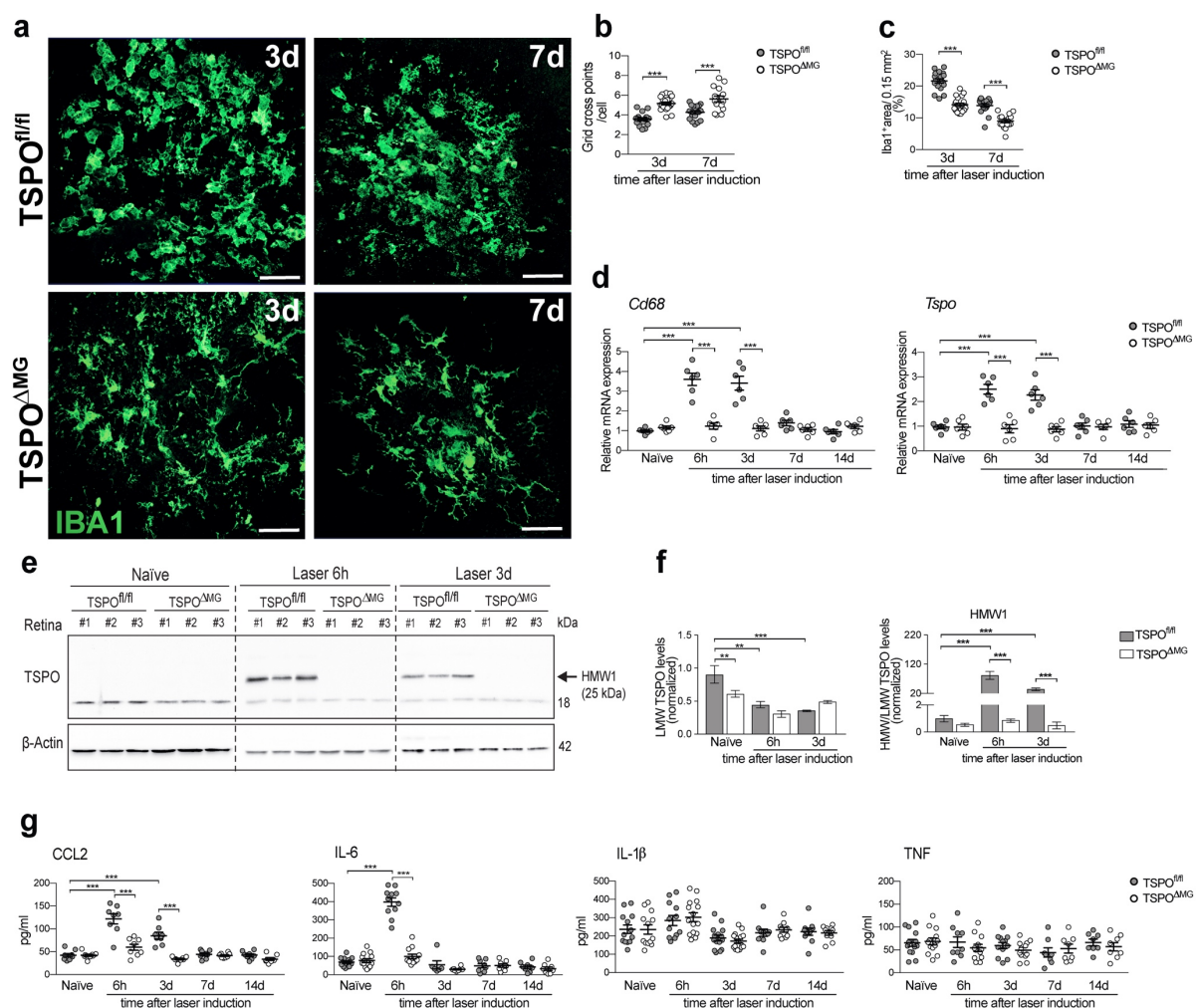
Figure 19: Absence of TSPO dampens mononuclear phagocyte reactivity in the retina after laser-induced CNV in mice. a Representative images show accumulation of Iba1^{+} cells within the laser lesion in retinal flat mounts. Scale bar: 50 μm. **b** Analysis of Iba1^{+} cell morphology within laser lesions. n= 18-21 spots. **c** Quantification of Iba1^{+} area of the laser lesions. n= 18-21 spots. **d** *Cd68* and *Tspo* mRNA levels in retina from

TSPO$^{fl/fl}$ and TSPO$^{\Delta MG}$ mice at indicated time points after laser-induced CNV. n= 6 retinas. **e** TSPO protein levels in whole retinal lysates of naïve and lasered TSPO$^{fl/fl}$ and TSPO$^{\Delta MG}$ mice at indicated time points. Each lane represents an individual retina. Dotted line indicates individual blots, which were processed in parallel. **f** Densitometric analysis of Western blots. LMW TSPO (18 kDa) signals were normalized to β-Actin and HMW:LMW TSPO ratio determined. n= 6 retinas from two independent experiments. LMW, lower molecular weight; HMW, higher molecular weight. **g** Pro-inflammatory cytokine levels in retinas of naïve and lasered TSPO$^{fl/fl}$ and TSPO$^{\Delta MG}$ mice at indicated time points. CCL2 (n= 8 retinas); IL-6, IL-1β and TNF (n= 8-13 retinas). Data are presented as mean ± SEM. Linear mixed model was used for statistical analyses; ** $P<0.01$ and *** $P\leq 0.001$.

Similar to the retina, the analysis of phagocytes in RPE/choroidal flat mounts showed reduced Iba1^{+} cell infiltration and reactivity in TSPO$^{\Delta MG}$ mice compared to TSPO$^{fl/fl}$ mice (Figure 20a-c). Laser-induced *Cd68* and *Tspo* expression were also prevented in TSPO$^{\Delta MG}$ mice but not in TSPO$^{fl/fl}$ mice (Figure 20d). In addition, laser-induced formation of HMW1 and HMW2 TSPO were absent in the RPE/choroid of TSPO$^{\Delta MG}$ mice (Figure 20e, f). Moreover, laser-induced secretion of CCL2, IL-6, and IL-1β in the RPE/choroid was blocked in TSPO$^{\Delta MG}$ mice (Figure 20g). Together, these data demonstrate that microglia-specific TSPO-KO prevented laser-induced MNP reactivity and ameliorates inflammation.
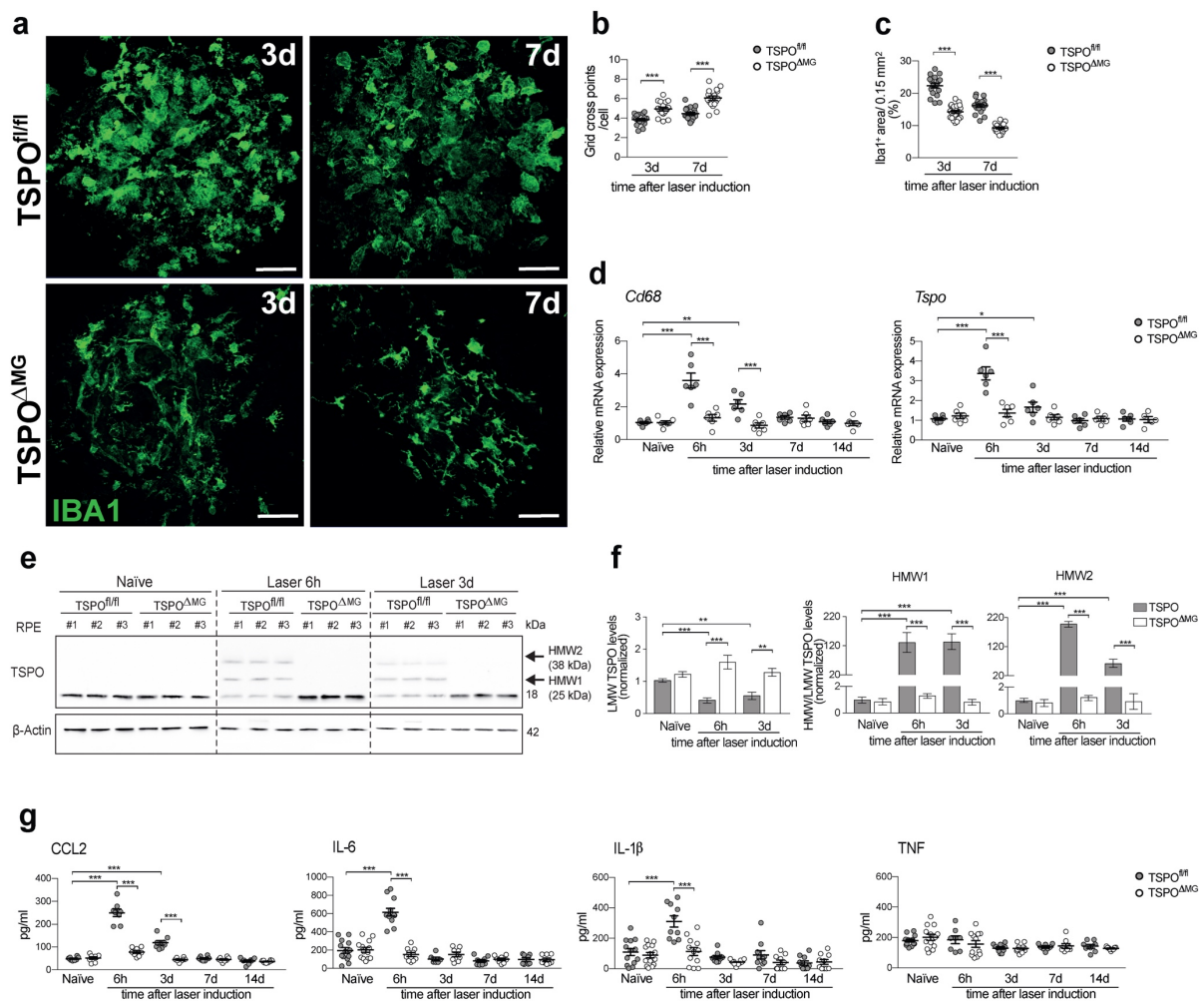
Figure 20: Absence of TSPO dampens mononuclear phagocyte reactivity in the RPE/choroid after laser-induced CNV in mice. a Representative images of Iba1$^+$ cells within the laser lesion in RPE/choroidal flat mounts. Scale bar: 50 μm. **b** Analysis of Iba1$^+$ cell morphology within laser lesions. n= 18 spots. **c** Quantification of Iba1$^+$ area of the laser lesions. n= 18 spots. **d** *Cd68* and *Tspo* mRNA levels in RPE/choroid from TSPO$^{fl/fl}$ and TSPO$^{\Delta MG}$ mice at indicated time points after laser-induced CNV. n= 6 RPE/choroids. **e** Western blots showing TSPO expression in whole RPE/choroidal lysates of naïve and lasered TSPO$^{fl/fl}$ and TSPO$^{\Delta MG}$ mice at indicated time points. Each lane represents an individual retina. Dotted line indicates individual blots, which were processed in parallel. **f** Densitometric analysis of Western blots. LMW TSPO (18 kDa) signals were normalized to β-Actin and HMW:LMW TSPO ratio determined. n= 6 RPE/choroids from two independent experiments. LMW, lower molecular weight; HMW, higher molecular weight. **g** Pro-inflammatory cytokine levels in RPE/choroids of naïve and lasered TSPO$^{fl/fl}$ and TSPO$^{\Delta MG}$ mice. CCL2 (n= 8 RPE/choroids); IL-6, IL-1β and TNF (n= 8-13 RPE/choroids). Data are presented as mean ± SEM. Linear mixed model was used for statistical analyses; * P<0.05, ** P<0.01 and *** P≤ 0.001.

3.2.4 TSPO deficiency blocks stimulation-induced ROS production in primary microglia

When analyzing extracellular ROS production of microglia after different stimuli, we found that ROS production after stimulation with the PKC activator PMA was not affected upon genomic deletion of TSPO specifically in these cells, whereas their capacity to produce this neurotoxin after stimulation with photoreceptor cell debris was completely abolished (Figure

21a). Notably, XBD173 treatment did not further reduce ROS levels in TSPO$^{\Delta MG}$ microglia suggesting a TSPO-specific inhibitory effect on ROS production (Figure 21b). As TSPO is a mitochondrial protein, we also analyzed the effects of TSPO deficiency on ROS levels originating from the mitochondria. Here, no differences in cytosolic ROS or ROS production into the mitochondrial matrix at basal levels or after stimulation were found in TSPO$^{\Delta MG}$ versus TSPO$^{fl/fl}$ microglia (Figure 21c, d). These data indicate that TSPO is necessary for microglial production of extracellular and phagosomal ROS upon stimulation.
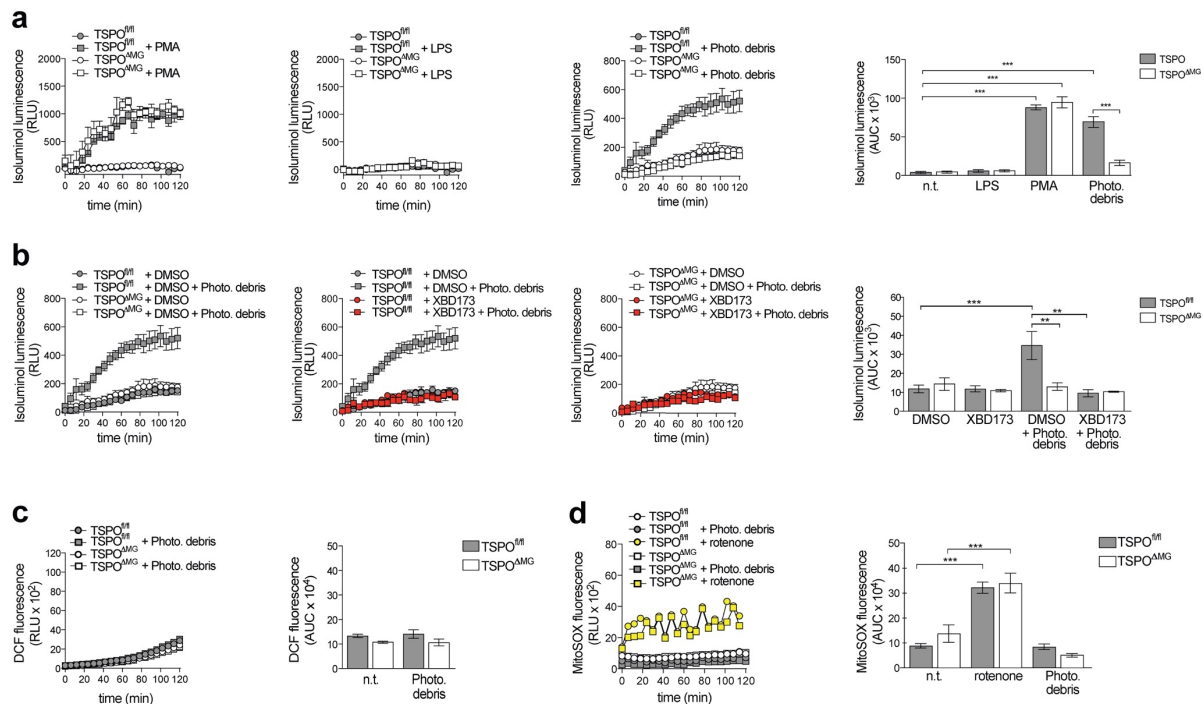
Figure 21: TSPO-KO blocks stimulation-induced extracellular ROS production in primary microglia.
a Quantification of extracellular ROS production by primary microglia from TSPO$^{fl/fl}$ and TSPO$^{\Delta MG}$ mice. Primary microglia were stimulated with LPS, PMA or photoreceptor cell debris. Kinetics of ROS production and the area under the curve (AUC) are shown. n= 10 independent experiments. **b** Quantification of stimulation-induced extracellular ROS production by primary microglia from TSPO$^{fl/fl}$ and TSPO$^{\Delta MG}$ mice treated with XBD173. Kinetics of ROS production and the area under the curve (AUC) are shown. n= 10 independent experiments, (+ XBD173, n= 3 independent experiments). **c** Cytosolic ROS production in TSPO$^{fl/fl}$ and TSPO$^{\Delta MG}$ mice. Primary microglia were stimulated photoreceptor cell debris. Kinetics of ROS production and the area under the curve (AUC) are shown. n= 4 independent experiments. **d** Matrix-derived ROS production in TSPO$^{fl/fl}$ and TSPO$^{\Delta MG}$ microglia. Primary microglia were stimulated with photoreceptor cell debris or rotenone as a positive control to induce ROS production into the mitochondrial matrix. Kinetics of ROS production and the area under the curve (AUC) are shown. n= 4 independent experiments. Data are presented as mean ± SEM; unpaired two-tailed Student's *t* test, **$P< 0.01$ and ***$P< 0.001$.

3.2.5 TSPO-KO in microglia prevents laser-induced vascular leakage and CNV

Since deletion of TSPO in microglia strongly reduced their inflammatory potential, we invested their effects on vascular leakage and CNV. TSPO$^{fl/fl}$ mice showed typical laser-induced vascular leakage that was strongly reduced in TSPO$^{\Delta MG}$ mice at all analyzed time

points (Figure 22a-c) and the overall CNV size was significantly smaller in TSPO$^{\Delta MG}$ mice than in controls (Figure 22d, e). While a prominent laser-induced secretion of VEGF-A, ANG-1, ANG-2 and IGF-1 was found in the retinas and RPE/choroids of TSPO$^{fl/fl}$ mice, only basal levels of these pro-angiogenic factors were detected in TSPO$^{\Delta MG}$ mice (Figure 22f, g).
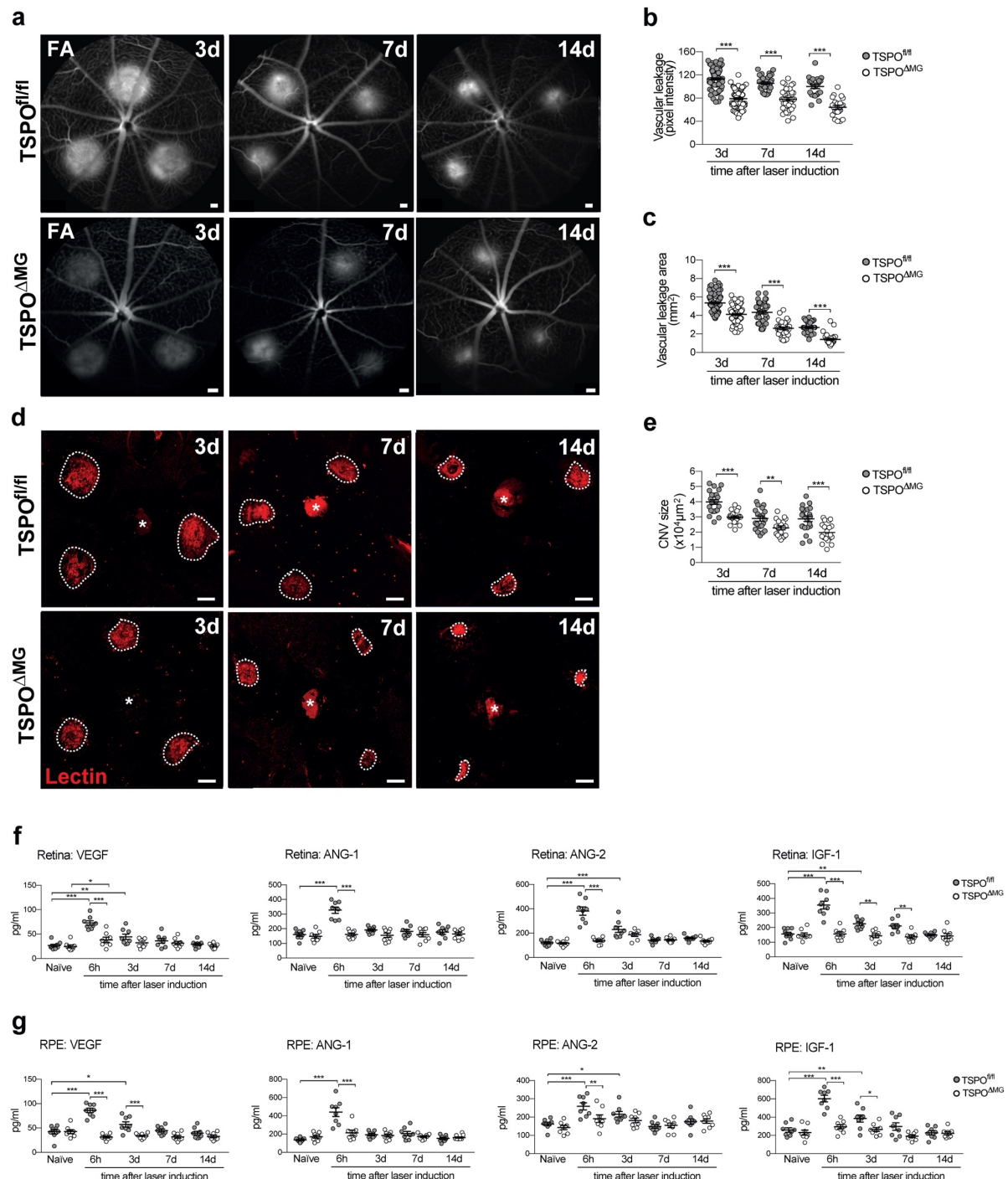
Figure 22: Absence of TSPO inhibits laser-induced vascular leakage and pathological CNV in mice.
a Representative late phase FFA images at indicated time points post laser injury. Scale bar: 200 μm; FA, fluorescein angiography. **b** Quantification of vascular leakage intensity after laser-induced CNV. n= 22-85 eyes. **c** Quantification of vascular leakage area after laser-induced CNV. n= 30-91 eyes. **d** Representative images of laser-induced CNV stained with isolectin B4 in RPE/choroidal flat mounts. Scale bar: 100 μm. **e** Quantification of laser-induced CNV area in RPE/choroidal flat mounts. n= 22 RPE/choroids. **f** Pro-angiogenic growth factor levels in retinas of naïve and lasered TSPO$^{fl/fl}$ and TSPO$^{\Delta MG}$ mice at indicated time

points. n= 8 retinas. **g** Pro-angiogenic growth factor levels in RPE/choroids of naïve and lasered TSPO^{fl/fl} and TSPO[ΔMG] mice at indicated time points. n= 8 RPE/choroids. Data are presented as mean ± SEM. Linear mixed model was used for statistical analyses; *$P < 0.05$, **$P < 0.01$ and ***$P ≤ 0.001$.

Finally, we assessed the wound healing process in TSPO[ΔMG] mice. These mice showed attenuated laser lesion sizes and significantly reduced fibrosis compared to TSPO^{fl/fl} mice (Figure 23a, b). Thus, TSPO-KO in retinal microglia considerably reduced inflammation-associated vascular leakage and neovascular lesions.
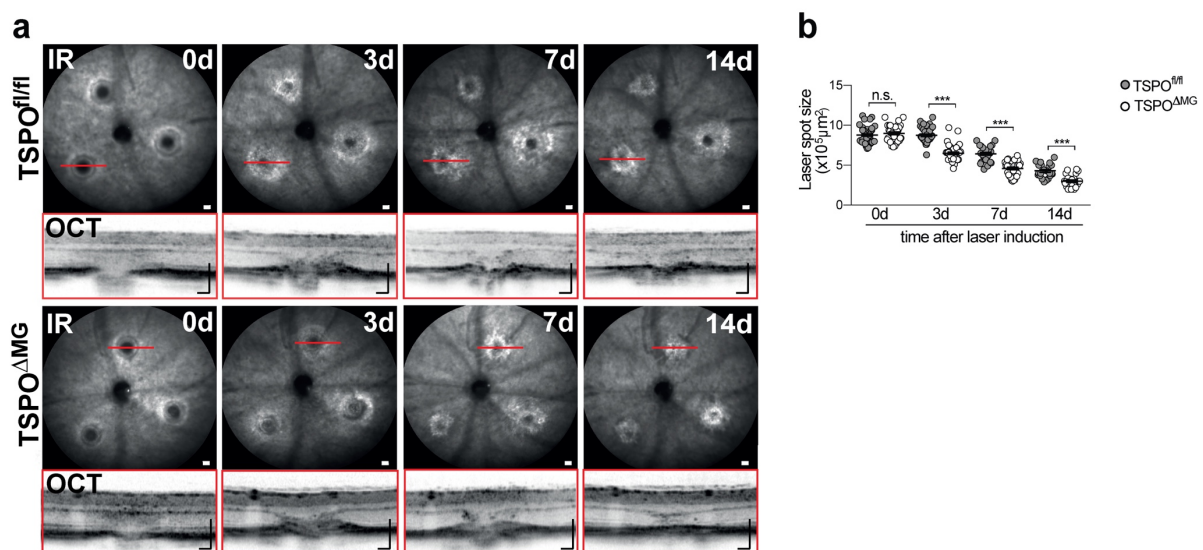
Figure 23: Microglia-specific TSPO-KO attenuates laser lesion size and promotes wound healing. **a** Representative IR fundus images at indicated time points post laser injury. Lower panel shows OCT scan from one laser spot marked by a red line. Scale bars: 200 µm. **b** Quantification of laser spot size. n= 25-45 eyes. Data are presented as mean ± SEM. Linear mixed model was used for statistical analyses; ***$P ≤ 0.001$. n.s., not significant.

3.3 TSPO as a regulator of phagocytic ROS production in the retina

3.3.1 Targeting TSPO reduces laser-induced *Nox1* expression

Since our observations from XBD173 treatment and microglia-specific TSPO-KO indicate a novel role for TSPO in phagocyte ROS production, we further evaluated the molecular pathways. The enzyme family of NADPH oxidases (NOX) is mainly responsible for regulated ROS production and consists of the membrane-bound enzymes NOX1, NOX2, NOX3, NOX4, NOX5 and the dual oxidases DUOX1 and DUOX2. All isoforms transfer electrons from NADPH across biological membranes to molecular oxygen generating superoxide ($O_2^{.-}$) and subsequently H_2O_2 (Bedard and Krause, 2007).

Although NOX2 is often considered as the major source of ROS in phagocytes, including macrophages, we assessed the expression pattern of all NOX isotypes in the retina and RPE. Since NOX5 is absent in rodents (Cheng et al., 2001), its expression was not addressed in this study. In both tissues, all NOX family members except *Nox3*, which is mainly found in the inner ear (Banfi et al., 2004), were expressed at low basal levels (Figure 24a). Interestingly, only *Nox1* expression was strongly increased in the retina and RPE 6h after laser-induced injury while the expression levels of *Nox2*, *Nox4*, *Duox1* or *Duox2* did not change compared with naïve mice (Figure 24b, c). Notably, the laser-induced expression of *Nox1* was not only abolished after XBD173 treatment (Figure 24b, c) but also in TSPO$^{\Delta MG}$ mice after laser-CNV (Figure 25a, b). These findings indicate that in retinal microglia NOX1 could be the major source of ROS after laser-induced CNV.
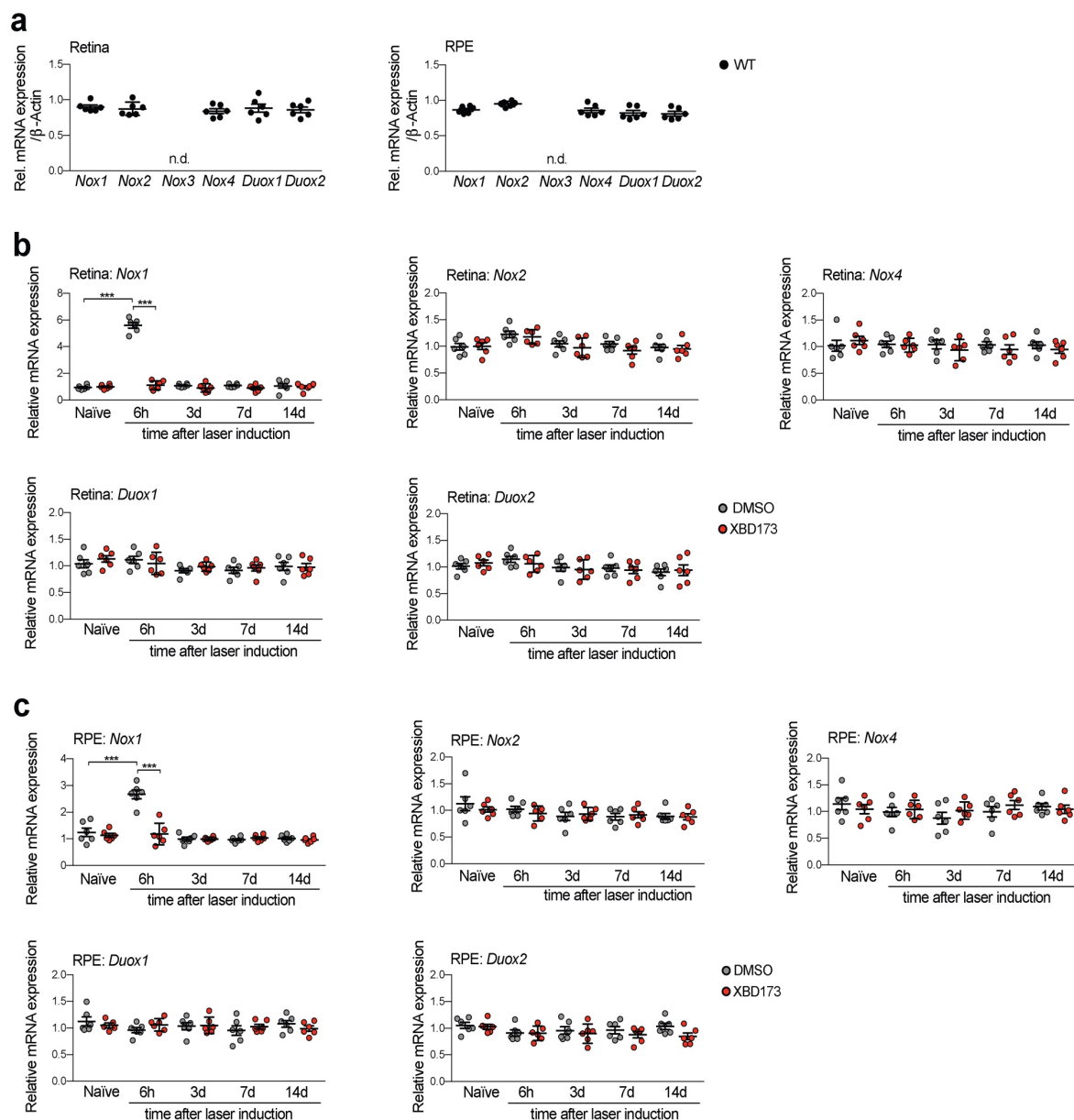
Figure 24: XBD173 reduces laser-induced *NADPH oxidase 1 (Nox1)* expression. a Relative expression of

Nox family members in WT retinas and RPE/choroids. Transcript levels for each enzyme were normalized to *β-Actin*. n= 6 retinas/RPEs. **b-c** Laser-induced gene expression of *Nox* enzymes in retina **(b)** and RPE/choroid **(c)** of DMSO- or XBD173 treated mice. Transcript levels for each enzyme were normalized to *β-Actin*. n= 6 retinas/RPEs. Data are presented as mean ± SEM. Linear mixed model was used for statistical analyses; ***$P \leq$ 0.001. N.d., not detected.
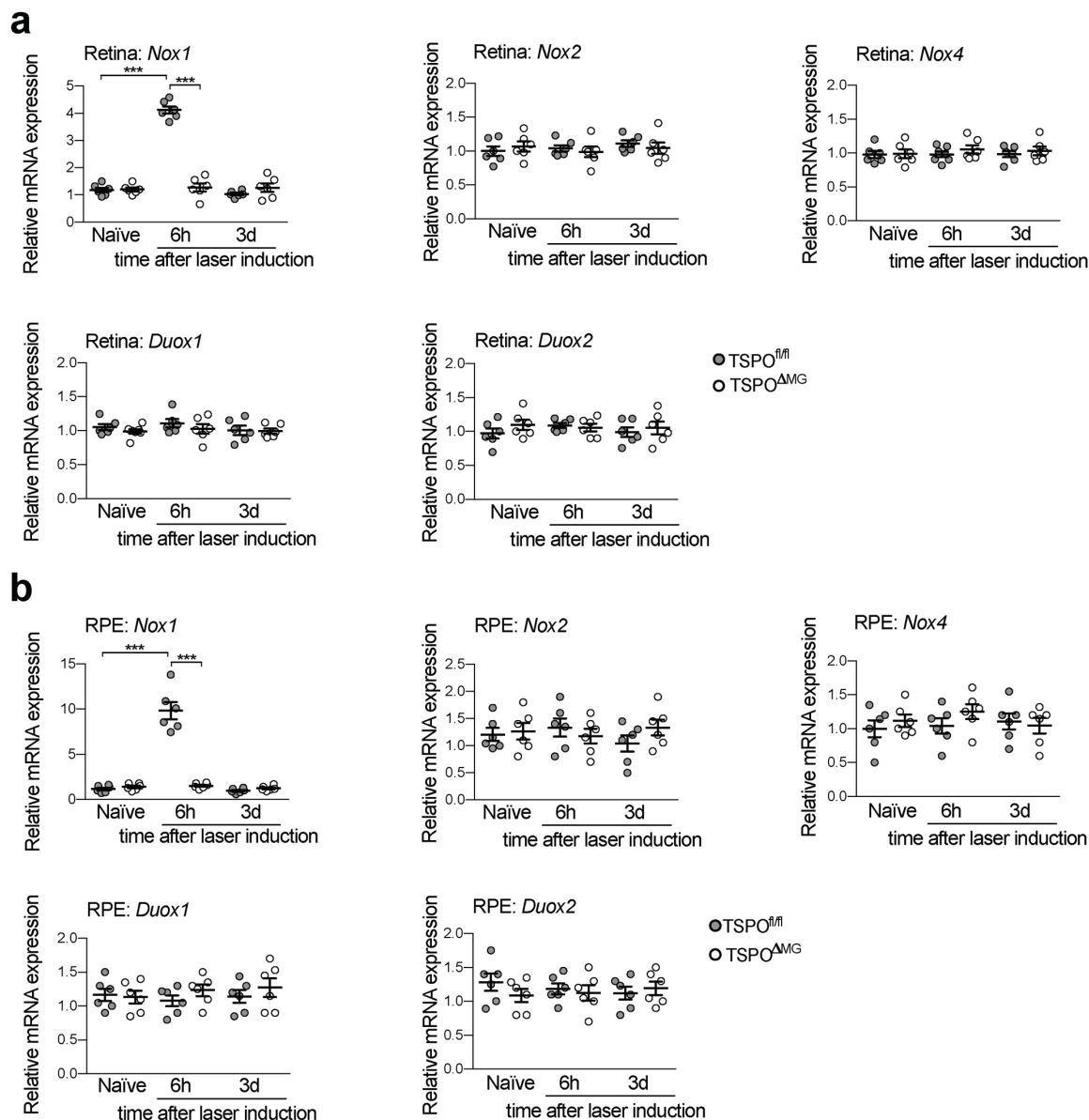
Figure 25: Microglia-specific TSPO-KO reduces laser-induced *Nox1* expression. **a-b** Laser-induced gene expression of *Nox* enzymes in retina **(a)** and RPE/choroid **(b)** of TSPO^{fl/fl} and TSPO[ΔMG] mice. Transcript levels for each enzyme were normalized to *β-Actin*. n= 6 retinas/RPEs. Data are presented as mean ± SEM. Linear mixed model was used for statistical analyses; ***$P \leq$ 0.001.

3.3.2 TSPO triggers ROS production in microglia via NOX1

To validate the findings above, extracellular microglial ROS production was analyzed in different Nox-deficient mice. Microglia deficient for p22[phox] (p22[phox]-KO), the common

catalytic subunit of NOX1-4, were lacking stimulation-induced extracellular ROS production (Figure 26a). Thus, DUOX1 and DUOX2 can be excluded as ROS sources as both are not dependent on p22^{phox} (Lambeth et al., 2007). When analyzing Nox1-deficient microglia, no stimulation-induced ROS production was detected (Figure 26b), while microglia from Nox2- and Nox4-deficient mice were still able to produce stimulation-induced extracellular ROS, which was abolished after XBD173 treatment (Figure 26c, d). These results indicate that NOX1 is the key enzyme for ROS production in retinal phagocytes and critically depends on the presence of TSPO.
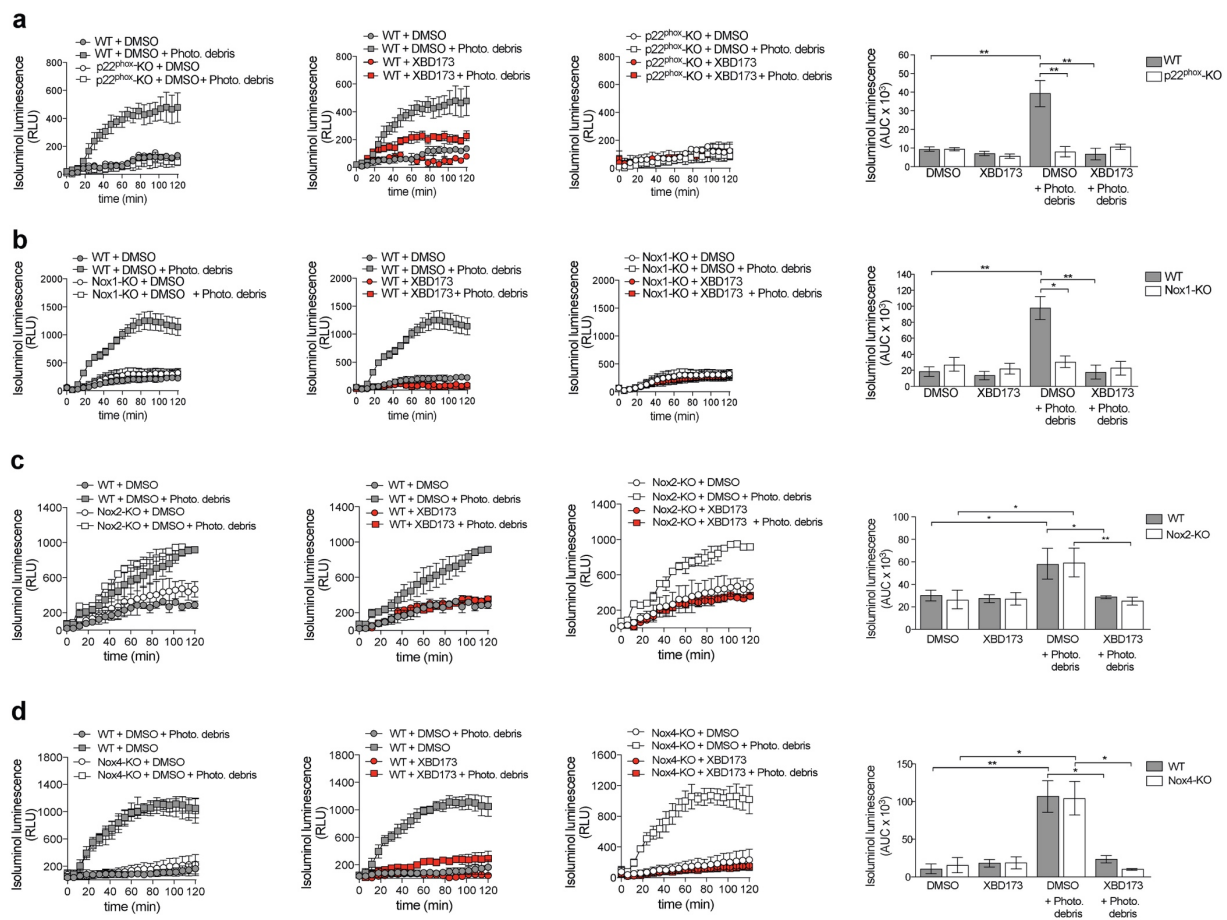
Figure 26: ROS production by primary microglia involves TSPO-dependent NOX1 activation.
a-d Quantification of extracellular ROS production by primary microglia from WT and p22^{phox}-KO mice **(a)**, Nox1-KO mice **(b)**, Nox2-KO mice **(c)** and Nox4-KO mice **(d)**. Kinetics of ROS production and the area under the curve (AUC) are shown. Where indicated, primary microglia were stimulated with photoreceptor cell debris. n= 3 independent experiments. Data are presented as mean ± SEM; unpaired two-tailed Student's t test; *$P < 0.05$ and ** $P < 0.01$.

3.3.3 TSPO associated increase in cytosolic calcium is essential for NOX1-derived extracellular ROS production

Next, we further investigated the functional coupling between TSPO and NOX1 in microglia. Calcium (Ca^{2+}) is an important second messenger that regulates a variety of cellular functions (Berridge, 2012) and is responsible for the activation of ROS-generating enzymes (Gordeeva et al., 2003). As TSPO is assumed to be involved in Ca^{2+} homeostasis and to play a potential role in redox homeostasis, we first analyzed the effects of modulating Ca^{2+} levels on ROS production. Microglia from WT (Figure 27a), TSPO$^{fl/fl}$ and TSPO$^{\Delta MG}$ mice (Figure 27b) completely failed to produce ROS in the absence of extracellular Ca^{2+}. Increasing cytosolic Ca^{2+} with the Ca^{2+}-ionophore ionomycin was sufficient to induce extracellular ROS production in non-stimulated microglia (Figure 27a, b). This indicates that the influx of extracellular Ca^{2+} is essential for the induction of NOX1-dependent ROS production in response to stimulation with photoreceptor debris. Interestingly, not only stimulus-dependent NOX1 activity but also increased *Nox1* expression in primary microglia was detected after phagocytosis of photoreceptor cell debris, which was strongly reduced by XBD173 or in microglia-specific TSPO-KO (Figure 27c). Notably, this upregulation of *Nox1* gene expression was also depended on extracellular Ca^{2+} levels (Figure 27c), indicating that the increased ROS production is, at least in part, due to increased *Nox1* expression in primary microglia.
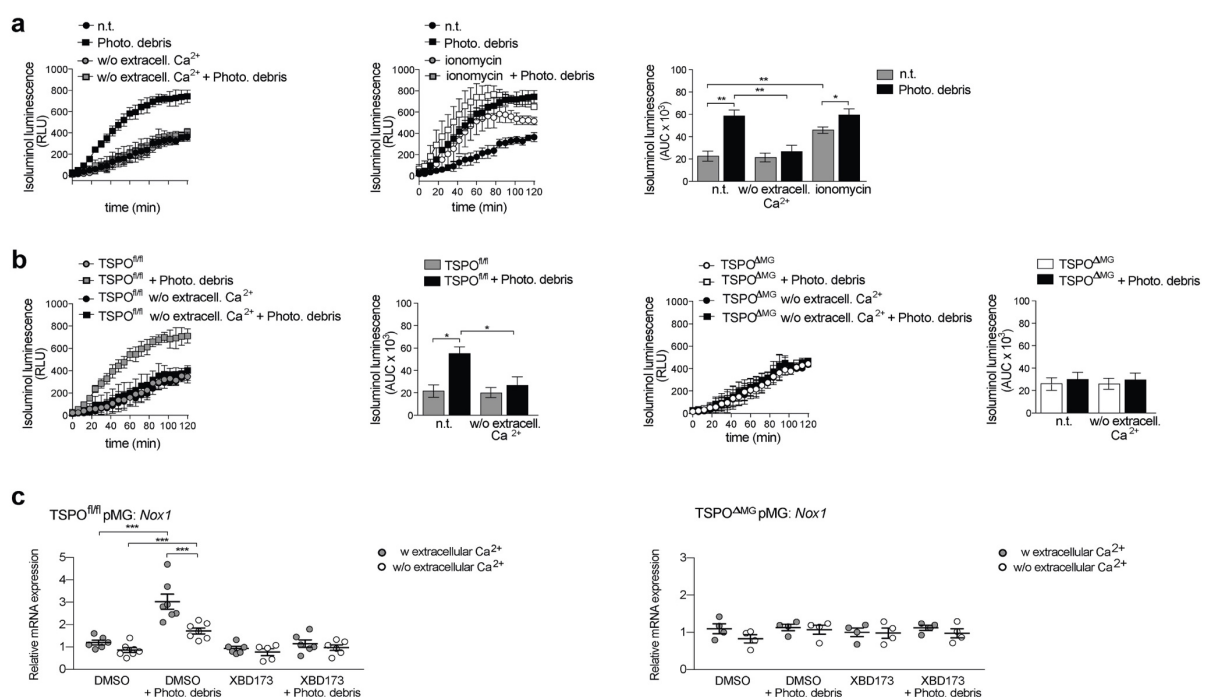
Figure 27: Lack of extracellular Ca^{2+} reduces NOX1 activity and expression in primary microglia.
a-b Quantification of extracellular ROS production by primary microglia from WT **(a)**, TSPO$^{fl/fl}$ and TSPO$^{\Delta MG}$

mice **(b)**. Kinetics of ROS production and the area under the curve (AUC) are shown. Where indicated, primary microglia were stimulated with photoreceptor cell debris in the presence or absence of extracellular Ca^{2+} or cytosolic Ca^{2+} was increased with the Ca^{2+} ionophore ionomycin as a positive control. n= 4 **(a)**, n= 3 **(b)** independent experiments. **c** *Nox1* mRNA levels in pMG from TSPO$^{fl/fl}$ and TSPO$^{\Delta MG}$ mice 6h after stimulation with photoreceptor cell debris in the presence or absence of extracellular Ca^{2+}. n= 6 for TSPO$^{fl/fl}$ pMG and n= 4 independent experiments for TSPO$^{\Delta MG}$ pMG. Data are presented as mean ± SEM; unpaired two-tailed Student's t test; **$P<$ 0.01, ***$P\leq$ 0.001. w/o, without; w, with; n.t., non-treated.

Mitochondria are not only the cellular organelles responsible for energy generation but also act as intracellular Ca^{2+} stores (Demaurex et al., 2009). Ca^{2+} storage within the mitochondrial matrix is mainly achieved by the formation of Ca^{2+} phosphate complexes (Prins and Michalak, 2011). Thus, we next analyzed cytosolic and mitochondrial Ca^{2+} levels of microglia using synthetic fluorescent Ca^{2+} indicators.

Fura-2-acetoxymethyl ester (Fura-2-AM) is a membrane permeable ratiometric fluorescent Ca^{2+} indicator that measures cytosolic Ca^{2+} levels (Figure 28a). Once it crosses the cell membranes, the AM form is hydrolyzed via cellular esterases, regenerating Fura-2. Binding of Ca^{2+} to Fura-2 causes a shift in the excitation spectrum which can be easily detected (Contreras et al., 2010). In order to measure mitochondrial Ca^{2+} levels Rhod-2-AM is used. Rhod-2-AM is also cell permeable and due to its delocalized positive charge and the negative MMP, it mainly accumulates inside the mitochondrial matrix (Figure 28a). In contrast to Fura-2, Rhod-2 responds to Ca^{2+} rises with an increase in fluorescence intensity (Contreras et al., 2010). When analyzing mitochondrial Ca^{2+} levels in primary microglia of TSPO$^{fl/fl}$ and TSPO$^{\Delta MG}$ mice, we did not detect a stimulation-induced increase in these Ca^{2+} levels (Figure 28b). Also, no difference in the basal mitochondrial Ca^{2+} levels between WT and TSPO-deficient microglia was observed (Figure 28b). In contrast, stimulated phagocytosis of primary microglia increased their cytosolic Ca^{2+} levels (Figure 28c). Notably, XBD173 prevented the stimulation-induced increase in cytosolic Ca^{2+}, as did the microglia-specific knockout of TSPO itself (Figure 28c).

These results demonstrate that the TSPO-dependent increase of cytosolic Ca^{2+} after stimulation is essential not only for *Nox1* expression but also for stimulated NOX1-dependent ROS production.
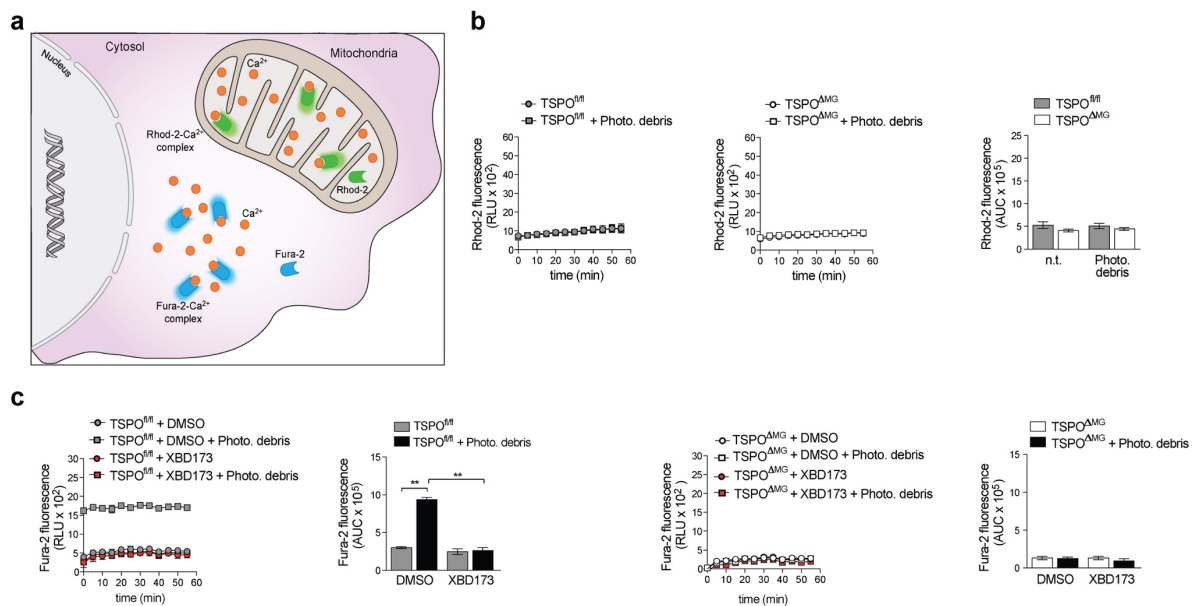
Figure 28: TSPO associated increase in cytosolic calcium is essential for NOX1-derived extracellular ROS production. a Schematic representation of different calcium detection methods. Rhod-2-AM detects calcium within mitochondria and Fura-2-AM detects cytosolic calcium levels. **b** Quantification of mitochondrial calcium levels in primary microglia from TSPO$^{fl/fl}$ and TSPO$^{\Delta MG}$ mice. Where indicated, primary microglia were stimulated with photoreceptor cell debris. n= 3 independent experiments. **c** Quantification of cytosolic calcium levels in primary microglia from TSPO$^{fl/fl}$ and TSPO$^{\Delta MG}$ mice. Where indicated, primary microglia were stimulated with photoreceptor cell debris. n= 3 independent experiments. Data are presented as mean ± SEM; unpaired two-tailed Student's t test; **P< 0.01. n.t., non-treated.

3.3.4 Microglia-derived extracellular ROS damage photoreceptor cells in a paracrine manner

Excessive ROS production is often referred to as oxidative stress and associated with damage of cellular molecules such as DNA, lipids and proteins (Lambeth and Neish, 2014; Schumacher et al., 2008). However, a slight elevation of ROS levels has important signaling functions during immunological and biological processes (Finkel, 2012; Reczek and Chandel, 2015). Thereby, not only the ROS-inducing stimuli, ROS sources and its subspecies play a role but also the compartmentalization of ROS production is an important factor that determines if it acts as a neurotoxin or signaling molecule (Kaludercic et al., 2014; Ushio-Fukai, 2009). Recognition of PAMPs by phagocytes leads to a substantial and fast increase of extracellular and phagosomal ROS production catalyzed by NOX enzymes that damage invading pathogens (Gluschko et al., 2018). Here, we identified NOX1-dependent ROS production by microglia upon stimulated phagocytosis, which takes place at the plasma membrane resulting in extracellular and phagosomal ROS. Thus, we finally investigated the paracrine potential of microglia-derived extracellular ROS as damaging neurotoxins.

For this, 661W photoreceptor cells were co-cultured in a trans-well system with primary microglia stimulated with photoreceptor cell debris to induce their extracellular ROS production. 661W cells cultured alone were used to determine the ratio of dead cells that occur during the cell harvesting for flow cytometric analysis. Here, the number of propidium iodide positive (PI^+) photoreceptor cells did not significantly increase when these cells were challenged with photoreceptor cell debris (Figure 29a, g). During co-culture with resting microglia only few PI^+ photoreceptor cells were detected via flow cytometry while cell death of photoreceptor cells tremendously increased after induction of extracellular ROS production via photoreceptor cell debris stimulation of microglia (Figure 29b, e, g). Accordingly, a strong reduction of PI^+ photoreceptor cells could be observed when co-cultured with XBD173-treated $TSPO^{fl/fl}$ microglia (Figure 29c, g), microglia deficient for TSPO (Figure 29d, g) or microglia deficient for NOX1 (Figure 29f, g), which all were incapable of producing extracellular ROS after stimulation (Figure 13b, 21c, 26b). These findings clearly indicate a paracrine damaging effect of microglia-derived extracellular ROS on photoreceptor cells.
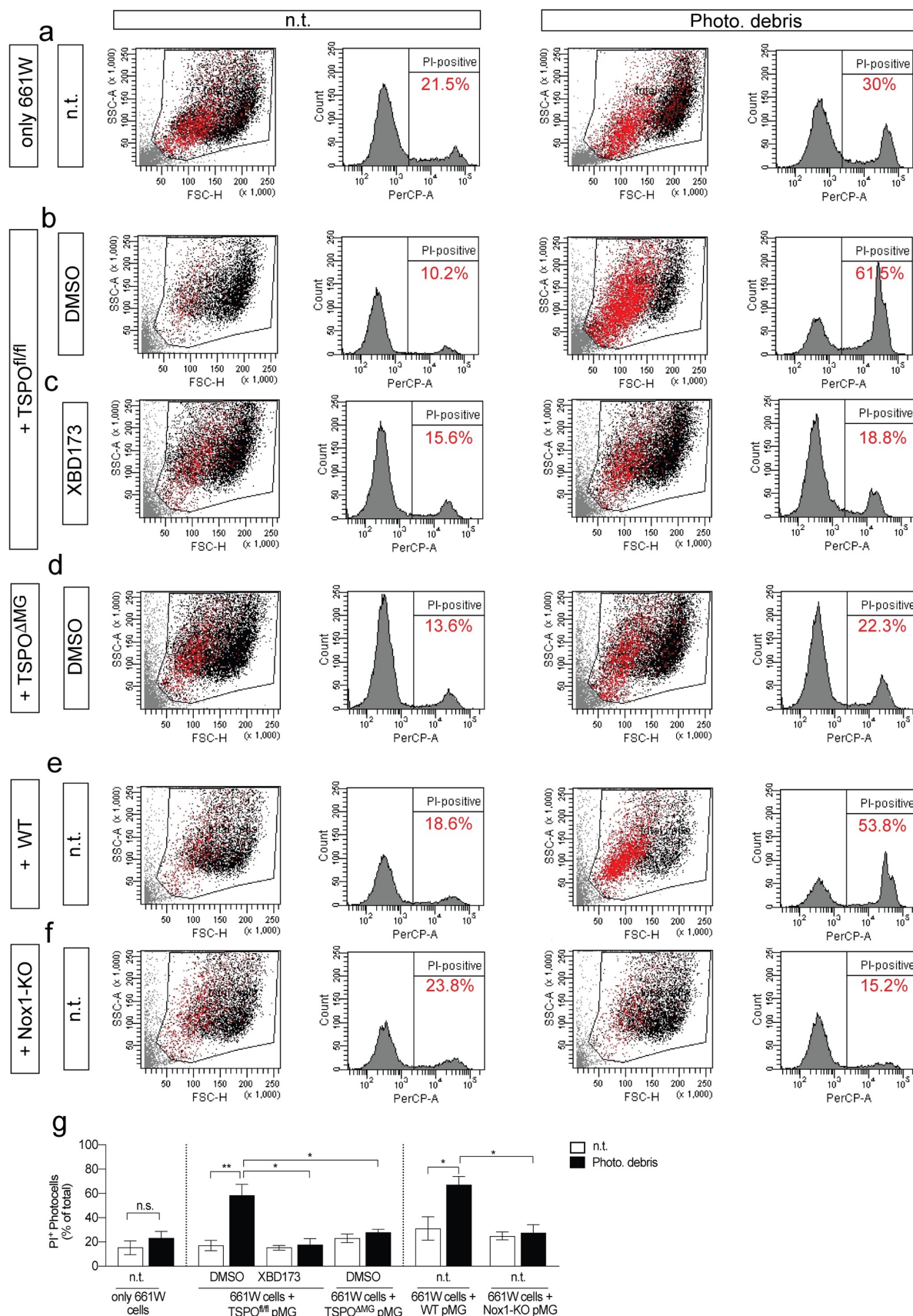
Figure 29: Extracellular ROS damage photoreceptor cells in a paracrine manner. a-f Representative flow cytometric cytograms and histograms of PI-stained 661W photoreceptor cells. Cell death of 661W photoreceptor cells alone **(a)** or in trans-well co-culture with primary microglia **(b-f)** was determined by analyzing the percentage of PI^+-photoreceptor cells isolated from the co-culture inlays. Photoreceptor cells and primary microglia were unstimulated (left panel) or treated with photoreceptor cell debris (right panel) to induce ROS production in microglia. Photoreceptor cells were co-cultured with $TSPO^{fl/fl}$ microglia treated

with the vehicle control DMSO **(b)**, with TSPO$^{fl/fl}$ microglia treated with XBD173 **(c)** or with TSPO$^{\Delta MG}$ microglia **(d)**. Photoreceptor cells were co-cultured with Nox1-WT microglia **(e)** or Nox1-KO microglia **(f)**. **g** Bar chart showing the quantification of photoreceptor cell death. 5,000 cells were counted per sample. n= 3-5 independent experiments. Data are presented as mean ± SEM; unpaired two-tailed Student's t test; *$P<$ 0.05 and **$P<$ 0.01. n.s., not significant, n.t., non-treated.

3.4 Effects of NOX1 deficiency on laser-induced CNV

3.4.1 NOX1 deficiency reduces MNP infiltration in laser-damaged retinas and RPE/choroids

Based on the above results, showing that TSPO-deficient microglia failed to produce stimulation-induced ROS which was shown to damage photoreceptor cells in a paracrine manner, we next examined whether the protective effects in the laser-induced CNV model emerging from XBD173 and microglia-specific TSPO-KO were due to the blockade of NOX1 activation. First, the expression levels of NOX enzyme family members after laser injury were analyzed in order to exclude compensatory upregulation of other *Nox* enzymes when NOX1 is absent (Figure 30). Here, only *Nox1* expression was strongly increased in WT retinas and RPE/choroids 6h after laser-induced injury compared with naïve mice, while in Nox1-KO mice neither *Nox1* was expressed nor compensatory upregulation of other *Nox* enzymes was detected (Figure 30a, b). Thus, we next examined if the absence of NOX1 affects the phagocyte response in the laser-induced CNV mouse. Immunostaining of retinal flat mounts from Nox1-KO mice showed reduced accumulation of Iba1$^+$ cells within the laser lesion compared to WT mice (Figure 31a-c) albeit no morphological differences in their ramification were detected (Figure 31b). Nox1-deficient mice also displayed lower *Cd68* expression in the retina after laser injury while increased expression levels of *Tspo* were still detected (Figure 31d). Moreover, the lesion-associated formation of HMW1 TSPO was slightly decreased in retinas from Nox1-KO mice compared to WT littermates (Figure 31e, f). While IL-6 secretion did not change in Nox1-KO retinas, CCL2 levels were significantly reduced compared to WT retinas (Figure 31g).
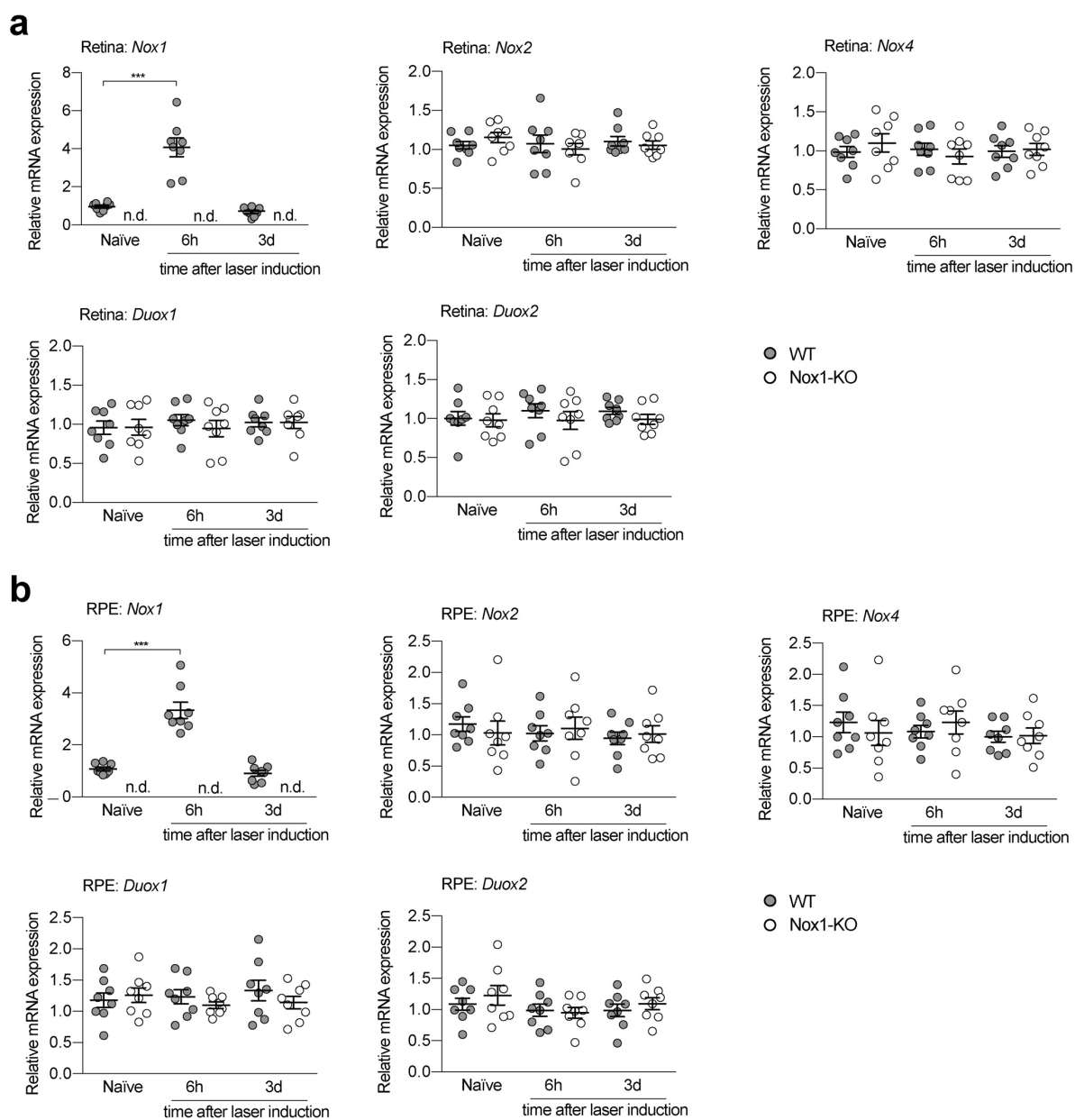
Figure 30: Laser-induced CNV does not induce compensatory *Nox* expression in Nox1-deficient mice.
a-b Laser-induced gene expression of *Nox* enzymes in retinas **(a)** and RPE/choroids **(b)** of WT and Nox1-KO mice. Transcript levels for each enzyme were normalized to *β-Actin*. n= 8 retinas/RPEs. Data are presented as mean ± SEM. Linear mixed model was used for statistical analyses; ***P≤ 0.001. n.d., not detected.
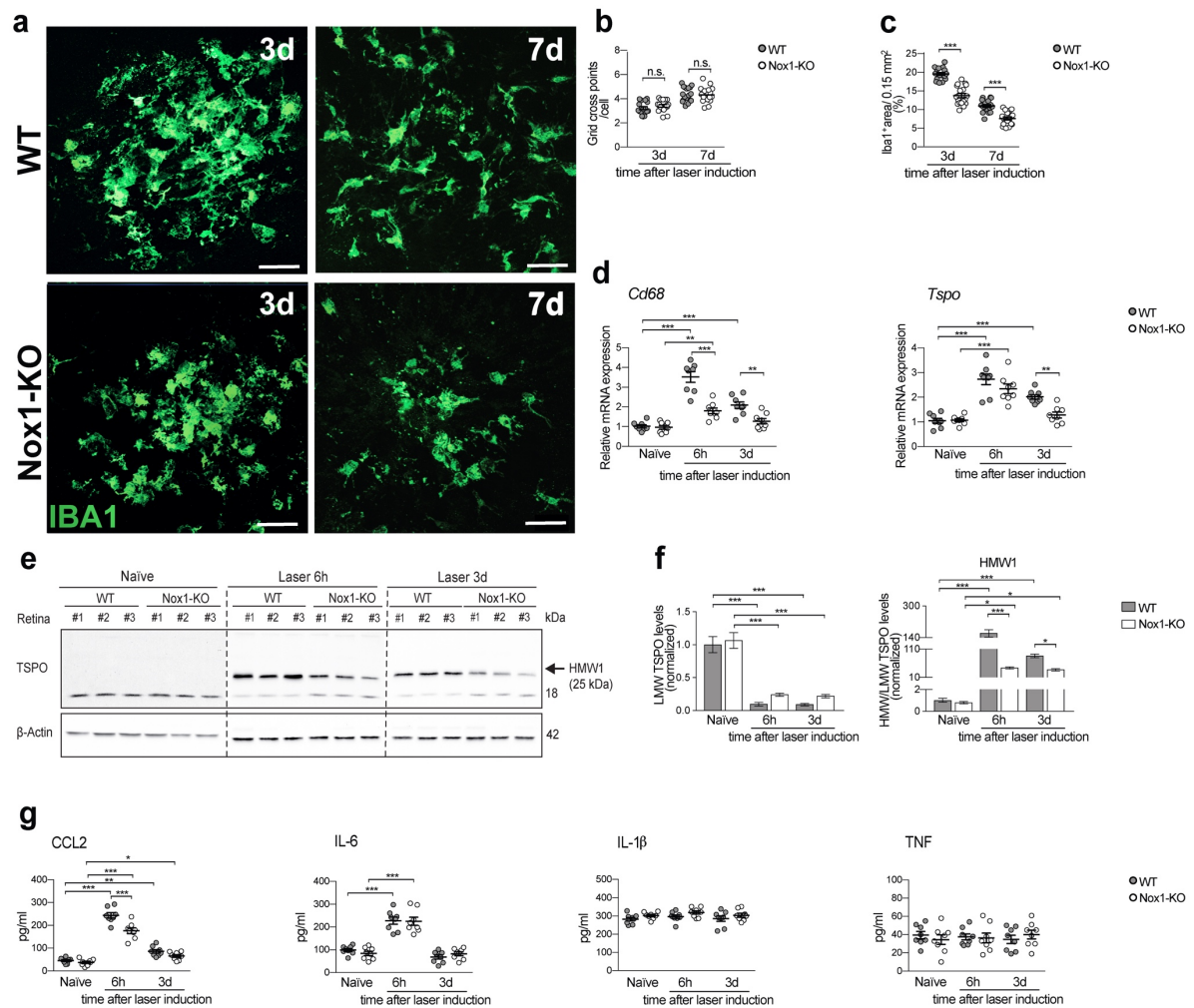
Figure 31: NOX1 deficiency reduces mononuclear phagocyte infiltration in the retina after laser-induced CNV in mice. a Representative images show accumulation of Iba1^{+} cells within the laser lesion in retinal flat mounts. Scale bar: 50 μm. **b** Analysis of Iba1^{+} cell morphology within laser lesions. n= 18-22 spots. **c** Quantification of Iba1^{+} area of the laser lesions. n= 18-22 spots. **d** *Cd68* and *Tspo* mRNA levels in retina from WT and Nox1-KO mice at indicated time points after laser-induced CNV. n= 8 retinas. **e** TSPO protein levels in whole retinal lysates of naïve and lasered WT and Nox1-KO mice at indicated time points. Each lane represents an individual retina. Dotted line indicates individual blots, which were processed in parallel. **f** Densitometric analysis of Western blots. LMW TSPO (18 kDa) signals were normalized to β-Actin and HMW:LMW TSPO ratio determined. n= 6 retinas from two independent experiments. LMW, lower molecular weight; HMW, higher molecular weight. **g** Pro-inflammatory cytokine levels in retinas of naïve and lasered WT and Nox1-KO mice at indicated time points. n= 8 retinas. Data are presented as mean ± SEM. Linear mixed model was used for statistical analyses; * P<0.05, ** P<0.01 and *** P≤ 0.001. n.s., not significant.

Similar results were observed in RPE/choroidal flat mount analyses, where NOX1 deficiency reduced Iba1^{+} cell infiltration (Figure 32a-c) and disease-associated expression of *Cd68* (Figure 32d). Furthermore, the formation of HMW1 and HMW2 TSPO was reduced (Figure 32e, f) and CCL2 levels were decreased in the RPE/choroids from Nox1-KO mice, while IL-6 and IL-1β levels showed no differences (Figure 32g). Together, these data demonstrate that, Nox1-KO alleviates MNP infiltration in laser-damaged retinas and RPE/choroids.
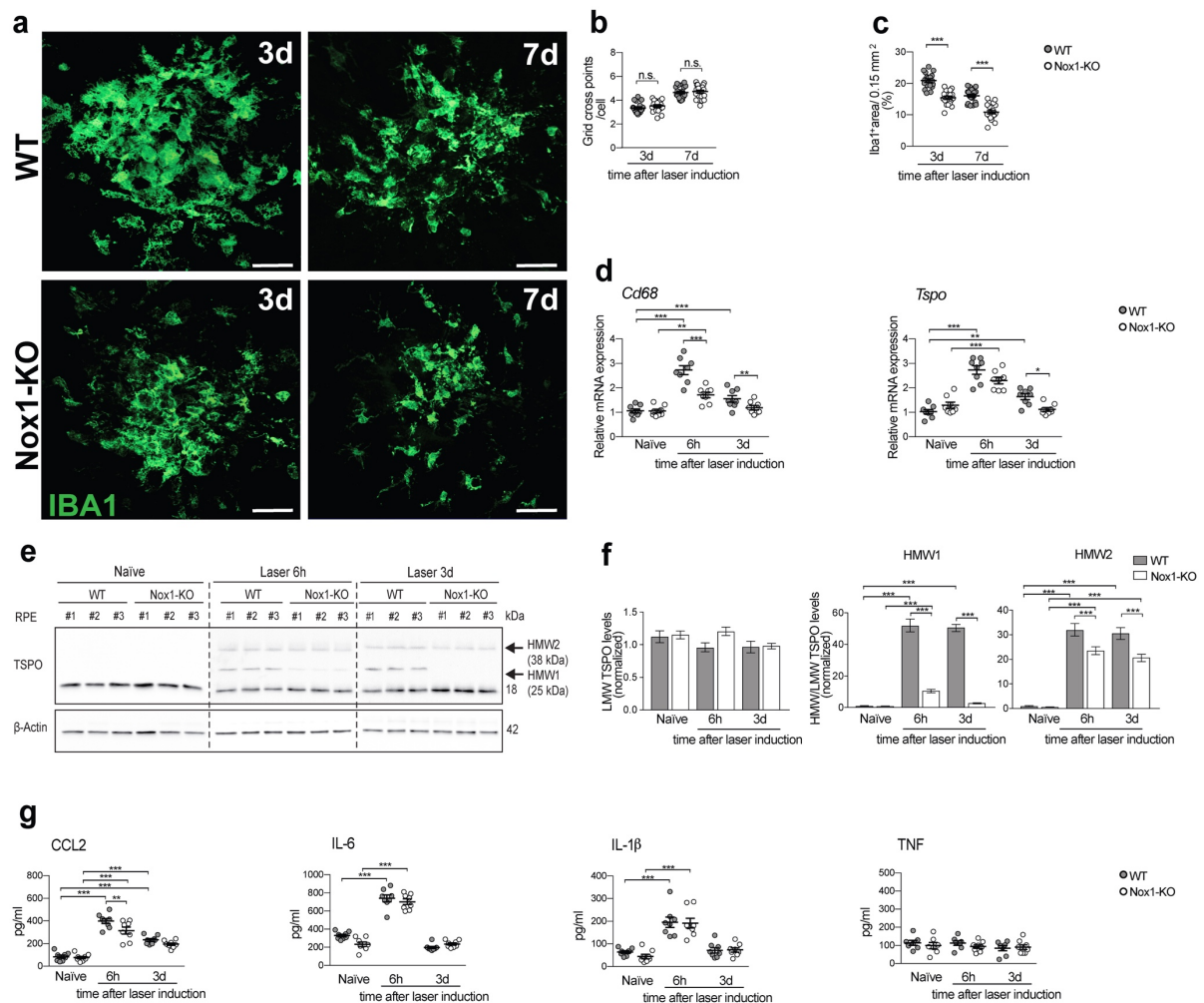
Figure 32: NOX1 deficiency reduces mononuclear phagocyte infiltration in the RPE/choroid after laser-induced CNV in mice. a Representative images of Iba1^{+} cells within the laser lesion in RPE/choroidal flat mounts. Scale bar: 50 μm. **b** Analysis of Iba1^{+} cell morphology within laser lesions. n= 18-22 spots. **c** Quantification of Iba1^{+} area of the laser lesions. n= 18-22 spots. **d** *Cd68* and *Tspo* mRNA levels in RPE/choroid from WT and Nox1-KO mice at indicated time points after laser-induced CNV. n= 8 retinas. **e** Western blots showing TSPO expression in whole RPE/choroidal lysates of naïve and lasered WT and Nox1-KO mice at indicated time points. Each lane represents an individual retina. Dotted line indicates individual blots, which were processed in parallel. **f** Densitometric analysis of Western blots. n= 6 RPE/choroids from two independent experiments. LMW, lower molecular weight; HMW, higher molecular weight. **g** Pro-inflammatory cytokine levels in RPE/choroids of naïve and lasered WT and Nox1-KO mice. n= 8 RPE/choroids. Data are presented as mean ± SEM. Linear mixed model was used for statistical analyses; * P<0.05, ** P<0.01 and *** P≤ 0.001. n.s., not significant.

3.4.2 NOX1 deficiency limits laser-induced vascular leakage and pathological CNV in mice

Finally, we investigated the effect of NOX1 deficiency on laser-induced vascular leakage and CNV. Nox1-KO mice showed a strongly reduced vascular leakage (Figure 33a-c) and CNV size (Figure 33d, e). NOX1 deficiency did not affect laser-induced secretion of VEGF-A, ANG-1, ANG-2, and IGF-1 (Figure 33f, g). Moreover, analysis of the wound healing process

in Nox1-KO mice revealed attenuated laser lesion sizes and significantly reduced fibrosis compared to WT mice (Figure 34). Thus, NOX1 and NOX1-derived ROS are a critical modifier of disease progression and outcome in the laser-induced CNV mouse model.
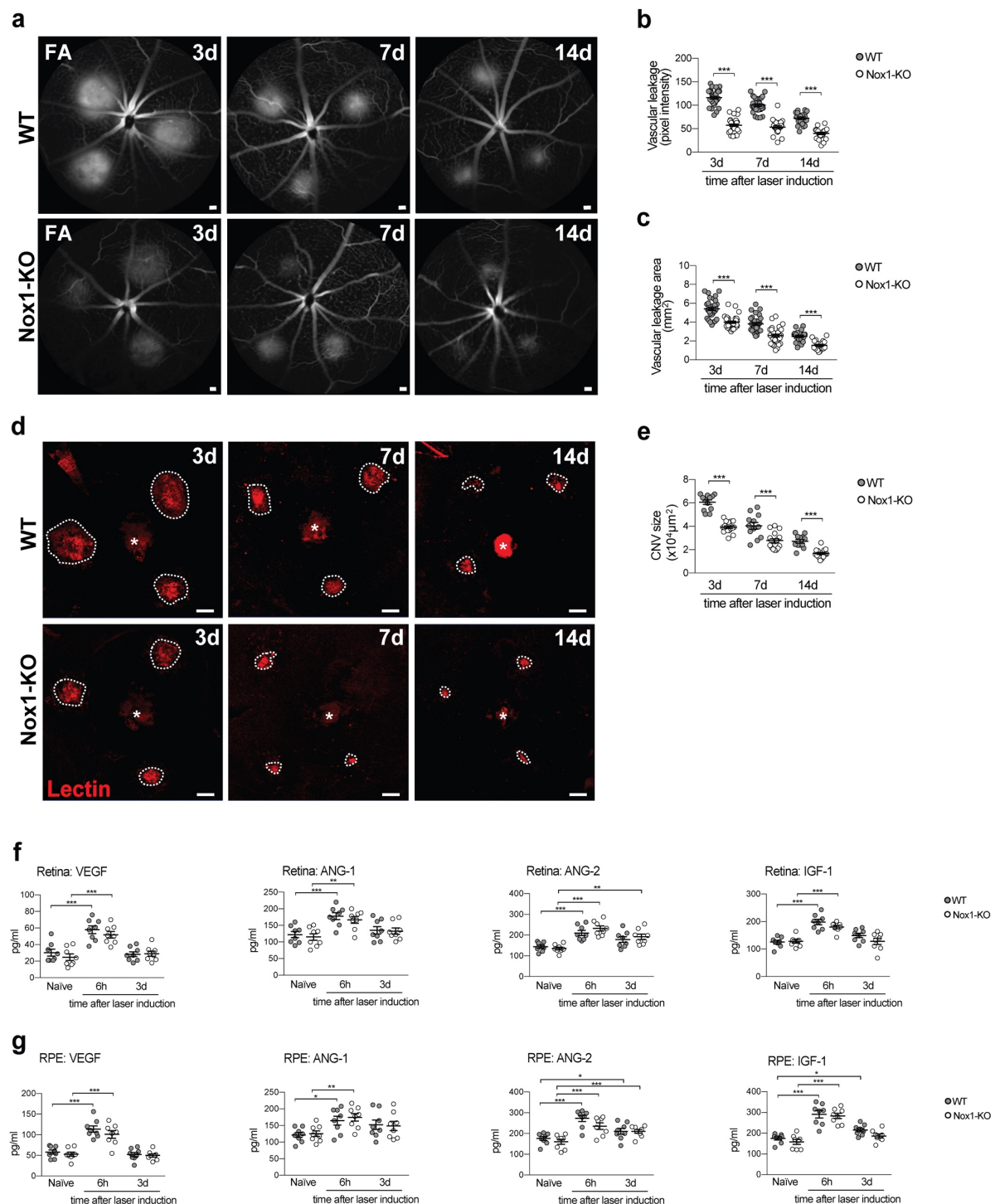
Figure 33: NOX1 deficiency limits laser-induced vascular leakage and pathological CNV in mice. **a** Representative late phase FFA images at indicated time points post laser injury. Scale bar: 200 μm; FA, fluorescein angiography. **b** Quantification of vascular leakage intensity after laser-induced CNV. n= 22-32 eyes. **c** Quantification of vascular leakage area after laser-induced CNV. n= 22-32 eyes. **d** Representative images of laser-induced CNV stained with isolectin B4 in RPE/choroidal flat mounts. Scale bar: 100 μm. **e** Quantification of laser-induced CNV area in RPE/choroidal flat mounts. n= 12-18 RPE/choroids. **f** Pro-angiogenic growth factor levels in retinas of naïve and lasered WT and Nox1-KO mice at indicated time points.

n= 8 eyes. **g** Pro-angiogenic growth factor levels in RPE/choroids of naïve and lasered WT and Nox1-KO mice at indicated time points. n= 8 eyes. Data are presented as mean ± SEM. Linear mixed model was used for statistical analyses; * P<0.05, ** P<0.01 and *** P≤ 0.001.
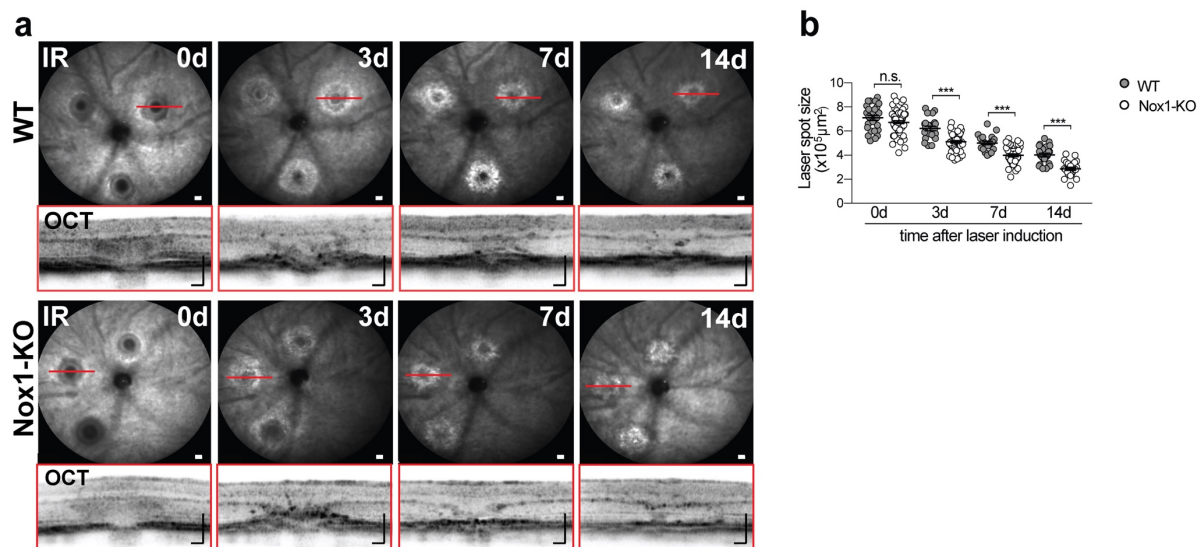
Figure 34: NOX1 deficiency attenuates laser lesion size and promotes a faster wound healing.
a Representative IR fundus images at indicated time points post laser injury. Lower panel shows OCT scan from one laser spot marked by a red line. Scale bar: 200 µm. **b** Quantification of laser lesion size. n= 22-68 eyes. Data are presented as mean ± SEM. Linear mixed model was used for statistical analyses; *** P≤ 0.001. n.s., not significant.

3.5 Model of TSPO-mediated ROS production in reactive retinal phagocytes

Based on the data described in this thesis, we postulate that TSPO is critical for the Ca^{2+} associated, NOX1-mediated production of extracellular ROS in retinal phagocytes and that targeting TSPO by gene knockout or by using the specific ligand XBD173 limits retinal innate immune cell responses and pathological angiogenesis.

In response to pathological signals and damage, resident microglia transform into amoeboid phagocytes, migrate to the lesion sites and recruit macrophages from the periphery. They phagocytose cell debris of the damaged tissue and react with the release of pro-inflammatory and pro-angiogenic factors and with a robust production of NOX1-derived ROS in a Ca^{2+} associated, TSPO-dependent manner. Targeting TSPO with its synthetic ligand XBD173 decreased not only the expression and secretion of pro-inflammatory and pro-angiogenic factors but also prevented NOX1-derived ROS

production by blocking the TSPO-dependent increase of cytosolic Ca^{2+}, thereby limiting photoreceptor cell death and pathological CNV (Figure 35).
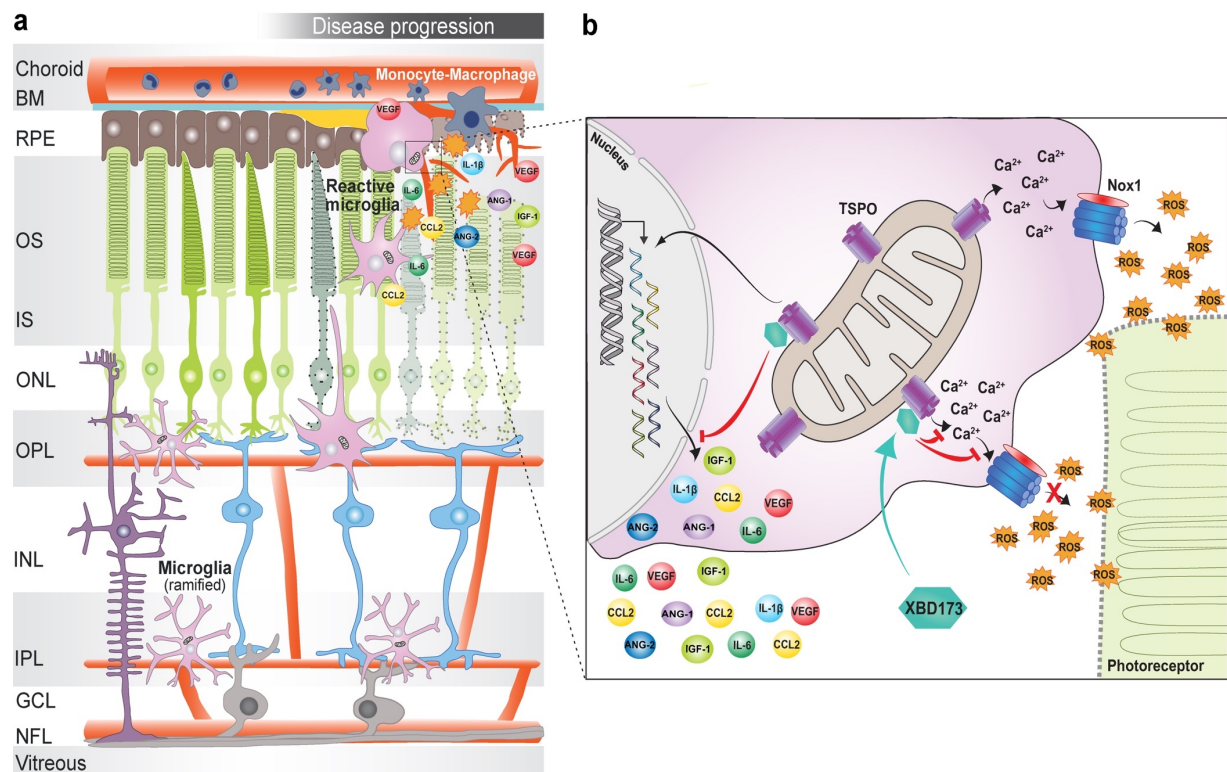
Figure 35: **Model of TSPO-mediated ROS production in retinal phagocytes. a** In the healthy retina, resident microglia reside in the plexiform layers, where they constantly scan their environment with their long protrusions and phagocytose cell debris. Different insults leading to abnormal cell functions or degeneration of the RPE and photoreceptors rapidly alert microglia. Resident microglia transform into amoeboid phagocytes, migrate to the lesion sites and recruit macrophages from the periphery. **b** In response to these pathological signals, microglia increase pro-inflammatory and pro-angiogenic cytokines expression to resolve neuroinflammation and promote tissue recovery. In addition, reactive microglia upregulate mitochondrial TSPO leading to increased cytosolic calcium levels, which is essential for NOX1-mediated extracellular ROS production. However, chronic activation of microglia is detrimental and promotes retinal degeneration. Binding of the synthetic ligand XBD173 to TSPO limits the magnitude of inflammatory responses and inhibits the increase of cytosolic calcium levels thus preventing from ROS damage. XBD173 support the transition of reactive microglia towards a ramified neuroprotective phenotype, limiting pathological CNV. BM, Bruch's membrane; OS, outer segment; IS, inner segment; ONL, outer nuclear layer; OPL, outer plexiform layer; INL, inner nuclear layer; IPL, inner plexiform layer; GCL, ganglion cell layer; NFL, nerve fiber layer.

4.   Discussion

Chronic inflammation is a hallmark of many neurodegenerative diseases including AMD. Microglia, the resident phagocytes of the retina, represent a broad target for therapy as their chronic pro-inflammatory reactivity negatively contributes to disease progression. Thus, pharmacological approaches of microglia-related immunomodulation to preserve their homeostatic functions, are promising therapeutic strategies. Targeting TSPO, a reliable biomarker of gliosis, using different synthetic ligands improved disease outcome in various preclinical model systems including Alzheimer's (Barron et al., 2013), Parkinson's (Gong et al., 2019), MS (Daugherty et al., 2013) and degenerative diseases of the retina (Scholz et al., 2015a). However, the underlying molecular mechanisms of TSPO-mediated immunomodulation and its precise molecular function has not been elucidated in these studies and remain largely elusive.

In this study, the molecular function of TSPO in retinal immune homeostasis and pathological angiogenesis was examined using the laser-induced CNV model. Although rodents lack a macula, this mouse model recapitulates key pathological features of neovascular AMD in humans. The laser-induced rupture of BM results is an acute local inflammatory response concomitant with a rapid recruitment of MNPs and CNV formation (Lambert et al., 2013). Nevertheless, this model has some limitations as it does not recapitulate the aging aspect of AMD including drusen and the complex interplay between genetic and environmental factors. As an acute injury model, the wound healing process even leads to spontaneous disease regression (Gong et al., 2015; Lambert et al., 2013). However, the laser-induced CNV model remains one of the most commonly used mouse models to study neovascular AMD and to test the efficacy of anti-VEGF therapies.

Based on the concept of endogenous TSPO ligand-mediated immunomodulation of retinal microglia, we investigated whether the synthetic TSPO ligand XBD173 possesses immunomodulatory and neuroprotective effects in this mouse model of neovascular AMD. Additionally, we aimed to elucidate the direct function of TSPO in retinal immune cells using conditional microglia-specific knockout mice.

4.1 Immunomodulatory effects of XBD173 on laser-induced CNV

In this study we have shown that targeting TSPO by using the specific ligand XBD173 limits retinal innate immune cell responses and pathological angiogenesis in the laser-induced CNV mouse model. Previous studies have also shown immunomodulatory and neuroprotective effects of XBD173 in various neurodegenerative mouse models including light-induced retinal degeneration (Scholz et al., 2015a), retinal ischemia (Mages et al., 2019) and MPTP-induced parkinsonism (Gong et al., 2019). However, the effect of XBD173 in retinal ischemia was mainly confined to retinal Müller cells with less effect on microglia (Mages et al., 2019). We have demonstrated before that TSPO is constitutively expressed in the RPE and showed no inflammation-induced expression (Scholz et al., 2015a), suggesting that the TSPO increase after laser injury mainly derives from resident and invading mononuclear phagocytes.

Interestingly, our Western blots revealed for the first time the presence of HMW TSPO in the retina and RPE after laser injury *in vivo*. While in the laser-damaged retina only one HMW TSPO band was detected, two appeared in the RPE/choroid, indicating a different cell-type specific reorganization of TSPO. The appearance of these HMW bands could be due to post-translational modifications and subsequent oligomerization since a putative phosphorylation motif has been identified in the C-terminal domain of TSPO (Whalin et al., 1994). Also, a study using colonic cells showed that the TSPO ligand PK11195 can induce TSPO polymerization by stabilizing the dimeric form (Issop et al., 2016). However, our data showed that XBD173 prevented the formation of these HMW TSPO bands. The current understanding of the TSPO structure at molecular level is based on the NMR structure of mouse TSPO (mTSPO) (Jaremko et al., 2014; 2015) and two crystal structures of the bacterial homologs from *Rhodobacter sphaeroides* and *Bacilluscereus* (Guo et al., 2015; Li et al., 2013). Mouse TSPO was mainly reported to be monomeric in detergent systems but there are also reports indicating that a fraction of mouse TSPO may exist as oligomers in lipid bilayers (Jaipuria et al., 2017; Papadopoulos et al., 1994; Teboul et al., 2012). This suggests that different oligomeric states of TSPO may be associated with different functions. However, a recent study showed that the lipid-mimetic system which is used to solubilize mouse TSPO for NMR studies, thermodynamically destabilizes the protein, introduces structural perturbations and in addition alters the characteristics of ligand binding (Xia et al., 2019). Therefore, the precise composition and role of these TSPO proteins in the retina and RPE/choroid after laser injury remain elusive and deserves further studies.

Concomitant with reducing TSPO expression, XBD173 treatment also reduced the secretion of pro-inflammatory cytokines after laser injury. This is in line with a previous mouse study on MPTP-induced parkinsonism, reporting that XBD173-specific transcriptional changes include pathways related to cytokine production (Gong et al., 2019).

The fact that laser injury did not induce IL-1β levels in the retina but in the RPE suggests an important role of RPE cells and invading MNPs for inflammasome-dependent IL-1β secretion (Mohr et al., 2015). Of note, experimental data suggest that CCL2/CCR2 signaling contributes to the pathogenesis of wet AMD, as knockout of these factors prevents inflammatory MNP recruitment and CNV progression after laser injury (Luhmann et al., 2009; Tsutsumi et al., 2003). Also, clinical studies support the possible involvement of CCL2 in the pathogenesis of wet AMD, as increased intraocular levels of CCL2 have been found in AMD patients (Jonas, 2010; Newman et al., 2012). Here, we found that XBD173 treatment potently reduced laser-induced CCL2 levels, resulting in diminished MNP recruitment to the subretinal space and neoganiogenesis, corroborating the critical role of MNPs in the development of CNV.

In addition, we also showed that XBD173 reduced pro-angiogenic growth factor expression and subsequently diminished CNV via modulation of MNPs. Indeed, Iba1^{+} MNPs actively produced VEGF during laser injury (Balser et al., 2019) and macrophage depletion correlates with reduced VEGF expression and laser-induced CNV (Sakurai et al., 2003). Furthermore, autocrine IL-1β can potently induce VEGF production by RPE cells (Nagineni et al., 2012) and the reduced IL-1β levels found upon XBD173 treatment may also dampen RPE-derived VEGF levels indicating a complex paracrine interplay of pro-inflammatory and pro-angiogenic factors on the tissue and cellular level. A potential mechanism by which XBD173 acts anti-inflammatory could be through inhibition of NF-κB and activator protein 1 (AP-1) signaling. Both transcription factors are important regulators of pro-inflammatory gene expression and vinpocetine, another TSPO ligand, have been shown to reduce their expression levels thereby limiting pro-inflammatory cytokine production and neurotoxicity of microglia *in vitro* (Zhao et al., 2011) and *in vivo* (Wang et al., 2014a).

In summary, we have shown that XBD173 treatment in the laser-induced CNV mouse model improves disease outcome by reducing MNP reactivity and migration, thereby limiting phagocyte-triggered neoangiogenesis.

4.2 Immunoprotective effects of microglia-specific TSPO-KO on laser-induced CNV

Here, we generated a conditional microglia-specific TSPO-KO mouse in order to determine if TSPO function in MNPs modulates their reactivity during laser-induced CNV. Our data demonstrated that microglia lacking TSPO showed no morphological differences compared to control microglia. Furthermore, microglia from TSPO$^{\Delta MG}$ mice showed no alterations in predictors of mitochondrial health, including mitochondrial morphology or MMP. Analysis of total cellular ATP levels showed that microglia use both glycolysis and mitochondrial respiration to generate ATP. While inhibition of glycolysis through the glucose derivative 2-DG showed that both non-activated and stimulated microglia to some degree depend on glycolysis for ATP generation, inhibition of the mitochondrial ATP synthase via oligomycin A treatment showed that ATP is mainly generated by mitochondrial respiration and this was not changed in TSPO-KO microglia. However, this is in contrast to studies reporting reduced mitochondrial metabolism in mouse and human microglia cell lines after TSPO knockdown or knockout (Bader et al., 2019; Milenkovic et al., 2019). This discrepancy could be due to the fact that endogenous levels from immortalized cultured cell lines and primary microglia differ in their TSPO expression levels and function. Thus, a report on liver-specific TSPO-KO mice also observed neither mitochondrial ultrastructural alterations nor membrane potential or ATP level differences (Sileikyte et al., 2014). Also, experiments using TSPO-deficient MA-10 testicular Leydig cells (Tu et al., 2016) or isolated mitochondria from ventricles of cardiac-specific TSPO-KO mice showed no signs of dysfunction (Thai et al., 2018).

Although myeloid cells, such as retinal microglia and recruited monocyte-derived macrophages accumulate in areas of neovascularization, the extent to which these cells contribute to this process is not clear (Green, 1991; Sousa et al., 2017). In this study, we reported that conditional deletion of TSPO in long-lived retinal microglia phenocopied the beneficial effect of XBD173 treatment on laser-induced CNV, pointing towards a significant contribution of this cell type on disease formation. This is in line with a recent study showing that resident retinal microglia are the predominant cell population in areas of retinal neovascularization whereas blood-derived monocytes play a minor role in terms of quantity (Boeck et al., 2020). In addition, two studies demonstrated that astroglia-specific TSPO-KO was protective in a mouse model of MS (Daugherty et al., 2016) and that a cardiac-specific TSPO-KO protected from pressure overload induced heart failure (Thai et al., 2018).

Thus, our data have shown that TSPO is not required for mitochondrial integrity, health or energy metabolism in microglia and that microglia-specific TSPO-KO limits retinal innate immune cell responses and pathological angiogenesis in the laser-induced CNV mouse model.

4.3 The TSPO-NOX1 axis controls phagocyte-triggered pathological CNV in the retina

4.3.1 TSPO regulates NOX1-derived ROS production in a Ca^{2+}-dependent manner

In this study, we have shown that targeting TSPO with XBD173 or microglia-specific TSPO-KO blocks stimulation-induced extracellular phagocyte ROS production. Involvement of TSPO in ROS production was suggested before (Gatliff et al., 2014; 2017; Guilarte et al., 2016) and deregulation of redox balance such as chronic ROS production is strongly linked to neurodegeneration (Tarafdar and Pula, 2018). The regulated production of ROS is mediated by members of the NOX enzyme family (Lambeth and Neish, 2014). Although NOX2 is the predominant source of ROS in phagocytes (Haslund-Vinding et al., 2017), several studies also described a role for NOX1- and NOX4-dependent ROS production in microglia (Bin Li et al., 2009; Chéret et al., 2008). While animal studies with genetically modified NOX enzymes in eye diseases are scarce (Chan et al., 2016; Yokota et al., 2011) and only a few *in vivo* studies investigated the role of NOX2 or NOX4 in deficient mice (Hou et al., 2018; Ma et al., 2017; 2018), most of the research on microglia was performed with cell lines. NOX enzymes were either knocked down (Cheng et al., 2018; Gatliff et al., 2017; Zeng et al., 2018) or ROS production was chemically inhibited with diphenyleneiodonium or apocyanin (Appukuttan et al., 2018; Chen et al., 2017; Gatliff et al., 2017; Hou et al., 2018). While commonly termed specific NOX inhibitors, these compounds show numerous side effects and their specificity is questioned (Altenhöfer et al., 2015).

Here, we showed for the first time that *Nox1* but no other *Nox* or *Duox* enzymes were up-regulated *in vivo* after laser-injury and accordingly, by using different NOX-KO mouse strains, we revealed that microglia produce extracellular ROS exclusively via NOX1, while other NOX enzymes were dispensable for this response. Furthermore, we showed that TSPO was crucial for the induction of NOX1-derived ROS as both XBD173 treatment and microglia-specific TSPO-KO not only blocked laser-induced *Nox1* expression but also extracellular ROS

production. TSPO was also implicated in mitochondrial ROS production before, which was associated with cellular signaling functions (Choi et al., 2010; Gatliff et al., 2014). However, we did not observe ROS production in the cytosol or the mitochondrial matrix after stimulation. This discrepancy could be due to the different methodological approaches and ROS detection probes used in these studies. Cytosolic ROS were either detected with 2',7'-dichlorohydrofluorescein diacetate (H_2DCFDA) (Choi et al., 2010) or dihydroethydium (DHE) (Gatliff et al., 2014) and both approaches are unspecific in terms of compartmentalization of ROS production (Hempel et al., 1999; Dikalov and Harrison, 2014; Zielonka and Kalyanaraman, 2010).

A TSPO-dependent regulation of NOX enzymes was described before and heme and/or cholesterol transport was suggested as a possible regulatory mechanism (Gatliff et al., 2017; Guilarte et al., 2016). However, after PMA stimulation, TSPO-KO microglia still showed a robust increase in extracellular ROS production, excluding non-functionality of NOX enzymes due to hampered heme or cholesterol transport in TSPO-KO microglia. Furthermore, two other studies demonstrated an interaction of TSPO with the channel VDAC1 and a potential role in redox homeostasis via Ca^{2+} (Gatliff et al., 2014; 2017). Therefore, we decided to analyze the role of TSPO in calcium homeostasis and subsequent NOX1-derived ROS production. In accordance with a former study demonstrating elevated cytosolic Ca^{2+} levels in TSPO-overexpressing cells (Gatliff et al., 2017), we observed a strong reduction in cytosolic Ca^{2+} in TSPO-deficient microglia. Notably, the TSPO-mediated increase of cytosolic Ca^{2+} levels was prevented by XBD173, which subsequently abolished not only *Nox1* expression, but also acute NOX1-derived ROS production after stimulation. This is in line with a previous study showing that the TSPO ligand PK11195 was able to reduce LPS-induced increase of intracellular Ca^{2+} in human microglial cells (Choi et al., 2002). Interestingly, in the absence of extracellular Ca^{2+}, *Nox1* expression and NOX1-dependent ROS production upon stimulation was significantly reduced in microglia, indicating that extracellular ROS production is regulated via both, *Nox1* expression and activation in a Ca^{2+}-dependent manner.

While DUOX1-2 and NOX5 are directly activated via their EF-hand calcium-binding domains (Görlach et al., 2015; Lambeth and Neish, 2014), ROS production in microglia depends on the catalytic subunit p22^{phox}. This suggests that the rise in cytosolic Ca^{2+} indirectly activates NOX1 via calcium-dependent signaling mechanisms in the cytosol. Indeed, it was shown that NOX1 activity indirectly depends on cytosolic Ca^{2+} (Valencia and Kochevar, 2008) and that *Nox1* expression levels can also depend on cytosolic Ca^{2+} levels (Ge et al., 2010). The mechanisms

regulating the entry of Ca^{2+} into the cytosol that is required for NOX1 activation remained elusive, though.

The identification of these signaling cascades in microglia will be a topic for further investigations. Here, receptors previously reported to be involved in ROS production in microglia such as complement receptor 3 (CR3), CD36, ionotropic and metabolic purinergic receptors are promising targets (Haslund-Vinding et al., 2017). Especially the latter are not only specialized in detecting ATP, a molecule released by damaged cells (e.g. PCD), but also require Ca^{2+} entry into the cytosol for the induction of ROS production after ATP binding (Kim et al., 2007; Martel-Gallegos et al., 2013).

In summary, our data revealed that influx of Ca^{2+} from the extracellular milieu into the cytosol is required for stimulation of NOX1 activity and expression in microglia and that this influx is regulated by TSPO.

4.3.2 NOX1 deficiency improves disease outcome of laser-induced CNV

Here, we identified NOX1-dependent ROS production by microglia upon stimulated phagocytosis that lead to a substantial and fast increase of extracellular ROS. Notably, we also showed that these NOX1-derived extracellular ROS induce photoreceptor cell death in a paracrine manner, confirming their potential as damaging neurotoxins.

In Nox1-KO mice, no compensatory upregulation of other *Nox* or *Duox* enzymes after laser injury was detected and accordingly, NOX1 deficiency improved disease outcome in these mice, while other features of microglia reactivity were not affected. Our data show that NOX1 is terminally in the TSPO-NOX1 axis and thus, the production of pro-inflammatory cytokines and angiogenic growth factors are mediated via TSPO-dependent but NOX1-independent mechanisms. Although some studies suggested that NOX2-derived ROS can influence the pro-inflammatory response after infection (Deffert et al., 2012; Han et al., 2013), it was recently shown that NOX2-derived extracellular ROS are dispensable for cytokine secretion in infected macrophages (Herb et al., 2019). In a mouse model of amyotrophic lateral sclerosis (ALS), deletion of NOX1 was reported to increase the survival, while the cellular sources of NOX1 remained undetermined in this study (Marden et al., 2007). In addition, another study showed that mice deficient in inducible nitric oxide-synthase (iNOS) develop less CNV after laser

injury (Ando et al., 2002), highlighting reactive nitrogen species (RNS)/ROS as drivers of disease progression.

In summary, our data have shown that NOX1-mediated production of ROS can damage photoreceptor cells in a paracrine manner and that Nox1-KO mice show the same beneficial effects on CNV and wound healing as XBD173 treatment or microglia-specific TSPO-KO.

4.4 Conclusion

In this study, we demonstrated a critical function of TSPO signaling in phagocyte-triggered neoangiogenesis of the retina, a model system that recapitulates key pathological features of neovascular AMD. We showed that TSPO acts as a regulatory node and regulates microglia functions through both NOX1-dependent and NOX1-independent mechanisms. While TSPO mediates NOX1-derived extracellular ROS production that damage photoreceptor cells in a paracrine manner, its regulation of pro-inflammatory cytokines and angiogenic growth factors are independent from NOX1. Indeed, the TSPO-NOX1 axis is crucial in the laser-induced CNV model, as Nox1-KO mice showed the same beneficial effects on CNV and wound healing as XBD173 treatment or microglia-specific TSPO-KO.

Collectively, this thesis defines a distinct role for TSPO in retinal phagocyte reactivity and highlights the protein as a drug target for immunomodulatory and antioxidant therapies for AMD.

5.   References

Ajami, B., Bennett, J.L., Krieger, C., Tetzlaff, W., and Rossi, F.M.V. (2007). Local self-renewal can sustain CNS microglia maintenance and function throughout adult life. Nat. Neurosci. *10*, 1538–1543.

Akhtar-Schäfer, I., Wang, L., Krohne, T.U., Xu, H., and Langmann, T. (2018). Modulation of three key innate immune pathways for the most common retinal degenerative diseases. EMBO Molecular Medicine *10*, e8259.

Altenhöfer S, Radermacher K, Kleikers P, Wingler K , and Schmidt H. (2015). Evolution of NADPH Oxidase Inhibitors: Selectivity and Mechanisms for Target Engagement. Antioxid. Redox Signal. *23*, 406–427.

Alters, S. (2000). Biology: understanding life.

Amor, S., Peferoen, L.A.N., Vogel, D.Y.S., Breur, M., van der Valk, P., Baker, D., and van Noort, J.M. (2014). Inflammation in neurodegenerative diseases – an update. Immunology *142*, 151–166.

Anderson, D.H., Radeke, M.J., Gallo, N.B., Chapin, E.A., Johnson, P.T., Curletti, C.R., Hancox, L.S., Hu, J., Ebright, J.N., Malek, G., et al. (2010). The pivotal role of the complement system in aging and age-related macular degeneration: Hypothesis re-visited. Prog Retin Eye Res *29*, 95–112.

Ando, A., Yang, A., Mori, K., Yamada, H., Yamada, E., Takahashi, K., Saikia, J., Kim, M., Melia, M., Fishman, M., et al. (2002). Nitric oxide is proangiogenic in the retina and choroid. J. Cell. Physiol. *191*, 116–124.

Andriessen, E.M., Wilson, A.M., Mawambo, G., Dejda, A., Miloudi, K., Sennlaub, F., and Sapieha, P. (2016). Gut microbiota influences pathological angiogenesis in obesity-driven choroidal neovascularization. EMBO Molecular Medicine *8*, 1366–1379.

Anholt, R.R., De Souza, E.B., Oster-Granite, M.L., and Snyder, S.H. (1985). Peripheral-type benzodiazepine receptors: autoradiographic localization in whole-body sections of neonatal rats. J. Pharmacol. Exp. Ther. *233*, 517–526.

Anholt, R.R., Pedersen, P.L., De Souza, E.B., and Snyder, S.H. (1986). The peripheral-type benzodiazepine receptor. Localization to the mitochondrial outer membrane. J. Biol. Chem. *261*, 576–583.

Appukuttan, B., Ma, Y., Stempel, A., Ashander, L.M., Deliyanti, D., Wilkinson-Berka, J.L., and Smith, J.R. (2018). Effect of NADPH oxidase 1 and 4 blockade in activated human retinal endothelial cells. Clinical and Experimental Ophthalmology *46*, 652–660.

Ba, J., Peng, R.-S., Xu, D., Li, Y.-H., Shi, H., Wang, Q., and Yu, J. (2015). Intravitreal anti-VEGF injections for treating wet age-related macular degeneration: a systematic review and meta-analysis. Drug Design, Development and Therapy *9*, 5397–5405.

Bader, S., Wolf, L., Milenkovic, V.M., Gruber, M., Nothdurfter, C., Rupprecht, R., and Wetzel, C.H. (2019). Differential effects of TSPO ligands on mitochondrial function in mouse microglia cells. Psychoneuroendocrinology *106*, 65–76.

Baines, C.P., Kaiser, R.A., Sheiko, T., Craigen, W.J., and Molkentin, J.D. (2007). Voltage-dependent anion channels are dispensable for mitochondrial-dependent cell death. Nat. Cell Biol. *9*, 550–555.

Balsemão-Pires, E., Jaillais, Y., Olson, B.J., Andrade, L.R., Umen, J.G., Chory, J., and Sachetto-Martins, G. (2011). The Arabidopsis translocator protein (At TSPO) is regulated at multiple levels in response to salt stress and perturbations in tetrapyrrole metabolism. BMC Plant Biol *11*, 1–17.

Balser, C., Wolf, A., Herb, M., and Langmann, T. (2019). Co-inhibition of PGF and VEGF blocks their expression in mononuclear phagocytes and limits neovascularization and leakage in the murine retina. J Neuroinflammation *16,* 26.

Banati, R.B., Middleton, R.J., Chan, R., Hatty, C.R., Kam, W.W.Y., Quin, C., Graeber, M.B., Parmar, A., Zahra, D., Callaghan, P., et al. (2014). Positron emission tomography and functional characterization of a complete PBR/TSPO knockout. Nature Communications 2014 5 *5*, 5452.

Banfi, B., Malgrange, B., Knisz, J., Steger, K., Dubois-Dauphin, M., and Krause, K.-H. (2004). NOX3, a superoxide-generating NADPH oxidase of the inner ear. J. Biol. Chem. *279*, 46065–46072.

Barron, A.M., Garcia-Segura, L.M., Caruso, D., Jayaraman, A., Lee, J.-W., Melcangi, R.C., and Pike, C.J. (2013). Ligand for Translocator Protein Reverses Pathology in a Mouse Model of Alzheimer's Disease. J. Neurosci. *33*, 8891–8897.

Batoko, H., Veljanovski, V., and Jurkiewicz, P. (2015). Enigmatic Translocator protein (TSPO) and cellular stress regulation. Trends Biochem. Sci. *40*, 497–503.

Baylor, D.A., Lamb, T.D., and Yau, K.W. (1979). Responses of retinal rods to single photons. J. Physiol. (Lond.) *288*, 613–634.

Beatty, S., Koh, H.-H., Phil, M., Henson, D., and Boulton, M. (2000). The Role of Oxidative Stress in the Pathogenesis of Age-Related Macular Degeneration. Survey of Ophthalmology *45*, 115–134.

Bedard, K., and Krause, K.-H. (2007). The NOX Family of ROS-Generating NADPH Oxidases: Physiology and Pathophysiology. Physiological Reviews *87*, 245–313.

Berridge, M.J. (2012). Calcium signalling remodelling and disease. Biochemical Society Transactions *40*, 297–309.

Bin Li, Bedard, K., Sorce, S., Hinz, B., Dubois-Dauphin, M., and Krause, K.-H. (2009). NOX4 Expression in Human Microglia Leads to Constitutive Generation of Reactive Oxygen Species and to Constitutive IL-6 Expression. Jin *1*, 570–581.

Block, M.L., and Hong, J.S. (2007). Chronic microglial activation and progressive dopaminergic neurotoxicity. Biochemical Society Transactions *35*, 1127–1132.

Bodeutsch, N., and Thanos, S. (2000). Migration of phagocytotic cells and development of the murine intraretinal microglial network: An in vivo study using fluorescent dyes. Glia *32*, 91–101.

Boeck, M., Thien, A., Wolf, J., Hagemeyer, N., Laich, Y., Yusuf, D., Backofen, R., Zhang, P., Boneva, S., Stahl, A., et al. (2020). Temporospatial distribution and transcriptional profile of retinal microglia in the oxygen-induced retinopathy mouse model. Glia *12*, 467.

Bok, D. (1985). Retinal Photoreceptor-Pigment Epithelium Interactions - Friedenwald Lecture. Invest. Ophthalmol. Vis. Sci. *26*, 1659–1694.

Braestrup, C., Albrechtsen, R., and SQUIRES, R.F. (1977). High densities of benzodiazepine receptors in human cortical areas. Nature *269*, 702–704.

Broderick, C., Hoek, R.M., Forrester, J.V., Liversidge, J., Sedgwick, J.D., and Dick, A.D. (2002). Constitutive Retinal CD200 Expression Regulates Resident Microglia and Activation State of Inflammatory Cells during Experimental Autoimmune Uveoretinitis. The American Journal of Pathology *161*, 1669–1677.

Brown, P.K., and Wald, G. (1964). Visual Pigments in Single Rods and Cones of the Human Retina. Science *144*, 45–52.

Bruttger, J., Karram, K., Wörtge, S., Regen, T., Marini, F., Hoppmann, N., Klein, M., Blank, T., Yona, S., Wolf, Y., et al. (2015). Genetic Cell Ablation Reveals Clusters of Local Self-Renewing Microglia in the Mammalian Central Nervous System. Immunity *43*, 92–106.

Buchanan, J.B., Sparkman, N.L., Chen, J., and Johnson, R.W. (2008). Cognitive and neuroinflammatory consequences of mild repeated stress are exacerbated in aged mice. Psychoneuroendocrinology *33*, 755–765.

Burnstock, G., Krügel, U., Abbracchio, M.P., and Illes, P. (2011). Purinergic signalling: From normal behaviour to pathological brain function. Progress in Neurobiology *95*, 229–274.

Buschini, E., Piras, A., Nuzzi, R., and Vercelli, A. (2011). Age related macular degeneration and drusen: neuroinflammation in the retina. Progress in Neurobiology *95*, 14–25.

Caballero, B., Veenman, L., and Gavish, M. (2013). Role of Mitochondrial Translocator Protein (18 kDa) on Mitochondrial- Related Cell Death Processes *7*, 86-101

Calovi, S., Mut-Arbona, P., and Sperlágh, B. (2019). Microglia and the Purinergic Signaling System. Neuroscience *405*, 137–147.

Cardona, A.E., Pioro, E.P., Sasse, M.E., Kostenko, V., Cardona, S.M., Dijkstra, I.M., Huang, D., Kidd, G., Dombrowski, S., Dutta, R., et al. (2006). Control of microglial neurotoxicity by the fractalkine receptor. Nat. Neurosci. *9*, 917–924.

Carnesecchi, S., Deffert, C., Donati, Y., Basset, O., Hinz, B., Preynat-Seauve, O., Guichard, C., Arbiser, J.L., Banfi, B., Pache, J.-C., et al. (2011). A Key Role for NOX4 in Epithelial Cell Death During Development of Lung Fibrosis. Antioxid. Redox Signal. *15*, 607–619.

Carter, D., and Dick, A. (2009). CD200 maintains microglial potential to migrate in adult human retinal explant model. Curr. Eye Res. *28*, 427–436.

Casalotti, S.O., Pelaia, G., Yakovlev, A.G., Csikós, T., Grayson, D.R., and Krueger, K.E. (1992). Structure of the rat gene encoding the mitochondrial benzodiazepine receptor. Gene *121*, 377–382.

Casano, A.M., and Peri, F. (2015). Microglia: Multitasking Specialists of the Brain. Dev. Cell *32*, 469–477.

Castellano, B., González, B., and Nieto-Sampedro, M. (2012). Understanding glial cells.

Chader, G.J., and Taylor, A. (2013). Preface: The Aging Eye: Normal Changes, Age-Related Diseases, and Sight-Saving Approaches. Invest. Ophthalmol. Vis. Sci. *54*, ORSF1–ORSF4.

Chakravarthy, U., Wong, T.Y., Fletcher, A., Piault, E., Evans, C., Zlateva, G., Buggage, R., Pleil, A., and Mitchell, P. (2010). Clinical risk factors for age-related macular degeneration: a systematic review and meta-analysis. BMC Ophthalmol *10*, –13.

Chan, E.C., van Wijngaarden, P., Chan, E., Ngo, D., Wang, J.-H., Peshavariya, H.M., Dusting, G.J., and Liu, G.-S. (2016). NADPH oxidase 2 plays a role in experimental corneal neovascularization. Clinical Science *130*, 683–696.

Checchin, D., Sennlaub, F., Levavasseur, E., Leduc, M., and Chemtob, S. (2006). Potential role of microglia in retinal blood vessel formation. Invest. Ophthalmol. Vis. Sci. *47*, 3595–3602.

Chelli, B., Falleni, A., Salvetti, F., Gremigni, V., Lucacchini, A., and Martini, C. (2001). Peripheral-type benzodiazepine receptor ligands: Mitochondrial permeability transition induction in rat cardiac tissue. Biochemical Pharmacology *61*, 695–705.

Chen, M., Luo, C., Zhao, J., Devarajan, G., and Xu, H. (2019). Immune regulation in the aging retina. Prog Retin Eye Res *69*, 159–172.

Chen, S., Tisch, N., Kegel, M., Yerbes, R., Hermann, R., Hudalla, H., Zuliani, C., Gülcüler, G.S., Zwadlo, K., Engelhardt, von, J., et al. (2017). CNS Macrophages Control Neurovascular Development via CD95L. Cell Rep *19*, 1378–1393.

Cheng, G., Cao, Z., Xu, X., Meir, E.G.V., and Lambeth, J.D. (2001). Homologs of gp91phox: cloning and tissue expression of Nox3, Nox4, and Nox5. Gene *269*, 131–140.

Cheng, L., Chen, L., Wei, X., Wang, Y., Ren, Z., Zeng, S., Zhang, X., Wen, H., Gao, C., and Liu, H. (2018). NOD2 promotes dopaminergic degeneration regulated by NADPH oxidase 2 in 6-hydroxydopamine model of Parkinson's disease. J Neuroinflammation *15*, 243.

Chéret, C., Gervais, A., Lelli, A., Colin, C., Amar, L., Ravassard, P., Mallet, J., Cumano, A., Krause, K.-H., and Mallat, M. (2008). Neurotoxic Activation of Microglia Is Promoted by a Nox1-Dependent NADPH Oxidase. J. Neurosci. *28*, 12039–12051.

Choi, H.B., Khoo, C., Ryu, J.K., Van Breemen, E., Kim, S.U., and McLarnon, J.G. (2002). Inhibition of lipopolysaccharide-induced cyclooxygenase-2, tumor necrosis factor-α and $[Ca^{2+}]i$ responses in human microglia by the peripheral benzodiazepine receptor ligand PK11195. J. Neurochem. *83*, 546–555.

Choi, J., Ifuku, M., Noda, M., and Guilarte, T.R. (2010). Translocator protein (18 kDa)/peripheral benzodiazepine receptor specific ligands induce microglia functions consistent with an activated state. Glia *59*, 219–230.

Christensen, A., and Pike, C.J. (2018). TSPO ligand PK11195 improves Alzheimer-related outcomes in aged female 3xTg-AD mice. Neuroscience Letters *683*, 7–12.

Clark, V.M. (1986). The cell biology of the retinal pigment epithelium (The Retina: A Model for Cell Biology Studies).

Cleary, J., Johnson, K.M., Opipari, A.W., Jr., and Glick, G.D. (2007). Inhibition of the mitochondrial F1F0-ATPase by ligands of the peripheral benzodiazepine receptor. Bioorganic & Medicinal Chemistry Letters *17*, 1667–1670.

Cohen, S.Y., Dubois, L., Tadayoni, R., Delahaye-Mazza, C., Debibie, C., and Quentel, G. (2007). Prevalence of reticular pseudodrusen in age-related macular degeneration with newly diagnosed choroidal neovascularisation. Br J Ophthalmol *91*, 354–359.

Colijn, J.M., Buitendijk, G.H.S., Prokofyeva, E., Alves, D., Cachulo, M.L., Khawaja, A.P., Cougnard-Gregoire, A., Merle, B.M.J., Korb, C., Erke, M.G., et al. (2017). Prevalence of Age-Related Macular Degeneration in Europe. Ophthalmology *124*, 1753–1763.

Combadière, C., Feumi, C., Raoul, W., Keller, N., Rodéro, M., Pézard, A., Lavalette, S., Houssier, M., Jonet, L., Picard, E., et al. (2007). CX3CR1-dependent subretinal microglia cell accumulation is associated with cardinal features of age-related macular degeneration. J Clin Invest *117*, 2920–2928.

Contreras, L., Drago, I., Zampese, E., and Pozzan, T. (2010). Mitochondria: the calcium connection. Biochim. Biophys. Acta *1797*, 607–618.

Costa, E., and Guidotti, A. (1991). Diazepam binding inhibitor (DBI): A peptide with multiple biological actions. Life Sciences *49*, 325–344.

Crabb, J.W., Miyagi, M., Gu, X., Shadrach, K., West, K.A., Sakaguchi, H., Kamei, M., Hasan, A., Yan, L., Rayborn, M.E., et al. (2002). Drusen proteome analysis: An approach to the etiology of age-related macular degeneration. Proc. Natl. Acad. Sci. U.S.a. *99*, 14682–14687.

Danis, R.P., Lavine, J.A., and Domalpally, A. (2015). Geographic atrophy in patients with advanced dry age-related macular degeneration: current challenges and future prospects. Clin Ophthalmol *9*, 2159–2174.

Daugherty, D.J., Chechneva, O., Mayrhofer, F., and Deng, W. (2016). The hGFAP-driven conditional TSPO knockout is protective in a mouse model of multiple sclerosis. Sci Rep *6*, 22556.

Daugherty, D.J., Selvaraj, V., Chechneva, O.V., Liu, X.B., Pleasure, D.E., and Deng, W. (2013). A TSPO ligand is protective in a mouse model of multiple sclerosis. EMBO Molecular Medicine *5*, 891–903.

Davalos, D., Grutzendler, J., Yang, G., Kim, J.V., Zuo, Y., Jung, S., Littman, D.R., Dustin, M.L., and Gan, W.B. (2005). ATP mediates rapid microglial response to local brain injury in vivo. Nat. Neurosci. *8*, 752–758.

Dawson, L.D.C., and Lavail, M.M. (1979). Rods and cones in the mouse retina. II. Autoradiographic analysis of cell generation using tritiated thymidine. Journal of Comparative Neurology *188*, 263–272.

De Souza, E.B., Anholt, R.R., Murphy, K.M., Snyder, S.H., and Kuhar, M.J. (1985). Peripheral-type benzodiazepine receptors in endocrine organs: autoradiographic localization in rat pituitary, adrenal, and testis. Endocrinology *116*, 567–573.

DeAngelis, M.M., Owen, L.A., Morrison, M.A., Morgan, D.J., Li, M., Shakoor, A., Vitale, A., Iyengar, S., Stambolian, D., Kim, I.K., et al. (2017). Genetics of age-related macular degeneration (AMD). Hum. Mol. Genet. *26*, R246–R246.

Deffert, C., Carnesecchi, S., Yuan, H., Rougemont, A.L., Kelkka, T., Holmdahl, R., Krause, K.-H., and Schäppi, M.G. (2012). Hyperinflammation of chronic granulomatous disease is abolished by NOX2 reconstitution in macrophages and dendritic cells. J. Pathol. *228*, 341–350.

Delavoie, F., Li, H., Hardwick, M., Robert, J.C., Giatzakis, C., Peranzi, G., Yao, Z.X., Maccario, J., Lacapere, J.J., and Papadopoulos, V. (2003). In vivo and in vitro peripheral-type benzodiazepine receptor polymerization: Functional significance in drug ligand and cholesterol binding. Biochemistry *42*, 4506–4519.

Demaurex, N., Poburko, D., and Frieden, M. (2009). Regulation of plasma membrane calcium fluxes by mitochondria. Biochimica Et Biophysica Acta (BBA) - Bioenergetics *1787*, 1383–1394.

Dikalov, Sergey I., and Harrison, David D. (2014). Methods for Detection of Mitochondrial and Cellular Reactive Oxygen Species. Antioxid. Redox Signal. *20*, 372–382.

Doyle, S.L., Campbell, M., Ozaki, E., Salomon, R.G., Mori, A., Kenna, P.F., Farrar, G.J., Kiang, A.-S., Humphries, M.M., Lavelle, E.C., et al. (2012). NLRP3 has a protective role in age-related macular degeneration through the induction of IL-18 by drusen components. Nat. Med. *18*, 791–798.

Ebert, S., Weigelt, K., Walczak, Y., Drobnik, W., Mauerer, R., Hume, D.A., Weber, B.H.F., and Langmann, T. (2009). Docosahexaenoic acid attenuates microglial activation and delays early retinal degeneration. J. Neurochem. *110*, 1863–1875.

Edison, P., Archer, H.A., Gerhard, A., Hinz, R., Pavese, N., Turkheimer, F.E., Hammers, A., Tai, Y.F., Fox, N., Kennedy, A., et al. (2008). Microglia, amyloid, and cognition in Alzheimer's disease: An [11C] (R)PK11195-PET and [11C] PIB-PET study. Neurobiol. Dis. *32*, 412–419.

Elmore, M.R.P., Najafi, A.R., Koike, M.A., Dagher, N.N., Spangenberg, E.E., Rice, R.A., Kitazawa, M., Matusow, B., Nguyen, H., West, B.L., et al. (2014). Colony-stimulating factor 1 receptor signaling is necessary for microglia viability, unmasking a microglia progenitor cell in the adult brain. Neuron *82*, 380–397.

Espinosa-Heidmann, D.G., Suner, I.J., Catanuto, P., Hernandez, E.P., Marin-Castano, M.E., and Cousins, S.W. (2006). Cigarette Smoke–Related Oxidants and the Development of Sub-RPE Deposits in an Experimental Animal Model of Dry AMD. Invest. Ophthalmol. Vis. Sci. *47*, 729–737.

Eysel, U. (1998). Sehen. In Neuro- Und Sinnesphysiologie, (Berlin, Heidelberg: Springer, Berlin, Heidelberg), pp. 263–304.

Fan, J., Lindemann, P., G J Feuilloley, M., and Papadopoulos, V. (2012). Structural and Functional Evolution of the Translocator Protein (18 kDa). Current Molecular Medicine *12*, 369–386.

Fantin, A., Vieira, J.M., Gestri, G., Denti, L., Schwarz, Q., Prykhozhij, S., Peri, F., Wilson, S.W., and Ruhrberg, C. (2010). Tissue macrophages act as cellular chaperones for vascular anastomosis downstream of VEGF-mediated endothelial tip cell induction. Blood *116*, 829–840.

Ferreira, R., Santos, T., Cortes, L., Cochaud, S., Agasse, F., Silva, A.P., Xapelli, S., and Malva, J.O. (2012). Neuropeptide Y inhibits interleukin-1 beta-induced microglia motility. J. Neurochem. *120*, 93–105.

Ferzaz, B., Brault, E., Bourliaud, G., Robert, J.-P., Poughon, G., Claustre, Y., Marguet, F., Liere, P., Schumacher, M., Nowicki, J.-P., et al. (2002). SSR180575 (7-chloro-N,N,5-trimethyl-4-oxo-3-phenyl-3,5-dihydro-4H-pyridazino[4,5-b]indole-1-acetamide), a peripheral benzodiazepine receptor ligand, promotes neuronal survival and repair. J. Pharmacol. Exp. Ther. *301*, 1067–1078.

Finkel, T. (2012). Signal transduction by mitochondrial oxidants. J. Biol. Chem. *287*, 4434–4440.

Frade, J.M., and Barde, Y.A. (1998). Microglia-derived nerve growth factor causes cell death in the developing retina. Neuron *20*, 35–41.

Francis, P.J., Hamon, S.C., Ott, J., Weleber, R.G., and Klein, M.L. (2009). Polymorphisms in C2, CFB and C3 are associated with progression to advanced age related macular degeneration associated with visual loss. Journal of Medical Genetics *46*, 300–307.

Franze, K., Grosche, J., Skatchkov, S.N., Schinkinger, S., Foja, C., Schild, D., Uckermann, O., Travis, K., Reichenbach, A., and Guck, J. (2007). Müller cells are living optical fibers in the vertebrate retina. Proc. Natl. Acad. Sci. U.S.a. *104*, 8287–8292.

Fritsche, L.G., Fariss, R.N., Stambolian, D., Abecasis, G.R., Curcio, C.A., and Swaroop, A. (2014). Age-Related Macular Degeneration: Genetics and Biology Coming Together. Annu Rev Genomics Hum Genet *15*, 151–171.

Fritsche, L.G., Igl, W., Bailey, J.N.C., Grassmann, F., Sengupta, S., Bragg-Gresham, J.L., Burdon, K.P., Hebbring, S.J., Wen, C., Gorski, M., et al. (2016). A large genome-wide association study of age-related macular degeneration highlights contributions of rare and common variants. Nat. Genet. *48*, 134–143.

Fritsche, L.G., Loenhardt, T., Janssen, A., Fisher, S.A., Rivera, A., Keilhauer, C.N., and Weber, B.H.F. (2008). Age-related macular degeneration is associated with an unstable ARMS2 (LOC387715) mRNA. Nat. Genet. *40*, 892–896.

Gao, H.-M., Zhou, H., and Hong, J.-S. (2012). NADPH oxidases: novel therapeutic targets for neurodegenerative diseases. Trends in Pharmacological Sciences *33*, 295–303.

Gao, J., Liu, R.T., Cao, S., Cui, J.Z., Wang, A., To, E., and Matsubara, J.A. (2015). NLRP3 Inflammasome: Activation and Regulation in Age-Related Macular Degeneration. Mediators of Inflammation *2015*, 1–11.

Gatliff, J., East, D.A., Singh, A., Alvarez, M.S., Frison, M., Matic, I., Ferraina, C., Sampson, N., Turkheimer, F., and Campanella, M. (2017). A role for TSPO in mitochondrial Ca^{2+} homeostasis and redox stress signaling. Cell Death Dis *8*, e2896–e2896.

Gatliff, J., East, D., Crosby, J., Abeti, R., Harvey, R., Craigen, W., Parker, P., and Campanella, M. (2014). TSPO interacts with VDAC1 and triggers a ROS-mediated inhibition of mitochondrial quality control. Autophagy *10*, 2279–2296.

Gavazzi, G., Banfi, B., Deffert, C., Fiette, L., Schappi, M., Herrmann, F., and Krause, K.H. (2006). Decreased blood pressure in NOX1-deficient mice. FEBS Letters *580*, 497–504.

Gavish, M., Bachman, I., Shoukrun, R., Katz, Y., Veenman, L., Weisinger, G., and Weizman, A. (1999). Enigma of the Peripheral Benzodiazepine Receptor. Pharmacol Rev *51*, 629–650.

Ge, Y., Jiang, W., Gan, L., Wang, L., Sun, C., Ni, P., Liu, Y., Wu, S., Gu, L., Zheng, W., et al. (2010). Mouse embryonic fibroblasts from CD38 knockout mice are resistant to oxidative stresses through inhibition of reactive oxygen species production and Ca(2+) overload. Biochem. Biophys. Res. Commun. *399*, 167–172.

Geerlings, M.J., de Jong, E.K., and Hollander, den, A.I. (2017). The complement system in age-related macular degeneration: A review of rare genetic variants and implications for personalized treatment. Mol. Immunol. *84*, 65–76.

Gehlert, D.R., Yamamura, H.I., and Wamsley, J.K. (1985). Autoradiographic localization of "peripheral-type" benzodiazepine binding sites in the rat brain, heart and kidney. Naunyn-Schmiedeberg's Arch. Pharmacol. *328*, 454–460.

Geiszt, M., and Leto, T.L. (2004). The Nox family of NAD(P)H oxidases: host defense and beyond. J. Biol. Chem. *279*, 51715–51718.

Giorgio, V., Stockum, von, S., Antoniel, M., Fabbro, A., Fogolari, F., Forte, M., Glick, G.D., Petronilli, V., Zoratti, M., Szabó, I., et al. (2013). Dimers of mitochondrial ATP synthase form the permeability transition pore. Proc. Natl. Acad. Sci. U.S.a. *110*, 5887–5892.

Gluschko, A., Herb, M., Wiegmann, K., Krut, O., Neiss, W.F., Utermöhlen, O., Krönke, M., and Schramm, M. (2018). The β2 Integrin Mac-1 Induces Protective LC3-Associated Phagocytosis of Listeria monocytogenes. Cell Host Microbe *23*, 324–337.e325.

Gong, J., Szego, É.M., Leonov, A., Benito, E., Becker, S., Fischer, A., Zweckstetter, M., Outeiro, T., and Schneider, A. (2019). Translocator Protein Ligand Protects against Neurodegeneration in the MPTP Mouse Model of Parkinsonism. J. Neurosci. *39*, 3752–3769.

Gong, Y., Li, J., Sun, Y., Fu, Z., Liu, C.-H., Evans, L., Tian, K., Saba, N., Fredrick, T., Morss, P., et al. (2015). Optimization of an Image-Guided Laser-Induced Choroidal Neovascularization Model in Mice. Plos One *10*, e0132643.

Gordeeva, A.V., Zvyagilskaya, R.A., and Labas, Y.A. (2003). Cross-talk between reactive oxygen species and calcium in living cells. Biochemistry Mosc. *68*, 1077–1080.

Görlach, A., Bertram, K., Hudecova, S., and Krizanova, O. (2015). Calcium and ROS: A mutual interplay. Redox Biol *6*, 260–271.

Green, W.R. (1991). Clinicopathologic studies of treated choroidal neovascular membranes. A review and report of two cases. Retina (Philadelphia, Pa.) *11*, 328–356.

Green, W.R., McDonnell, P.J., and Yeo, J.H. (1985). Pathologic features of senile macular degeneration. Ophthalmology *92*, 615–627.

Guilarte, T.R., Loth, M.K., and Guariglia, S.R. (2016). TSPO Finds NOX2 in Microglia for Redox Homeostasis. Trends in Pharmacological Sciences *37*, 334–343.

Guo, Y., Kalathur, R.C., Liu, Q., Kloss, B., Bruni, R., Ginter, C., Kloppmann, E., Rost, B., and Hendrickson, W.A. (2015). Structure and activity of tryptophan-rich TSPO proteins. Science *347*, 551–555.

Gupta, N., Brown, K.E., and Milam, A.H. (2003). Activated microglia in human retinitis pigmentosa, late-onset retinal degeneration, and age-related macular degeneration. Exp. Eye Res. *76*, 463–471.

Halliwell, B. (2006). Oxidative stress and neurodegeneration: where are we now? J. Neurochem. *97*, 1634–1658.

Hamon, A., Morel, A., Hue, B., Verleye, M., and Gillardin, J.-M. (2003). The modulatory effects of the anxiolytic etifoxine on GABAA receptors are mediated by the β subunit. Neuropharmacology *45*, 293–303.

Han, W., Li, H., Cai, J., Gleaves, L.A., Polosukhin, V.V., Segal, B.H., Yull, F.E., and Blackwell, T.S. (2013). NADPH Oxidase Limits Lipopolysaccharide-Induced Lung Inflammation and Injury in Mice through Reduction-Oxidation Regulation of NF-κB Activity. The Journal of Immunology *190*, 4786–4794.

Harada, C., Harada, T., Quah, H.M.A., Maekawa, F., Yoshida, K., Ohno, S., Wada, K., Parada, L.F., and Tanaka, K. (2003). Potential role of glial cell line-derived neurotrophic factor receptors in Müller glial cells during light-induced retinal degeneration. Neuroscience *122*, 229–235.

Harada, T., Harada, C., Nakayama, N., Okuyama, S., Yoshida, K., Kohsaka, S., Matsuda, H., and Wada, K. (2000). Modification of Glial–Neuronal Cell Interactions Prevents Photoreceptor Apoptosis during Light-Induced Retinal Degeneration. Neuron *26*, 533–541.

Haslund-Vinding, J., McBean, G., Jaquet, V., and Vilhardt, F. (2017). NADPH oxidases in oxidant production by microglia: activating receptors, pharmacology and association with disease. Br. J. Pharmacol. *174*, 1733–1749.

He, Y., Taylor, N., Fourgeaud, L., and Bhattacharya, A. (2017). The role of microglial P2X7: modulation of cell death and cytokine release. J Neuroinflammation *14*, 135–13.

Hempel, S.L., Buettner, G.R., O'Malley, Y.Q., Wessels, D.A., and Flaherty, D.M. (1999). Dihydrofluorescein diacetate is superior for detecting intracellular oxidants: comparison with 2′,7′-dichlorodihydrofluorescein diacetate, 5(and 6)-carboxy-2′,7′-dichlorodihydrofluorescein diacetate, and dihydrorhodamine 123. Free Radical Biology and Medicine *27*, 146–159.

Herb, M., Gluschko, A., Wiegmann, K., Farid, A., Wolf, A., Utermöhlen, O., Krut, O., Krönke, M., and Schramm, M. (2019). Mitochondrial reactive oxygen species enable proinflammatory signaling through disulfide linkage of NEMO. Sci Signal *12*, eaar5926.

Hernangómez, M., Mestre, L., Correa, F.G., Loría, F., Mecha, M., Iñigo, P.M., Docagne, F., Williams, R.O., Borrell, J., and Guaza, C. (2012). CD200-CD200R1 interaction contributes to neuroprotective effects of anandamide on experimentally induced inflammation. Glia *60*, 1437–1450.

Hickman, S.E., Kingery, N.D., Ohsumi, T.K., Borowsky, M.L., Wang, L.-C., Means, T.K., and Khoury, El, J. (2013). The microglial sensome revealed by direct RNA sequencing. Nat. Neurosci. *16*, 1896–1905.

Hinojosa, A.E., Garcia-Bueno, B., Leza, J.C., and Madrigal, J.L. (2011). CCL2/MCP-1 modulation of microglial activation and proliferation. J Neuroinflammation *8*, 1–10.

Hoek, R.M., Ruuls, S.R., Murphy, C.A., Wright, G.J., Goddard, R., Zurawski, S.M., Blom, B., Homola, M.E., Streit, W.J., Brown, M.H., et al. (2000). Down-Regulation of the Macrophage Lineage Through Interaction with OX2 (CD200). Science *290*, 1768–1771.

Holmstroem, K.M., and Finkel, T. (2014). Cellular mechanisms and physiological consequences of redox-dependent signalling. Nat. Rev. Mol. Cell Biol. *15*, 411–421.

Horst, C.J., Johnson, L.V., and Besharse, J.C. (1990). Transmembrane assemblage of the photoreceptor connecting cilium and motile cilium transition zone contain a common immunologic epitope. Cell Motility and the Cytoskeleton *17*, 329–344.

Hou, L., Bao, X., Zang, C., Yang, H., Sun, F., Che, Y., Wu, X., Li, S., Zhang, D., and Wang, Q. (2018). Integrin CD11b mediates α-synuclein-induced activation of NADPH oxidase through a Rho-dependent pathway. Redox Biol *14*, 600–608.

Huang, Y., Xu, Z., Xiong, S., Qin, G., Sun, F., Yang, J., Yuan, T.-F., Zhao, L., Wang, K., Liang, Y.-X., et al. (2018a). Dual extra-retinal origins of microglia in the model of retinal microglia repopulation. Cell Discov *4*, 9–16.

Huang, Y., Xu, Z., Xiong, S., Sun, F., Qin, G., Hu, G., Wang, J., Zhao, L., Liang, Y.-X., Wu, T., et al. (2018b). Repopulated microglia are solely derived from the proliferation of residual microglia after acute depletion. Nat. Neurosci. *21*, 530–540.

Hume, D.A., Perry, V.H., and Gordon, S. (1983). Immunohistochemical Localization of a Macrophage-Specific Antigen in Developing Mouse Retina - Phagocytosis of Dying Neurons and Differentiation of Microglial Cells to Form a Regular Array in the Plexiform Layers. J. Cell Biol. *97*, 253–257.

Hurley, J.B., Lindsay, K.J., and Du, J. (2015). Glucose, lactate, and shuttling of metabolites in vertebrate retinas. J. Neurosci. Res. *93*, 1079–1092.

Issop, L., Ostuni, M.A., Lee, S., Laforge, M., Péranzi, G., Rustin, P., Benoist, J.-F., Estaquier, J., Papadopoulos, V., and Lacapère, J.-J. (2016). Translocator Protein-Mediated Stabilization of Mitochondrial Architecture during Inflammation Stress in Colonic Cells. Plos One *11*, e0152919.

Jacobs, G.H., Neitz, J., and Deegan, J.F. (1991). Retinal receptors in rodents maximally sensitive to ultraviolet light. Nature *353*, 655–656.

Jaipuria, G., Leonov, A., Giller, K., Vasa, S.K., Jaremko, L., Jaremko, M., Linser, R., Becker, S., and Zweckstetter, M. (2017). Cholesterol-mediated allosteric regulation of the mitochondrial translocator protein structure. Nature Communications 2014 5 *8*, –8.

Jamin, N., Neumann, J.M., Molecular, M.O., 2005 Characterization of the cholesterol recognition amino acid consensus sequence of the peripheral-type benzodiazepine receptor. Molecular Endocrinology *19*, 588-594.

Jaremko, L., Jaremko, M., Giller, K., Becker, S., and Zweckstetter, M. (2014). Structure of the mitochondrial translocator protein in complex with a diagnostic ligand. Science *343*, 1363–1366.

Jaremko, M., Jaremko, Ł., Jaipuria, G., Becker, S., and Zweckstetter, M. (2015). Structure of the mammalian TSPO/PBR protein. Biochemical Society Transactions *43*, 566–571.

Jin, W.-N., Shi, S.X.-Y., Li, Z., Li, M., Wood, K., Gonzales, R.J., and Liu, Q. (2017). Depletion of microglia exacerbates postischemic inflammation and brain injury. J. Cereb. Blood Flow Metab. *37*, 2224–2236.

Joachim, N., Colijn, J.M., Kifley, A., Lee, K.E., Buitendijk, G.H.S., Klein, B.E.K., Myers, C.E., Meuer, S.M., Tan, A.G., Holliday, E.G., et al. (2017). Five-year progression of unilateral age-related macular degeneration to bilateral involvement: The Three Continent AMD Consortium report. Br J Ophthalmol *101*, 1185–1192.

Johnson, K.M., Cleary, J., Fierke, C.A., Anthony W Opipari, J., and Glick, G.D. (2006). Mechanistic Basis for Therapeutic Targeting of the Mitochondrial F1Fo-ATPase. ACS Chem. Biol. *1*, 304–308.

Johnson, L.V., Leitner, W.P., Staples, M.K., and Anderson, D.H. (2001). Complement activation and inflammatory processes in drusen formation and age-related macular degeneration. Exp. Eye Res. *73*, 887–896.

Jonas, J.B. (2010). Monocyte Chemoattractant Protein 1, Intercellular Adhesion Molecule 1, and Vascular Cell Adhesion Molecule 1 in Exudative Age-Related Macular Degeneration. Arch. Ophthalmol. *128*, 1281–1286.

Jurgens, H.A., and Johnson, R.W. (2012). Dysregulated neuronal–microglial crosstalk during aging, stress and inflammation. Experimental Neurology *233*, 40–48.

Kaludercic, N., Deshwal, S., and Di Lisa, F. (2014). Reactive oxygen species and redox compartmentalization. Front Physiol *5*, 285.

Karlstetter, M., Ebert, S., and Langmann, T. (2010). Microglia in the healthy and degenerating retina: Insights from novel mouse models. Immunobiology *215*, 685–691.

Karlstetter, M., Kopatz, J., Aslanidis, A., Shahraz, A., Caramoy, A., Linnartz-Gerlach, B., Lin, Y., Lückoff, A., Fauser, S., Düker, K., et al. (2017). Polysialic acid blocks mononuclear phagocyte reactivity, inhibits complement activation, and protects from vascular damage in the retina. EMBO Molecular Medicine *9*, 154–166.

Karlstetter, M., Lippe, E., Walczak, Y., Moehle, C., Aslanidis, A., Mirza, M., and Langmann, T. (2011). Curcumin is a potent modulator of microglial gene expression and migration. J Neuroinflammation *8*.

Karlstetter, M., Nothdurfter, C., Aslanidis, A., Moeller, K., Horn, F., Scholz, R., Neumann, H., Weber, B.H.F., Rupprecht, R., and Langmann, T. (2014). Translocator protein (18 kDa) (TSPO) is expressed in reactive retinal microglia and modulates microglial inflammation and phagocytosis. J Neuroinflammation *11*, 3.

Karlstetter, M., Scholz, R., Rutar, M., Wong, W.T., Provis, J.M., and Langmann, T. (2015). Retinal microglia: Just bystander or target for therapy? Prog Retin Eye Res *45*, 30–57.

Karperien, A., Ahammer, H., and Jelinek, H. (2013). Quantitating the subtleties of microglial morphology with fractal analysis. Front Cell Neurosci *7*.

Katz, L.C., and Shatz, C.J. (1996). Synaptic activity and the construction of cortical circuits. Science *274*, 1133–1138.

Kettenmann, H., Hanisch, U.-K., Noda, M., and Verkhratsky, A. (2011). Physiology of Microglia. Physiological Reviews *91*, 461–553.

Khan, J.C., Thurlby, D.A., Shahid, H., Clayton, D.G., Yates, J.R.W., Bradley, M., Moore, A.T., and Bird, A.C. (2006). Smoking and age-related macular degeneration: the number of pack years of cigarette smoking is a major determinant of risk for both geographic atrophy and choroidal neovascularisation. Br J Ophthalmol *90*, 75–80.

Kierdorf, K., Erny, D., Goldmann, T., Sander, V., Schulz, C., Perdiguero, E.G., Wieghofer, P., Heinrich, A., Riemke, P., Hölscher, C., et al. (2013). Microglia emerge from erythromyeloid precursors via Pu.1- and Irf8-dependent pathways. Nat. Neurosci. *16*, 273–280.

Killingsworth, M.C., Sarks, J.P., and Sarks, S.H. (1990). Macrophages related to Bruch's membrane in age-related macular degeneration. Eye *4 (Pt 4)*, 613–621.

Kim, S.Y., Moon, J.H., Lee, H.G., Kim, S.U., and Lee, Y.B. (2007). ATP released from beta-amyloid-stimulated microglia induces reactive oxygen species production in an autocrine fashion. Exp. Mol. Med. *39*, 820–827.

Kinnally, K.W., Zorov, D.B., Antonenko, Y.N., Snyder, S.H., McEnery, M.W., and Tedeschi, H. (1993). Mitochondrial benzodiazepine receptor linked to inner membrane ion channels by nanomolar actions of ligands. Proc. Natl. Acad. Sci. U.S.a. *90*, 1374–1378.

Kita, A., Kohayakawa, H., Kinoshita, T., Ochi, Y., Nakamichi, K., Kurumiya, S., Furukawa, K., and Oka, M. (2004). Antianxiety and antidepressant-like effects of AC-5216, a novel mitochondrial benzodiazepine receptor ligand. Br. J. Pharmacol. *142*, 1059–1072.

Klein, R.J., Zeiss, C., Chew, E.Y., Tsai, J.-Y., Sackler, R.S., Haynes, C., Henning, A.K., SanGiovanni, J.P., Mane, S.M., Mayne, S.T., et al. (2005). Complement factor H polymorphism in age-related macular degeneration. Science *308*, 385–389.

Klein, R., Klein, B.E.K., and Linton, K.L.P. (1992). Prevalence of Age-related Maculopathy: The Beaver Dam Eye Study. Ophthalmology *99*, 933–943.

Kokona, D., Ebneter, A., Escher, P., and Zinkernagel, M.S. (2018). Colony-stimulating factor 1 receptor inhibition prevents disruption of the blood-retina barrier during chronic inflammation. J Neuroinflammation *15*, 340–18.

Kokoszka, J.E., Waymire, K.G., Levy, S.E., Sligh, J.E., Cai, J., Jones, D.P., MacGregor, G.R., and Wallace, D.C. (2004). The ADP/ATP translocator is not essential for the mitochondrial permeability transition pore. Nature *427*, 461–465.

Komatsu, H. (2006). The neural mechanisms of perceptual filling-in. Nature Reviews Neuroscience 2014 15:4 *7*, 220–231.

Krady, J.K., Lin, H.W., Liberto, C.M., Basu, A., Kremlev, S.G., and Levison, S.W. (2008). Ciliary neurotrophic factor and interleukin-6 differentially activate microglia. J. Neurosci. Res. *86*, 1538–1547.

Kubota, R., Boman, N.L., David, R., Mallikaarjun, S., Patil, S., and Birch, D. (2012). Safety and effect on rod function of acu-4429, a novel small-molecule visual cycle modulator. Retina (Philadelphia, Pa.) *32*, 183–188.

Kubota, Y., Takubo, K., Shimizu, T., Ohno, H., Kishi, K., Shibuya, M., Saya, H., and Suda, T. (2009). M-CSF inhibition selectively targets pathological angiogenesis and lymphangiogenesis. J. Exp. Med. *206*, 1089–1102.

la Cour, M., Kiilgaard, J.F., and Nissen, M.H. (2002). Age-Related Macular Degeneration. Drugs & Aging *19*, 101–133.

Lambert, V., Lecomte, J., Hansen, S., Blacher, S., Gonzalez, M.-L.A., Struman, I., Sounni, N.E., Rozet, E., de Tullio, P., Foidart, J.M., et al. (2013). Laser-induced choroidal neovascularization model to study age-related macular degeneration in mice. Nat Protoc *8*, 2197–2211.

Lambeth, J.D. (2004). NOX enzymes and the biology of reactive oxygen. Nat. Rev. Immunol. *4*, 181–189.

Lambeth, J.D., and Neish, A.S. (2014). Nox Enzymes and New Thinking on Reactive Oxygen: A Double-Edged Sword Revisited. Annual Review of Pathology: Mechanisms of Disease, Vol *99*, 119–145.

Lambeth, J.D., Kawahara, T., and Diebold, B. (2007). Regulation of Nox and Duox enzymatic activity and expression. Free Radical Biology and Medicine *43*, 319–331.

Langmann, T. (2007). Microglia activation in retinal degeneration. J. Leukoc. Biol. *81*, 1345–1351.

Lawson, L.J., Perry, V.H., and Gordon, S. (1992). Turnover of resident microglia in the normal adult mouse brain. Neuroscience *48*, 405–415.

Li, F., Xia, Y., Meiler, J., and Ferguson-Miller, S. (2013). Characterization and modeling of the oligomeric state and ligand binding behavior of purified translocator protein 18 kDa from Rhodobacter sphaeroides. Biochemistry *52*, 5884–5899.

Li, F., Jiang, D., and Samuel, M.A. (2019). Microglia in the developing retina. Neural Dev *14*, 12–13.

Li, H., Endocrinology, V.P., 1998 Peripheral-type benzodiazepine receptor function in cholesterol transport. Identification of a putative cholesterol recognition/interaction amino acid sequence and consensus pattern. Endocrinology *139*, 4991-4997.

Li, H., Yao, Z.-X., Degenhardt, B., Teper, G., and Papadopoulos, V. (2001). Cholesterol binding at the cholesterol recognition/ interaction amino acid consensus (CRAC) of the peripheral-type benzodiazepine receptor and inhibition of steroidogenesis by an HIV TAT-CRAC peptide. Proc. Natl. Acad. Sci. U.S.a. *98*, 1267–1272.

Li, M., Li, Z., Ren, H., Jin, W.-N., Wood, K., Liu, Q., Sheth, K.N., and Shi, F.-D. (2017a). Colony stimulating factor 1 receptor inhibition eliminates microglia and attenuates brain injury after intracerebral hemorrhage. J. Cereb. Blood Flow Metab. *37*, 2383–2395.

Li, M., Ren, H., Sheth, K.N., Shi, F.-D., and Liu, Q. (2017b). A TSPO ligand attenuates brain injury after intracerebral hemorrhage. The FASEB Journal *31*, 3278–3287.

Liang, K.J., Lee, J.E., Wang, Y.D., Ma, W., Fontainhas, A.M., Fariss, R.N., and Wong, W.T. (2009). Regulation of Dynamic Behavior of Retinal Microglia by CX3CR1 Signaling. Invest. Ophthalmol. Vis. Sci. *50*, 4444–4451.

Lin, D., Chang, Y.J., Strauss, J.F., III, and Miller, W.L. (1993). The human peripheral renzodiazepine receptor gene: Cloning and characterization of alternative splicing in normal tissues and in a patient with congenital lipoid adrenal hyperplasia. Genomics *18*, 643–650.

Liu, G.J., Middleton, R.J., Kam, W.W.Y., Chin, D.Y., Hatty, C.R., Chan, R.H.Y., and Banati, R.B. (2017). Functional gains in energy and cell metabolism after TSPO gene insertion. Cell Cycle *16*, 436–447.

Luhmann, U.F.O., Robbie, S., Munro, P.M.G., Barker, S.E., Duran, Y., Luong, V., Fitzke, F.W., Bainbridge, J.W.B., Ali, R.R., and MacLaren, R.E. (2009). The Drusenlike Phenotype in Aging Ccl2-Knockout Mice Is Caused by an Accelerated Accumulation of Swollen Autofluorescent Subretinal Macrophages. Invest. Ophthalmol. Vis. Sci. *50*, 5934–5943.

Lundqvist, H., and Dahlgren, C. (1996). Isoluminol-enhanced chemiluminescence: A sensitive method to study the release of superoxide anion from human neutrophils. Free Radical Biology and Medicine *20*, 785–792.

Lückoff, A., Caramoy, A., Scholz, R., Prinz, M., Kalinke, U., and Langmann, T. (2016). Interferon-beta signaling in retinal mononuclear phagocytes attenuates pathological neovascularization. EMBO Molecular Medicine *8*, 670–678.

Lückoff, A., Scholz, R., Sennlaub, F., Xu, H., and Langmann, T. (2017). Comprehensive analysis of mouse retinal mononuclear phagocytes. Nat Protoc *12*, 1136–1150.

Ma, M.W., Wang, J., Dhandapani, K.M., and Brann, D.W. (2017). NADPH Oxidase 2 Regulates NLRP3 Inflammasome Activation in the Brain after Traumatic Brain Injury. Oxid Med Cell Longev *2017*, 1–18.

Ma, M.W., Wang, J., Dhandapani, K.M., and Brann, D.W. (2018). Deletion of NADPH oxidase 4 reduces severity of traumatic brain injury. Free Radical Biology and Medicine *117*, 66–75.

Maeda, J., Higuchi, M., Inaji, M., Ji, B., Haneda, E., Okauchi, T., Zhang, M.-R., Suzuki, K., and Suhara, T. (2007). Phase-dependent roles of reactive microglia and astrocytes in nervous system injury as delineated by imaging of peripheral benzodiazepine receptor. Brain Res. *1157*, 100–111.

Mages, K., Grassmann, F., Jägle, H., Rupprecht, R., Weber, B.H.F., Hauck, S.M., and Grosche, A. (2019). The agonistic TSPO ligand XBD173 attenuates the glial response thereby protecting inner retinal neurons in a murine model of retinal ischemia. J Neuroinflammation *16*, 43.

Maller, J., George, S., Purcell, S., Fagerness, J., Altshuler, D., Daly, M.J., and Seddon, J.M. (2006). Common variation in three genes, including a noncoding variant in CFH , strongly influences risk of age-related macular degeneration. Nat. Genet. *38*, 1055–1059.

Manich, G., Recasens, M., Valente, T., Almolda, B., González, B., and Castellano, B. (2019). Role of the CD200-CD200R Axis During Homeostasis and Neuroinflammation. Neuroscience *405*, 118–136.

Marden, J.J., Harraz, M.M., Williams, A.J., Nelson, K., Luo, M., Paulson, H., and Engelhardt, J.F. (2007). Redox modifier genes in amyotrophic lateral sclerosis in mice. J Clin Invest *117*, 2913–2919.

Marinelli, S., Basilico, B., Marrone, M.C., and Ragozzino, D. (2019). Microglia-neuron crosstalk: Signaling mechanism and control of synaptic transmission. Semin. Cell Dev. Biol. *94*, 138–151.

Marín-Teva, J.L., Dusart, I., Colin, C., Gervais, A., van Rooijen, N., and Mallat, M. (2004). Microglia promote the death of developing Purkinje cells. Neuron *41*, 535–547.

Martel-Gallegos, G., Casas-Pruneda, G., Ortega-Ortega, F., Sanchez-Armass, S., Alberto Olivares-Reyes, J., Diebold, B., Perez-Cornejo, P., and Arreola, J. (2013). Oxidative stress induced by P2X7 receptor stimulation in murine macrophages is mediated by c-Src/Pyk2 and ERK1/2. Biochimica Et Biophysica Acta-General Subjects *1830*, 4650–4659.

Martyanova, E.K., conference, A.T.A.A., 2015 3D quantitative analysis of microglial morphology. Researchgate.Net

Masland, R.H. (2001). The fundamental plan of the retina. Nat. Neurosci. *4*, 877–886.

McEnery, M.W., Snowman, A.M., Trifiletti, R.R., and Snyder, S.H. (1992). Isolation of the mitochondrial benzodiazepine receptor: association with the voltage-dependent anion channel and the adenine nucleotide carrier. Proc. Natl. Acad. Sci. U.S.a. *89*, 3170–3174.

McLeod, D.S., Grebe, R., Bhutto, I., Merges, C., Baba, T., and Lutty, G.A. (2009). Relationship between RPE and Choriocapillaris in Age-Related Macular Degeneration. Invest. Ophthalmol. Vis. Sci. *50*, 4982–4991.

Meßmer, K., and Reynolds, G.P. (1998). Increased peripheral benzodiazepine binding sites in the brain of patients with Huntington's disease. Neuroscience Letters *241*, 53–56.

Mezey, E., Chandross, K.J., Harta, G., Maki, R.A., and McKercher, S.R. (2000). Turning blood into brain: cells bearing neuronal antigens generated in vivo from bone marrow. Science *290*, 1779–1782.

Midzak, A., Zirkin, B., and Papadopoulos, V. (2015). Translocator protein: pharmacology and steroidogenesis. Biochemical Society Transactions *43*, 572–578.

Milenkovic, V.M., Slim, D., Bader, S., Koch, V., Heinl, E.-S., Alvarez-Carbonell, D., Nothdurfter, C., Rupprecht, R., and Wetzel, C.H. (2019). CRISPR-Cas9 Mediated TSPO Gene Knockout alters Respiration and Cellular Metabolism in Human Primary Microglia Cells. Int J Mol Sci *20*, 3359.

Mocchetti, I., and Santi, M.R. (1991). Diazepam binding inhibitor peptide: Cloning and gene expression. Neuropharmacology *30*, 1365–1371.

Mohr, L.K.M., Hoffmann, A.V., Brandstetter, C., Holz, F.G., and Krohne, T.U. (2015). Effects of Inflammasome Activation on Secretion of Inflammatory Cytokines and Vascular Endothelial Growth Factor by Retinal Pigment Epithelial Cells. Invest. Ophthalmol. Vis. Sci. *56*, 6404–6413.

Morohaku, K., Pelton, S.H., Daugherty, D.J., Butler, W.R., Deng, W., and Selvaraj, V. (2014). Translocator protein/peripheral benzodiazepine receptor is not required for steroid hormone biosynthesis. Endocrinology *155*, 89–97.

Mukhin, A.G., Papadopoulos, V., Costa, E., and Krueger, K.E. (1989). Mitochondrial benzodiazepine receptors regulate steroid biosynthesis. Proc. Natl. Acad. Sci. U.S.a. *86*, 9813–9816.

Mullins, R.F., Russell, S.R., Anderson, D.H., and Hageman, G.S. (2000). Drusen associated with aging and age-related macular degeneration contain proteins common to extracellular deposits associated with atherosclerosis, elastosis, amyloidosis, and dense deposit disease. Faseb J. *14*, 835–846.

Nadal-Nicolás, F.M., Galindo-Romero, C., Valiente-Soriano, F.J., Barberà-Cremades, M., deTorre-Minguela, C., Salinas-Navarro, M., Pelegrín, P., and Agudo-Barriuso, M. (2016). Involvement of P2X7 receptor in neuronal degeneration triggered by traumatic injury. Sci Rep *6*, 1–14.

Nagineni, C.N., Kommineni, V.K., William, A., Detrick, B., and Hooks, J.J. (2012). Regulation of VEGF expression in human retinal cells by cytokines: Implications for the role of inflammation in age-related macular degeneration. J Cell Physiol. *227*, 116–126.

Nakano, Y., Longo-Guess, C.M., Bergstrom, D.E., Nauseef, W.M., Jones, S.M., and Banfi, B. (2008). Mutation of the Cyba gene encoding p22phox causes vestibular and immune defects in mice. J Clin Invest *118*, 1176–1185.

Nathans, J., Thomas, D., and Hogness, D.S. (1986). Molecular genetics of human color vision: the genes encoding blue, green, and red pigments. Science *232*, 193–202.

Nau, H., and Blaner, W.S. (2012). Retinoids: the biochemical and molecular basis of vitamin A and retinoid action.

Nayernia Zeynab, Jaquet Vincent, Krause Karl-Heinz (2014). New Insights on NOX Enzymes in the Central Nervous System. Antioxid. Redox Signal.

Newman, A.M., Gallo, N.B., Hancox, L.S., Miller, N.J., Radeke, C.M., Maloney, M.A., Cooper, J.B., Hageman, G.S., Anderson, D.H., Johnson, L.V., et al. (2012). Systems-level analysis of age-related macular degeneration reveals global biomarkers and phenotype-specific functional networks. Genome Med *4*, 16–18.

Nikodemova, M., Duncan, I.D., and Watters, J.J. (2006). Minocycline exerts inhibitory effects on multiple mitogen-activated protein kinases and IkappaBalpha degradation in a stimulus-specific manner in microglia. J. Neurochem. *96*, 314–323.

Nikolich-Žugich, J. (2018). The twilight of immunity: emerging concepts in aging of the immune system. Nat. Immunol. *19*, 10–19.

Nimmerjahn, A., Kirchhoff, F., and Helmchen, F. (2005). Resting microglial cells are highly dynamic surveillants of brain parenchyma in vivo. Science *308*, 1314–1318.

Ouchi, Y., Yoshikawa, E., Sekine, Y., Futatsubashi, M., Kanno, T., Ogusu, T., and Torizuka, T. (2005). Microglial activation and dopamine terminal loss in early Parkinson's disease. Ann. Neurol. *57*, 168–175.

Papadopoulos, V., Amri, H., Boujrad, N., Cascio, C., Culty, M., Garnier, M., Hardwick, M., Li, H., VIDIC, B., Brown, A.S., et al. (1997a). Peripheral benzodiazepine receptor in cholesterol transport and steroidogenesis. Steroids *62*, 21–28.

Papadopoulos, V., Amri, H., Li, H., Boujrad, N., VIDIC, B., and Garnier, M. (1997b). Targeted disruption of the peripheral-type benzodiazepine receptor gene inhibits steroidogenesis in the R2C Leydig tumor cell line. J. Biol. Chem. *272*, 32129–32135.

Papadopoulos, V., Berkovich, A., Krueger, K.E., Costa, E., and Guidotti, A. (1991). Diazepam binding inhibitor and its processing products stimulate mitochondrial steroid biosynthesis via an interaction with mitochondrial benzodiazepine receptors. Endocrinology *129*, 1481–1488.

Papadopoulos, V., Boujrad, N., IKONOMOVIC, M.D., FERRARA, P., and VIDIC, B. (1994). Topography of the Leydig-Cell Mitochondrial Peripheral-Type Benzodiazepine Receptor. Molecular and Cellular Endocrinology *104*, R5–R9.

Parekh, N., Voland, R.P., Moeller, S.M., Blodi, B.A., Ritenbaugh, C., Chappell, R.J., Wallace, R.B., Mares, J.A., CAREDS Research Study Group (2009). Association between dietary fat intake and age-related macular degeneration in the Carotenoids in Age-Related Eye Disease Study (CAREDS): an ancillary study of the Women's Health Initiative. Arch. Ophthalmol. *127*, 1483–1493.

Parkhurst, C.N., Yang, G., Ninan, I., Savas, J.N., Yates, J.R., Lafaille, J.J., Hempstead, B.L., Littman, D.R., and Gan, W.B. (2013). Microglia promote learning-dependent synapse formation through brain-derived neurotrophic factor. Cell *155*, 1596–1609.

Pascolini, D., and Mariotti, S.P. (2012). Global estimates of visual impairment: 2010. Br J Ophthalmol *96*, 614–618.

Perdiguero, E.G., Klapproth, K., Schulz, C., Immunity, K.B., 2015 The origin of tissue-resident macrophages: when an erythro-myeloid progenitor is an erythro-myeloid progenitor. Immunity *43*, 1023-1024

Perry, V.H., and Holmes, C. (2014). Microglial priming in neurodegenerative disease. Nat Rev Neurol *10*, 217–224.

Pollock, J.D., Williams, D.A., Gifford, M., Li, L.L., DU, X.X., Fisherman, J., Orkin, S.H., Doerschuk, C.M., and Dinauer, M.C. (1995). Mouse Model of X-Linked Chronic Granulomatous-Disease, an Inherited Defect in Phagocyte Superoxide Production. Nat. Genet. *9*, 202–209.

Prins, D., and Michalak, M. (2011). Organellar calcium buffers. Cold Spring Harb Perspect Biol *3*, a004069–a004069.

Priya, R.R., Chew, E.Y., and Swaroop, A. (2012). Genetic studies of age-related macular degeneration: lessons, challenges, and opportunities for disease management. Ophthalmology *119*, 2526–2536.

Purves, D., Lotto, R.B., Williams, S.M., Nundy, S., and Yang, Z. (2001). Why we see things the way we do: evidence for a wholly empirical strategy of vision. Philosophical Transactions of the Royal Society of London. Series B: Biological Sciences *356*, 285–297.

Radu, R.A., Hu, J., Peng, J., Bok, D., Mata, N.L., and Travis, G.H. (2008). Retinal pigment epithelium-retinal G protein receptor-opsin mediates light-dependent translocation of all-trans-retinyl esters for synthesis of visual chromophore in retinal pigment epithelial cells. J. Biol. Chem. *283*, 19730–19738.

Rashid, K., Wolf, A., and Langmann, T. (2018). Microglia Activation and Immunomodulatory Therapies for Retinal Degenerations. Front Cell Neurosci *12*, 176.

Ravichandran, K.S. (2003). "Recruitment Signals" from Apoptotic Cells: Invitation to a Quiet Meal. Cell *113*, 817–820.

Raymond, S.M., and Jackson, I.J. (1995). The retinal pigmented epithelium is required for development and maintenance of the mouse neural retina. Current Biology *5*, 1286–1295.

Rechichi, M., Salvetti, A., Chelli, B., Costa, B., Da Pozzo, E., Spinetti, F., Lena, A., Evangelista, M., Rainaldi, G., Martini, C., et al. (2008). TSPO over-expression increases motility, transmigration and proliferation properties of C6 rat glioma cells. Biochim. Biophys. Acta *1782*, 118–125.

Reczek, C.R., and Chandel, N.S. (2015). ROS-dependent signal transduction. Curr. Opin. Cell Biol. *33*, 8–13.

Rhoades, W., Dickson, D., and Do, D.V. (2015). Potential role of lampalizumab for treatment of geographic atrophy. Clin Ophthalmol *9*, 1049–1056.

Rice, R.A., Pham, J., Lee, R.J., Najafi, A.R., West, B.L., and Green, K.N. (2017). Microglial repopulation resolves inflammation and promotes brain recovery after injury. Glia *65*, 931–944.

Rice, R.A., Spangenberg, E.E., Yamate-Morgan, H., Lee, R.J., Arora, R.P.S., Hernandez, M.X., Tenner, A.J., West, B.L., and Green, K.N. (2015). Elimination of Microglia Improves Functional Outcomes Following Extensive Neuronal Loss in the Hippocampus. J. Neurosci. *35*, 9977–9989.

Ritter, M.R., Banin, E., Moreno, S.K., Aguilar, E., Dorrell, M.I., and Friedlander, M. (2006). Myeloid progenitors differentiate into microglia and promote vascular repair in a model of ischemic retinopathy. J Clin Invest *116*, 3266–3276.

Rivera, A., Fisher, S.A., Fritsche, L.G., Keilhauer, C.N., Lichtner, P., Meitinger, T., and Weber, B.H.F. (2005). Hypothetical LOC387715 is a second major susceptibility gene for age-related macular degeneration, contributing independently of complement factor H to disease risk. Hum. Mol. Genet. *14*, 3227–3236.

Robinson, K.M., Janes, M.S., Pehar, M., Monette, J.S., Ross, M.F., Hagen, T.M., Murphy, M.P., and Beckman, J.S. (2006). Selective fluorescent imaging of superoxide in vivo using ethidium-based probes. Proc. Natl. Acad. Sci. U.S.a. *103*, 15038–15043.

Rubino, S.J., Mayo, L., Wimmer, I., Siedler, V., Brunner, F., Hametner, S., Madi, A., Lanser, A., Moreira, T., Donnelly, D., et al. (2018). Acute microglia ablation induces neurodegeneration in the somatosensory system. Nature Communications 2014 5 *9*, 4578–13.

Rudnicka, A.R., Kapetanakis, V.V., Jarrar, Z., Wathern, A.K., Wormald, R., Fletcher, A.E., Cook, D.G., and Owen, C.G. (2015). Incidence of Late-Stage Age-Related Macular Degeneration in American Whites: Systematic Review and Meta-analysis. American Journal of Ophthalmology *160*, 85–93. e3.

Rupprecht, R., Papadopoulos, V., Rammes, G., Baghai, T.C., Fan, J., Akula, N., Groyer, G., Adams, D., and Schumacher, M. (2010). Translocator protein (18 kDa) (TSPO) as a therapeutic target for neurological and psychiatric disorders. Nat Rev Drug Discov *9*, 971–988.

Rupprecht, R., Rammes, G., Eser, D., Baghai, T.C., Schuele, C., Nothdurfter, C., Troxler, T., Gentsch, C., Kalkman, H.O., Chaperon, F., et al. (2009). Translocator Protein (18 kD) as Target for Anxiolytics Without Benzodiazepine-Like Side Effects. Science *325*, 490–493.

Rymo, S.F., Gerhardt, H., Wolfhagen Sand, F., Lang, R., Uv, A., and Betsholtz, C. (2011). A two-way communication between microglial cells and angiogenic sprouts regulates angiogenesis in aortic ring cultures. Plos One *6*, e15846.

Ryu, J.K., Choi, H.B., and McLarnon, J.G. (2005). Peripheral benzodiazepine receptor ligand PK11195 reduces microglial activation and neuronal death in quinolinic acid-injected rat striatum. Neurobiol. Dis. *20*, 550–561.

Sakurai, E., Anand, A., Ambati, B.K., van Rooijen, N., and Ambati, J. (2003). Macrophage Depletion Inhibits Experimental Choroidal Neovascularization. Invest. Ophthalmol. Vis. Sci. *44*, 3578–3585.

Salter, M.W., and Beggs, S. (2014). Sublime Microglia: Expanding Roles for the Guardians of the CNS. Cell *158*, 15–24.

Santos, A.M., Calvente, R., Tassi, M., Carrasco, M.-C., Martin-Oliva, D., Marín-Teva, J.L., Navascuies, J., and Cuadros, M.A. (2008). Embryonic and postnatal development of microglial cells in the mouse retina. Journal of Comparative Neurology *506*, 224–239.

Schafer, D.P., Lehrman, E.K., Kautzman, A.G., Koyama, R., Mardinly, A.R., Yamasaki, R., Ransohoff, R.M., Greenberg, M.E., Barres, B.A., and Stevens, B. (2012). Microglia Sculpt Postnatal Neural Circuits in an Activity and Complement-Dependent Manner. Neuron *74*, 691–705.

Scholz, R., Caramoy, A., Bhuckory, M.B., Rashid, K., Chen, M., Xu, H., Grimm, C., and Langmann, T. (2015a). Targeting translocator protein (18 kDa) (TSPO) dampens pro-inflammatory microglia reactivity in the retina and protects from degeneration. J Neuroinflammation *12*, 201.

Scholz, R., Sobotka, M., Caramoy, A., Stempfl, T., Moehle, C., and Langmann, T. (2015b). Minocycline counter-regulates pro-inflammatory microglia responses in the retina and protects from degeneration. J Neuroinflammation *12*, 209.

Schumacher, B., Garinis, G.A., and Hoeijmakers, J.H.J. (2008). Age to survive: DNA damage and aging. Trends in Genetics *24*, 77–85.

Schwartz, S.D., Regillo, C.D., Lam, B.L., Eliott, D., Rosenfeld, P.J., Gregori, N.Z., Hubschman, J.-P., Davis, J.L., Heilwell, G., Spirn, M., et al. (2015). Human embryonic stem cell-derived retinal pigment epithelium in patients with age-related macular degeneration and Stargardt's macular dystrophy: follow-up of two open-label phase 1/2 studies. The Lancet *385*, 509–516.

Selvaraj, V., and Stocco, D.M. (2015). The changing landscape in translocator protein (TSPO) function. Trends in Endocrinology & Metabolism *26*, 341–348.

Shastri, A., Bonifati, D.M., and Kishore, U. (2013). Innate Immunity and Neuroinflammation. Mediators of Inflammation *2013*, 1–19.

Shen, W., Zhu, L., Lee, S.-R., Chung, S.H., and Gillies, M.C. (2013). Involvement of NT3 and P75 NTR in photoreceptor degeneration following selective Müller cell ablation. J Neuroinflammation *10*, 1–13.

Sierra, A., de Castro, F., Del Río-Hortega, J., Rafael Iglesias-Rozas, J., Garrosa, M., and Kettenmann, H. (2016). The "Big-Bang" for modern glial biology: Translation and comments on Pío del Río-Hortega 1919 series of papers on microglia. Glia *64*, 1801–1840.

Sierra, A., Gottfried-Blackmore, A.C., McEwen, B.S., and Bulloch, K. (2007). Microglia derived from aging mice exhibit an altered inflammatory profile. Glia *55*, 412–424.

Sileikyte, J., Blachly-Dyson, E., Sewell, R., Carpi, A., Menabo, R., Di Lisa, F., Ricchelli, F., Bernardi, P., and Forte, M. (2014). Regulation of the Mitochondrial Permeability Transition Pore by the Outer Membrane Does Not Involve the Peripheral Benzodiazepine Receptor (Translocator Protein of 18 kDa (TSPO)). J. Biol. Chem. *289*, 13769–13781.

Simon-O'Brien, E., Gauthier, D., Riban, V., and Verleye, M. (2016). Etifoxine improves sensorimotor deficits and reduces glial activation, neuronal degeneration, and neuroinflammation in a rat model of traumatic brain injury. J Neuroinflammation *13*, 1–15.

Sousa, C., Biber, K., and Michelucci, A. (2017). Cellular and Molecular Characterization of Microglia: A Unique Immune Cell Population. Front. Immunol. *8*.

Stefater, J.A., Lewkowich, I., Rao, S., Mariggi, G., Carpenter, A.C., Burr, A.R., Fan, J., Ajima, R., Molkentin, J.D., Williams, B.O., et al. (2011). Regulation of angiogenesis by a non-canonical Wnt-Flt1 pathway in myeloid cells. Nature *474*, 511–515.

Streit, W.J. (2002). Microglia as neuroprotective, immunocompetent cells of the CNS. Glia *40*, 133–139.

Sung, C.-H., and Chuang, J.-Z. (2010). The cell biology of vision. J. Cell Biol. *190*, 953–963.

Swaroop, A., Chew, E.Y., Rickman, C.B., and Abecasis, G.R. (2009). Unraveling a Multifactorial Late-Onset Disease: From Genetic Susceptibility to Disease Mechanisms for Age-Related Macular Degeneration. Annu Rev Genomics Hum Genet *10*, 19–43.

Szalay, G., Martinecz, B., Lénárt, N., Környei, Z., Orsolits, B., Judák, L., Császár, E., Fekete, R., West, B.L., Katona, G., et al. (2016). Microglia protect against brain injury and their selective elimination dysregulates neuronal network activity after stroke. Nature Communications 2014 5 *7*, 1–13.

Szepesi, Z., Manouchehrian, O., Bachiller, S., and Deierborg, T. (2018). Bidirectional Microglia-Neuron Communication in Health and Disease. Front Cell Neurosci *12*, 323.

Tarafdar, A., and Pula, G. (2018). The Role of NADPH Oxidases and Oxidative Stress in Neurodegenerative Disorders. Int J Mol Sci *19*, 3824.

Tay, T.L., Savage, J.C., Hui, C.W., Bisht, K., and Tremblay, M.-È. (2017). Microglia across the lifespan: from origin to function in brain development, plasticity and cognition. J. Physiol. (Lond.) *595*, 1929–1945.

Teboul, D., Beaufils, S., Taveau, J.-C., Iatmanen-Harbi, S., Renault, A., Venien-Bryan, C., Vie, V., and Lacapère, J.-J. (2012). Mouse TSPO in a lipid environment interacting with a functionalized monolayer. Biochim. Biophys. Acta *1818*, 2791–2800.

Thai, P.N., Daugherty, D.J., Frederich, B.J., Lu, X., Deng, W., Bers, D.M., Dedkova, E.N., and Schaefer, S. (2018). Cardiac-specific Conditional Knockout of the 18-kDa Mitochondrial Translocator Protein Protects from Pressure Overload Induced Heart Failure. Sci Rep *8*, 16213.

Torres, S.R., Fröde, T.S., Nardi, G.M., Vita, N., Reeb, R., Ferrara, P., Ribeiro-do-Valle, R.M., and Farges, R.C. (2000). Anti-inflammatory effects of peripheral benzodiazepine receptor ligands in two mouse models of inflammation. European Journal of Pharmacology *408*, 199–211.

Truett, G.E., Heeger, P., Mynatt, R.L., Truett, A.A., Walker, J.A., and Warman, M.L. (2000). Preparation of PCR-quality mouse genomic DNA with hot sodium hydroxide and tris (HotSHOT). BioTechniques *29*, 52–54.

Tsutsumi, C., Sonoda, K.H., Egashira, K., Qiao, H., Hisatomi, T., Nakao, S., Ishibashi, M., Charo, I.F., Sakamoto, T., Murata, T., et al. (2003). The critical role of ocular-infiltrating macrophages in the development of choroidal neovascularization. J. Leukoc. Biol. *74*, 25–32.

Tu, L.N., Morohaku, K., Manna, P.R., Pelton, S.H., Butler, W.R., Stocco, D.M., and Selvaraj, V. (2014). Peripheral benzodiazepine receptor/translocator protein global knock-out mice are viable with no effects on steroid hormone biosynthesis. J. Biol. Chem. *289*, 27444–27454.

Tu, L.N., Zhao, A.H., Hussein, M., Stocco, D.M., and Selvaraj, V. (2016). Translocator Protein (TSPO) Affects Mitochondrial Fatty Acid Oxidation in Steroidogenic Cells. Endocrinology *157*, 1110–1121.

Tu, L.N., Zhao, A.H., Stocco, D.M., and Selvaraj, V. (2015). PK11195 effect on steroidogenesis is not mediated through the translocator protein (TSPO). Endocrinology *156*, 1033–1039.

Ushio-Fukai, M. (2009). Compartmentalization of redox signaling through NADPH oxidase-derived ROS. Antioxid. Redox Signal. *11*, 1289–1299.

Valencia, A., and Kochevar, I.E. (2008). Nox1-based NADPH oxidase is the major source of UVA-induced reactive oxygen species in human keratinocytes. J. Invest. Dermatol. *128*, 214–222.

Varga, Z.M., Wegner, J., and Westerfield, M. (1999). Anterior movement of ventral diencephalic precursors separates the primordial eye field in the neural plate and requires cyclops. Development *126*, 5533–5546.

Varvel, N.H., Grathwohl, S.A., Baumann, F., Liebig, C., Bosch, A., Brawek, B., Thal, D.R., Charo, I.F., Heppner, F.L., Aguzzi, A., et al. (2012). Microglial repopulation model reveals a robust homeostatic process for replacing CNS myeloid cells. Proc. Natl. Acad. Sci. U.S.a. *109*, 18150–18155.

Veenman, L., and Gavish, M. (2012). The role of 18 kDa mitochondrial translocator protein (TSPO) in programmed cell death, and effects of steroids on TSPO expression. Current Molecular Medicine *12*, 398–412.

Veiga, S., Azcoitia, I., and Garcia-Segura, L.M. (2005). Ro5-4864, a peripheral benzodiazepine receptor ligand, reduces reactive gliosis and protects hippocampal hilar neurons from kainic acid excitotoxicity. J. Neurosci. Res. *80*, 129–137.

Verma, A., Nye, J.S., and Snyder, S.H. (1987). Porphyrins are endogenous ligands for the mitochondrial (peripheraltype) benzodiazepine receptor. Proc. Natl. Acad. Sci. U.S.a. *84*, 2256–2260.

Vivash, L., and O'Brien, T.J. (2016). Imaging Microglial Activation with TSPO PET: Lighting Up Neurologic Diseases? J Nucl Med *57*, 165–168.

Wang, H., Zhang, K., Zhao, L., Tang, J., Gao, L., and Wei, Z. (2014a). Anti-inflammatory effects of vinpocetine on the functional expression of nuclear factor-kappa B and tumor necrosis factor-alpha in a rat model of cerebral ischemia-reperfusion injury. Neuroscience Letters *566*, 247–251.

Wang, H.-J., Fan, J., and Papadopoulos, V. (2012). Translocator protein (Tspo) gene promoter-driven green fluorescent protein synthesis in transgenic mice: an in vivo model to study Tspo transcription. Cell Tissue Res. *350*, 261–275.

Wang, M., and Wong, W.T. (2014). Microglia-Müller Cell Interactions in the Retina. In Retinal Degenerative Diseases, (New York, NY: Springer, New York, NY), pp. 333–338.

Wang, M., Wang, X., Zhao, L., Ma, W., Rodriguez, I.R., Fariss, R.N., and Wong, W.T. (2014b). Macroglia-Microglia Interactions via TSPO Signaling Regulates Microglial Activation in the Mouse Retina. J. Neurosci. *34*, 3793–3806.

Wang, X., Zhao, L., Zhang, J., Fariss, R.N., Ma, W., Kretschmer, F., Wang, M., Qian, H.H., Badea, T.C., Diamond, J.S., et al. (2016). Requirement for Microglia for the Maintenance of Synaptic Function and Integrity in the Mature Retina. J. Neurosci. *36*, 2827–2842.

Wenzel, A., Grimm, C., Samardzija, M., and Reme, C.E. (2005). Molecular mechanisms of light-induced photoreceptor apoptosis and neuroprotection for retinal degeneration. Prog Retin Eye Res *24*, 275–306.

Whalin, M.E., Boujrad, N., Papadopoulos, V., and Krueger, K.E. (1994). Studies on the phosphorylation of the 18 kDa mitochondrial benzodiazepine receptor protein. J. Recept. Res. *14*, 217–228.

Wheeler, D.L., Sariol, A., Meyerholz, D.K., and Perlman, S. (2018). Microglia are required for protection against lethal coronavirus encephalitis in mice. J Clin Invest *128*, 931–943.

Winkler, B.S. (1981). Glycolytic and oxidative metabolism in relation to retinal function. The Journal of General Physiology *77*, 667–692.

Winkler, B.S., Boulton, M.E., Gottsch, J.D., and Sternberg, P. (1999). Oxidative damage and age-related macular degeneration. Mol. Vis. *5*, 32.

Witmer, A. (2003). Vascular endothelial growth factors and angiogenesis in eye disease. Prog Retin Eye Res *22*, 1–29.

Wong, W.L., Su, X., Li, X., Cheung, C.M.G., Klein, R., Cheng, C.-Y., and Wong, T.Y. (2014). Global prevalence of age-related macular degeneration and disease burden projection for 2020 and 2040: a systematic review and meta-analysis. The Lancet Global Health *2*, e106–e116.

Wynn, T.A., and Vannella, K.M. (2016). Macrophages in Tissue Repair, Regeneration, and Fibrosis. Immunity *44*, 450–462.

Xia, Y., Ledwitch, K., Kuenze, G., Duran, A., Li, J., Sanders, C.R., Manning, C., and Meiler, J. (2019). A unified structural model of the mammalian translocator protein (TSPO). J. Biomol. NMR *73*, 347–364.

Xu, H., Chen, M., and Forrester, J.V. (2009). Para-inflammation in the aging retina. Prog Retin Eye Res *28*, 348–368.

Yang, S., Zhao, J., and Sun, X. (2016). Resistance to anti-VEGF therapy in neovascular age-related macular degeneration: a comprehensive review. Drug Design, Development and Therapy *10*, 1857–1867.

Yang, X., Ren, H., Wood, K., Li, M., Qiu, S., Shi, F.-D., Ma, C., and Liu, Q. (2018). Depletion of microglia augments the dopaminergic neurotoxicity of MPTP. The FASEB Journal *32*, 3336–3345.

Yeliseev, A.A., Krueger, K.E., and Kaplan, S. (1997). A mammalian mitochondrial drug receptor functions as a bacterial "oxygen" sensor. Proc. Natl. Acad. Sci. U.S.a. *94*, 5101–5106.

Yokota, H., Narayanan, S.P., Zhang, W., Liu, H., Rojas, M., Xu, Z., Lemtalsi, T., Nagaoka, T., Yoshida, A., Brooks, S.E., et al. (2011). Neuroprotection from Retinal Ischemia/Reperfusion Injury by NOX2 NADPH Oxidase Deletion. Invest. Ophthalmol. Vis. Sci. *52*, 8123–8131.

Yona, S., Kim, K.-W., Wolf, Y., Mildner, A., Varol, D., Breker, M., Strauss-Ayali, D., Viukov, S., Guilliams, M., Misharin, A., et al. (2013). Fate mapping reveals origins and dynamics of monocytes and tissue macrophages under homeostasis. Immunity *38*, 79–91.

Zeng, X., Ren, H., Zhu, Y., Zhang, R., Xue, X., Tao, T., and Xi, H. (2018). Gp91phox (NOX2) in Activated Microglia Exacerbates Neuronal Damage Induced by Oxygen Glucose Deprivation and Hyperglycemia in an in Vitro Model. Cell. Physiol. Biochem. *50*, 783–797.

Zhang, C., Lei, B., Lam, T.T., Yang, F., Sinha, D., and Tso, M. (2004). Neuroprotection of photoreceptors by minocycline in light-induced retinal degeneration. Invest. Ophthalmol. Vis. Sci. *45*, 2753–2759.

Zhang, Y., Zhao, L., Wang, X., Ma, W., Lazere, A., Qian, H.H., Zhang, J., Abu-Asab, M., Fariss, R.N., Roger, J.E., et al. (2018). Repopulating retinal microglia restore endogenous organization and function under CX3CL1-CX3CR1 regulation. Science Advances *4*, eaap8492.

Zhao, L., Zabel, M.K., Wang, X., Ma, W., Shah, P., Fariss, R.N., Qian, H., Parkhurst, C.N., Gan, W.B., and Wong, W.T. (2015). Microglial phagocytosis of living photoreceptors contributes to inherited retinal degeneration. EMBO Molecular Medicine *7*, 1179–1197.

Zhao, M., Mantel, I., Gelize, E., Li, X., Xie, X., Arboleda, A., Seminel, M., Levy-Boukris, R., Dernigoghossian, M., Prunotto, A., et al. (2019). Mineralocorticoid receptor antagonism limits experimental choroidal neovascularization and structural changes associated with neovascular age-related macular degeneration. Nature Communications 2014 5 *10*, 369–13.

Zhao, Y.-Y., Yu, J.-Z., Li, Q.-Y., Ma, C.-G., Lu, C.-Z., and Xiao, B.-G. (2011). TSPO-specific ligand vinpocetine exerts a neuroprotective effect by suppressing microglial inflammation. Neuron Glia Biol. *7*, 187–197.

Zielonka, J., and Kalyanaraman, B. (2010). Hydroethidine- and MitoSOX-derived red fluorescence is not a reliable indicator of intracellular superoxide formation: Another inconvenient truth. Free Radical Biology and Medicine *48*, 983–1001.

6. Danksagung

Eine wissenschaftliche Arbeit ist nie das Werk einer einzelnen Person, deshalb ist es jetzt an der Zeit, mich bei allen Menschen zu bedanken, die mir die Erstellung meiner Dissertation ermöglicht haben.

Ein ganz besonderer Dank gilt meinem Doktorvater Herrn Prof. Dr. Thomas Langmann, der nicht nur die wissenschaftliche Betreuung meiner Doktorarbeit übernommen und dessen Voranschreiten durch seine hilfreichen Ratschläge und anregenden Diskussionen begleitete, sondern mich auch im Hinblick auf meine fachliche und persönliche Weiterentwicklung stets gefördert hat.

Ein großer Dank geht auch an Prof. Dr. Elena Rugarli für die bereitwillige Übernahme des Zweitgutachtens und an Herrn Prof. Dr. Siegfried Roth für die Übernahme des Prüfungsvorsitzes.

Auch Dr. Michael Schramm und Dr. Marc Herb als meine Kooperationspartner sind hier besonders zu benennen, da Sie mir die technischen Möglichkeiten und das Know-how gegeben und vermittelt haben, die Arbeit in dieser methodischen Vielfalt durchzuführen. Für mich war es äußerst wertvoll, dass es ehrliche und offene Kritik gab und eine sehr gute Kooperationsarbeit. Für diese Ehrlichkeit, die Kollegialität der ganzen AG Schramm und die tolle Zusammenarbeit bin ich sehr dankbar.

Nicht versäumen will ich es, mich bei allen momentanen und ehemaligen Kollegen der AG Langmann zu bedanken. Für die angenehme Arbeitsatmosphäre und konstruktive Zusammenarbeit richte ich ein herzliches Dankeschön an Marcus Karlstetter, Alexander Aslanidis, Markus Sobotka, Khalid Rashid, Isha Akhtar-Schäfer, Mona Tabel, Carsten Balser, Verena Behnke, Johanna Wiedemann, Katharina Dannhausen, Amir Khan, Moyinoluwa Taiwo, Moran Homola, Anika Lückoff, Rebecca Scholz, Nils Laudenberg, Eva Scheiffert, Claudia Bismar, Ulrike Esendik, Anja Volkmann und Rodica Maniu.

Großer Dank gebührt auch allen meinen Freunden, die mich während meiner Arbeit unterstützt, mir den Rücken gestärkt und mir den nötigen Ausgleich zum Laboralltag verschafft haben.

Ein besonders herzlicher Dank gilt meiner Familie, insbesondere meinen Eltern Klaus und Susanne Wolf, denen ich diese Arbeit widme. Sie haben mir meine akademische Ausbildung ermöglicht und mir stets uneingeschränkten Rückhalt gegeben.

7.　Erklärung

Ich versichere, dass ich die von mir vorgelegte Dissertation selbständig angefertigt, die benutzten Quellen und Hilfsmittel vollständig angegeben und die Stellen der Arbeit − einschließlich Tabellen, Karten und Abbildungen −, die anderen Werken im Wortlaut oder dem Sinn nach entnommen sind, in jedem Einzelfall als Entlehnung kenntlich gemacht habe; dass diese Dissertation noch keiner anderen Fakultät oder Universität zur Prüfung vorgelegen hat; dass sie − abgesehen von unten angegebenen Teilpublikationen − noch nicht veröffentlicht worden ist, sowie, dass ich eine solche Veröffentlichung vor Abschluss des Promotionsverfahrens nicht vornehmen werde. Die Bestimmungen der Promotionsordnung sind mir bekannt. Die von mir vorgelegte Dissertation ist von Prof. Dr. Thomas Langmann betreut worden.

Teilpublikation:

Wolf, A., Herb, M., Schramm, M., Langmann, T. (2020). *The TSPO-NOX1 axis controls phagocyte-triggered pathological angiogenesis in the eye.* **Nature Communications**, 11 (2709); https://doi.org/10.1038/s41467-020-16400-8

Köln, 8 Juni 2020

_____
(Anne Wolf)

8. Curriculum vitae

Anne Wolf
Gustavstr. 15
D-50937 Köln
E-mail: annewolf.90@googlemail.com

Persönliche Daten

Geburtstag	14 Oktober 1990
Geburtsort	Merzig
Nationalität	deutsch

Hochschulausbildung

seit 10/2015	**Doktorandin** Zentrum für Augenheilkunde, Universität zu Köln Arbeitsgruppe von Prof. Dr. Thomas Langmann
10/2013 – 09/2015	**Master of Science in Biological Sciences** Zentrum für Augenheilkunde, Universität zu Köln Arbeitsgruppe von Prof. Dr. Thomas Langmann
10/2010 – 09/2013	**Bachelor of Science in Biological Sciences** Institut für Genetik, Universität zu Köln Arbeitsgruppe von Prof. Dr. med. Jens C. Brüning

Berufliche Erfahrung

09/2014 – 02/2015	**Forschungspraktikantin** Zentrum für Augenheilkunde, Universität zu Köln Arbeitsgruppe von Prof. Dr. Thomas Langmann
04/2014 – 02/2015	**Wissenschaftliche Mitarbeiterin** Institut für Botanik, Universität zu Köln Arbeitsgruppe von Prof. Dr. Martin Hülskamp
04/2014 – 05/2014	**Forschungspraktikantin** Max-Planck-Institut für Biologie des Alterns Arbeitsgruppe von Prof. Dr. Nils-Göran Larsson
03/2014– 04/2014	**Forschungspraktikantin** Institut für Genetik, Universität zu Köln Arbeitsgruppe von Prof. Dr. med Jens C. Brüning
02/2013 – 03/2013 04/2013 – 04/2013	**Praktikantin** Molekular Pathologie Trier (MPT)
07/2009 – 07/2010	**Freiwilliges Soziales Jahr** SOS Kinderdorf, Merzig,
07/2008 – 08/2014	**Hauswirtschafterin** Altenheim 'Wohnstift Myosotis', Britten

Stipendien und Auszeichnungen

2019	Retina Suisse Award
2019	IPaK Reisestipendium
2018	ProRetina Reisestipedium
2015 - 2019	Promotionsstipendium, VELUX Stiftung
2013	Auszeichnung als Jahrgangsbeste, Bachelor of Science in Biologie, Universität zu Köln

Publikationen

Wolf, A., Herb, M., Schramm, M., Langmann, T. (2020). *The TSPO-NOX1 axis controls phagocyte-triggered pathological angiogenesis in the eye.* **Nature Communications,** 11 (2709) https://doi.org/10.1038/s41467-020-16400-8

Behnke, V., **Wolf, A.**, Langmann, T. (2020). *The role of lymphocytes and phagocytes in age-related macular degeneration (AMD).* **Cellular and Molecular Life Sciences**: CMLS, 158 (193–199), 808–8. http://doi.org/10.1007/s00018-019-03419-4

Wolf, A., Langmann, T. (2019). Anti-VEGF-A/ANG2 combotherapy limits pathological angiogenesis in the eye: a replication study. **EMBO Molecular Medicine**, 11 (5), e10362. http://doi.org/10.15252/emmm.201910362

Balser, C. **and Wolf, A.**, Herb, M., Langmann, T. (2019). *Co-inhibition of PGF and VEGF blocks their expression in mononuclear phagocytes and limits neovascularization and leakage in the murine retina.* **Journal of Neuroinflammation**, 16 (1). http://doi.org/10.1186/s12974-019-1419-2

Herb, M., Gluschko, A., Wiegmann, K., F arid, A., **Wolf, A.**, Utermöhlen, O., et al. (2019). *Mitochondrial reactive oxygen species enable proinflammatory signaling through disulfide linkage of NEMO.* **Science Signaling**, 12 (568), eaar5926. http://doi.org/10.1126/scisignal.aar5926

Rashid K., **Wolf A.**, Langmann T. (2018) *Microglia Activation and Immunomodulatory Therapies for Retinal Degenerations.* **Frontiers in Cellular Neuroscience**, 12:176. http://doi: 10.3389/fncel.2018.00176

Rashid, K., Geissl, L., **Wolf, A.**, Karlstetter, M., Langmann, T. (2018). *Transcriptional regulation of Translocator protein (18 kDa) (TSPO) in microglia requires Pu.1, Ap1 and Sp factors.* **Biochimica Et Biophysica Acta - Gene Regulatory Mechanisms**, 1861 (12), 1119–1133. http://doi.org/10.1016/j.bbagrm.2018.10.018

Wolf A., Aslanidis A., Langmann T. (2017) *Retinal expression and localization of Mef2c support its important role in photoreceptor gene expression.* **Biochemical and Biophysical Research Communication**, 483 (1):346-351. http://doi.org/10.1016/j.bbrc.2016.12.141